NTNU – Trondheim
Norwegian University of
Science and Technology

Dynamic Analysis of Floating Dock Structures

Joakim Le Boulvais Børkja

Marine Technology
Submission date: March 2015
Supervisor: Svein Sævik, IMT

Norwegian University of Science and Technology
Department of Marine Technology

Dynamic Analysis of Floating Dock Structures

Joakim Børkja

March 2015

MASTER THESIS

Department of Marine Technology

Faculty of Engineering Science and Technology

Norwegian University of Science and Technology

Supervisor: Professor Svein Sævik

Preface

This paper is a Master's thesis in Marine constructions written as a final project for the Master's degree program Marine Technology at NTNU. The work was done during the autumn semester of 2014 and during the spring semester of 2015. The project was offered by managing director Stein Are Berg at Bi-Brygga AS. The contact with the company was maintained by email. A case study of a failed floating dock system was supplied by Bi-Brygga AS. There are currently no regulations concerning the design of floating docks, as such the Master's project was seen as a possibility to explore existing regulations for similar structures, and to establish a basis on which future regulations could be made. Marintek's relatively new software SIMA seemed suited for such an analysis. Although, the actual model was made with the older software SIMO. The Master's project therefore developed into a dynamic analysis of the floating dock system offered by Bi-Brygga AS done in SIMA. The parameters to be used in SIMA would be determined by a literature study of regulations concerning structures similar to floating docks. In order to fully grasp the theory and methods used in this paper a basic knowledge of marine constructions, marine hydrodynamics and statistics is required, and the paper is therefore mostly intended for marine and civil engineers.

Trondheim, 2015-03-25

Joakim Børkja

Acknowledgment

I would like to thank the following persons for their great help during the writing of this paper. Firstly, I would like to thank Stein Are Berg at Bi-Brygga AS for supplying a very interesting and challenging project, and for all his help given in determining the case study data. Secondly, I would like to thank Knut Moe at Marintek for providing crucial assistance in the development of the floating docks model. Finally, I would like to thank my supervisor professor Svein Sævik at NTNU for his excellent guidance and thought provoking inquiries.

J.B.

Summary

This paper concerns a dynamic analysis preformed on a floating dock structure. The structure was installed by Bi-Brygga AS and failed in 2013 during a winter storm. Bi-Brygga AS offered this structure as a case study for a Master's thesis. There are currently no regulations detailing the design of floating docks. The case study was to be done in part to establish a basis on which future regulations could be based. This was to be achieved by studying standards for similar structures such as fish farms. The program SIMA was to be used to model the floating dock structure.

In the paper, a literature study was done in order to establish the necessary parameters required to perform a dynamic analysis on the floating dock model in SIMA. All assumptions and simplifications made were presented along side the determined analysis parameters. Then the model was subjected to a 50 year design storm and to the 2013 winter storm. The peak forces of 30 different design storms were Gumbel distributed and the 90 percentile values were chosen as design values. The results revealed that the floating dock structure was severely underdimensioned. In order to survive the 50 year design storm the mooring lines would have to have their capacity increased threefold from 30 tons to 90 tons. Several lines also suffered failure when subjected to the 2013 winter storm, which corresponds to reality. The 90 percentile values may however be overestimating the actual loads somewhat.

The floating dock model was also subjected to varying environmental conditions. It was determined that the current forces were negligible in this case. Different wave spectra were considered and it was found that they yield nearly identical responses. This was likely due to a inadequately chosen parameter in the time domain simulation. The shallow water spectrum was considered to be the most accurate based on theory. The effect of mooring line tautness was also investigated. It was found that slack in the mooring line significantly increases the mooring line peak tension. This increase was caused by snapping.

The design wave method was evaluated as a possible simplified wave model. However, it was

found lacking as it could not accurately account for the dynamic effects acting on the floating structure, because it underestimated the total forces. It was concluded that the simplest method for accurately calculating the loads on a floating docks structure is the dynamic model presented in this paper.

Sammendrag

Denne rapporten omhandler en dynamisk analyse utført på en flytebrygge struktur. Strukturen ble installert av Bi-Brygga AS og sviktet i 2013 under en vinterstorm. Bi-Brygga AS tilbød denne strukturen som en case study for en Masteroppgave. I skrivende stund eksistere det ingen forskrifter som dekker design av flytebrygger. Case studyen hadde blant annet som mål å etablere en basis som fremtidige forskrifter kunne basere seg på. Dette skulle oppnås ved å studere standarder for lignende flytende strukturer, som for eksempl fiskeoppdrettsanlegg. Dataprogrammet SIMA skulle brukes til å modellere den flytende bryggestrukturen.

Først av alt ble en litteraturstudie gjennomført for å etablere de nødvendige parameterne som trengtes for å gjennomføre en dynamisk analyse på flytebryggemodellen i SIMA. Alle antagelser og forenklinger som ble gjort ble presentert sammen med de bestemte analyseparameterne. Flytebryggemodellen ble deretter utsatt for en 50 års designstorm og for 2013 vinterstormen. Designverdiene ble valgt som 90 persentil verdiene av Gumbel distribusjoner basert på maksverdiene til 30 forskjellige designstormer. Resultatene viste at flytebrygge strukturen var underdimensjonert. For å overleve 50 års designstormen er det nødvendig å øke kapasiteten til ankerlinene 3 ganger, fra 30 tonn til 90 tonn. Flere ankerliner ville også røket under 2013 vinterstormen, noe som stemmer med virkeligheten. Det er mulig at 90 persentil verdiene overvurdere belastningen på linene noe.

Flytebryggemodellen ble også utsatt for varierende miljøtilstander. Det ble vist at strømningskreftene var neglisjerbare i dette tilfellet. Forskjellige bølgespektra ble vurdert, og det viste seg at de gav nesten identisk respons. Dette skyldtes mest sannsynlig en utilstrekkelig valgt parameter i tidsdomene simuleringen. Grunt vann spektrumet ble sett på som mest nøyaktig basert på teori. Effekten av stramhet i ankerlinene ble også evaluert. Det viste seg at slakkhet i linene økte maksspenningen i ankerlinene betraktelig. Denne økningen skyldtes napping.

Designbølgemetoden ble vurdert som en mulig forenklet bølgemodell, men det viste seg at den ikke kunne ta hensyn til de dynamiske effektene i analysen, fordi den undervurderte de totale

kreftene i systemet. Det ble konkludert at den enkleste metoden for å nøyaktig kalkulere belastningen på en flytebrygge er den dynamiske modellen som ble presentert i denne rapporten.

Contents

List of Figures

List of Tables

Chapter 1

Introduction

1.1 Background

Floating docks are commonly used to moor small recreational vessels. Unlike other floating structures like fish farms no regulation currently exist in Norway for floating docks. This presents a challenge for the companies that install such structures. In particular with respect to insurance, as insurance companies may be reluctant to accept decisions made independently of government recommendations. This has created an incentive to establish regulations for floating docks. A moored floating structure is a complicated dynamic system, as such calculating the response of a floating dock requires a lot of resources. As floating docks are relatively cheap structures, the resources available for long and detailed analyses are limited. As such, the creation of a set of regulations would be helpful as it would allow one to save time when establishing the parameters of a dynamic analysis of a floating dock. The companies which sell and install floating docks have seen an added benefit in being the ones proposing the regulations, as this would give them a better chance of obtaining well tailored regulations.

In the winter of 2013 a winter storm hit a floating dock system installed by Bi-Brygga AS in Sande, Vestfold. The storm was intense enough to snap several of the system's mooring lines. This event was then offered by Bi-Brygga AS to NTNU as a possible case study. The hope was that the foundations of a regulatory standard could be laid down. The intent was that the response of the floating docks be calculated based on a study of regulations created for other industries. This

would then form the basis of a new standard. With this in mind, the goal of this paper is to establish a dynamic analysis of the floating dock system based on the data supplied by Bi-Brygga AS, and on regulation made for similar cases. In particular, floating fish farms design regulations. The environmental data will be varied to provide a clearer image of the local conditions. The possibility of establishing a simplified model for the environmental forces will be considered.

Three main sources will be used to create a functioning model. Firstly, *Norsk Standard NS 9415 Flytende oppdrettsanlegg Krav til utforming, dimensjonering, utførelse, installasjon og drift* [5] is a Norwegian standard for the design of floating fish farms. It will be used as a potential analogue for the design of floating docks. Secondly, the environmental parameters will be chosen largely based on the recommendations given in *DNV-RP-C205 ENVIRONMENTAL CONDITIONS AND ENVIRONMENTAL LOADS* [2]. The environmental data will be gathered from the meteorological data published freely by Meterologisk institutt. Thirdly, the wave heights and wave periods will be determined as detailed in *Port designer's handbook* [6]. Additionally, *Sea loads on ships and offshore structures* [1] will be extensively used to establish both environmental and structural parameters required when creating the dynamic model. Several other sources will also be referenced in the following parts of the paper, but the above stated sources are the most important ones. The required structural data is supplied by Bi-Brygga AS. Unfortunately, all the data is not exact, so some assumptions must be made in these cases.

The dynamic analysis of the floating dock system will be done in the computer program SIMA. Within SIMA, a SIMO model will be established based on the information presented in the previous. The SIMA post-processor will be used to process the results from the dynamic analysis.

1.2 Objectives

The main objectives of this paper may be listed as:

1. A literature study will be done of the theoretical background behind SIMO, and of the relevant rules and regulations which may be used to establish an accurate dynamic floating dock model.

2. A floating dock model will be established in SIMO based on a case study supplied by Bi-Brygga AS. The model parameters should account for mechanical properties, structural geometry details, hydrodynamic coefficients, environmental conditions etc.

3. The performance of the model will be evaluated with several different environmental conditions. Such as current velocities, wave spectra and different weather conditions. The capacity of the floating docks will be considered.

4. The possibility of establishing a simplified model to estimate extreme wave loads will be considered.

5. Recommendations for further work will be made.

1.3 Limitations

The case which will be investigated in this paper is a complex structure. This means that some assumptions must be made in order to create a functioning SIMO model. The main constraint is the shallow water depth. This makes the environment quite complicated to model. SIMA allows one to account for shallow waters to an extent with numerical wave spectra. Nevertheless, the modeling of waves can only be done approximately in SIMA as there isn't a wave spectrum which is a strong fit to the conditions investigated in this paper. Additionally, the mooring lines will be short, and therefore very sensitive to large motions. The data obtained from Bi-Brygga AS is only approximate when it comes to the mooring lines. This is a cause for concern, as the short lines should be modeled as accurately as possible. Finally, the geometrical shape of the floating docks is approximated to that of a rectangular barge. This influences the hydrodynamical behaviour of the structure. In this respect, the limitations of the paper follows the limitations given by SIMA.

The dynamic analysis will consider the 2013 winter storm which caused the mooring system to fail. Additionally, the 50 year storm will be investigated as a possible design storm. The influence of current velocity, different wave spectra and the importance of mooring line tension will

be studied. Finally, the design wave method will be considered as a possible simplified model for extreme wave loads.

1.4 Structure of the Report

The report is organized as follows. Chapter 2 will present the theory behind SIMO and the theory used to create the SIMO model. Chapter 3 will detail the modeling basis obtained from the case study. As well as assumptions made in order to permit the SIMO model to be established. Chapter 4 will detail the parameters which will be used in the creation of the SIMO model, and show how the environmental parameters may be obtained. Chapter 5 will present the different analyses procedures. Chapter 6 will contain the results from the analyses. Chapter 7 will discuss the results found in chapter 6 and suggest possible further work. Finally, chapter 8 will conclude the paper.

Chapter 2

Theory

In this part the theory behind the modeling and the calculations done in this paper will be presented.

2.1 Environmental modeling

2.1.1 General

This part will cover the environmental conditions a floating moored structure may be subjected to. Primary interest is given to the phenomena which induce loads on the structure. Namely, wind, waves and currents. Additionally, the the effects of shallow water will be explored were this is relevant. The text will mainly concern itself with the information which is needed to model the environment for a moored floating structure in shallow waters as accurately as possible.

2.1.2 Shallow water

The behaviour of deep water waves changes as the water depth decreases. For deep water waves the water particles in the waves have a circular orbital motion. The sea surface is first noticed by the wave when the depth becomes approximately half the wave length ($d < \frac{\lambda}{2}$). The depth then disrupts the circular motion of the wave orbitals. The motion is flattened and takes on an elliptical orbital shape. This change means that the energy in the wave shifts, causing the wave length to shorten, the wave propagation velocity to decrease, and the wave height to increase.

As the depth decreases to less than a 20th of the wave length ($d < \frac{\lambda}{20}$), the orbitals of the water particles are disrupted and the motions of the particles become turbulent.

The properties of shallow water waves may be found analytically in the following manner by potential theory [7]. First, the velocity potential ϕ of the wave must be established. In order to do this four assumptions must be made.

1. The continuity of an incompressible potential fluid may be described by the Laplace equation:
$$\frac{\partial^2\phi}{\partial x^2} + \frac{\partial^2\phi}{\partial z^2} = 0 \tag{2.1}$$

2. The velocity potential is zero at the bottom due to the no slip condition:
$$\left(\frac{\partial\phi}{\partial z}\right)_{z=-h} = 0 \tag{2.2}$$
where h is the water depth.

3. Bernoulli's equation must be true for the water surface. This is called the dynamic condition.
$$g\zeta + \left(\frac{\partial\phi}{\partial t}\right)_{z=0} = 0 \tag{2.3}$$

4. The kinematic condition says that the fluid particles on the surface of the waves stay on the top of the waves. This is described by:
$$\frac{\partial\zeta}{\partial t} - \left(\frac{\partial\phi}{\partial z}\right)_{z=0} = 0 \tag{2.4}$$

Using the above conditions the velocity potential of a shallow wave may be found as:

$$\phi = \frac{g\zeta_A}{\omega}\frac{cosh\, k(h+z)}{cosh\, kh} sin(kx - \omega t) \tag{2.5}$$

From this the dispersion relation for shallow waves is given as:

$$\omega^2 = kg\, tan\, kh \tag{2.6}$$

The velocity potential ϕ may now be used to show the elliptical orbitals of the water particles. The motion of the water particles may be given by:

$$u = \frac{\partial \phi}{\partial x} \tag{2.7}$$

$$y = \frac{\partial \phi}{\partial z} \tag{2.8}$$

Integrating over time gives:

$$x_A = \int_0^t \frac{\partial \phi}{\partial x} dt = -\zeta_A \frac{cosh\, k(h+z)}{sinh\, kh} [sin(kx - \omega t) - sin\, kx] = -\partial x + \partial x_m \tag{2.9}$$

and:

$$z_A = \int_0^t \frac{\partial \phi}{\partial z} dt = \zeta_A \frac{sinh\, k(h+z)}{sinh\, kh} [cos(kx - \omega t) - cos\, kx] = \partial z + \partial_m \tag{2.10}$$

Now ∂x and ∂z may be expressed as:

$$\partial x = -a\, sin(kx - \omega t) \tag{2.11}$$

$$\partial z = b\, cos(kx - \omega t) \tag{2.12}$$

This then yields:

$$\frac{\partial^2 x}{a^2} + \frac{\partial^2 y}{b^2} = 1 \tag{2.13}$$

Thus, the water particles motions are described by elliptical orbits with a middle point of $(x + \partial x_m, z + \partial z_m)$, and from this follows the effects mentioned earlier in this section. Knowing that for deep water:

$$tanh\, kh = 1 \tag{2.14}$$

and that for shallow water:

$$tanh\, kh < 1 \tag{2.15}$$

One can surmise the effects of shallow water from the equations below [7]:

Wave elevation:

$$\zeta(t) = \zeta_A cos(kx - wt) \tag{2.16}$$

Wave length:

$$\lambda = \frac{2\pi g}{\omega^2} tanh\, kh \tag{2.17}$$

Wave velocity:

$$c_w^2 = \frac{g\lambda}{2\pi} tanh\, kh \tag{2.18}$$

2.1.3 Short term wave conditions

General

When considering short term wave conditions, one may assume that for periods of 3-6 hours a sea state may be looked upon as stationary. In this context a sea state is considered stationary when it may be described by a a set of constant environmental parameters. In the following the main parameters considered are the significant wave height H_s and the peak period T_p. The significant wave height is defined as the average height of the one-third highest wave heights in a given time period. The peak period is the inverse of the frequency at which the wave energy spectrum has its maximum value. [2]

Wave spectrum

A wave spectrum is a power spectral density function of a given vertical sea surface displacement. That is to say that it describes the distribution of the wave energy as a function of the angular spectral wave frequency ω. Short term stationary irregular sea states are commonly modeled by such wave spectra. The spectra are chosen based on geographical area and the conditions of the studied sea state. In the following three wave spectra will be described.

Pierson-Moskowitz spectrum

The Pierson-Moskowitz (PM) spectrum is based on the assumption that if the wind blows for a long time over a large area, then the waves will reach an equilibrium with the wind. This is

called a fully developed sea state. [8] Several wave spectra were calculated based on given wind speeds, which showed that the different spectra had the same general form. From these findings one derived the PM spectrum. The PM spectrum is described by the following expression:

$$S_{PM}(\omega) = \frac{5}{16} \cdot H_s^2 \omega_p^4 \cdot \omega^{-5} \exp\left(-\frac{5}{4}\left(\frac{\omega}{\omega_p}\right)^{-4}\right) \tag{2.19}$$

where ω_p is the angular spectral peak frequency.

JONSWAP spectrum

The JONSWAP was created from data recorded in the Joint North Sea Wave Observation Project (JONSWAP). [9] This study found that the a wave spectrum is completely fully developed. It will always be influenced by non linear effects, with the most important effect being interactions between waves. Therefore, the PM spectrum was modified with a peak shape factor γ in order to fit it to the observed data. The result may be expressed as shown below:

$$S_J(\omega) = A_\gamma S_{PM}(\omega) \gamma^{\exp\left(-0.5\left(\frac{\omega-\omega_p}{\sigma\omega_p}\right)^2\right)} \tag{2.20}$$

where

A_γ is a normalizing factor

$S_{PM}(\omega)$ is the Pierson-Moskowitz spectrum

γ is the peak shape factor

σ is the spectral width parameter

The normalizing factor A_γ is obtained from:

$$A_\gamma = 1 - 0.287 \cdot ln(\gamma) \tag{2.21}$$

The spectral width parameter is defined by:

$$\sigma = \begin{cases} 0.07, & \omega \leq \omega_p \\ 0.09, & \omega \geq \omega_p. \end{cases} \tag{2.22}$$

Peakedness factor

The peak shape factor influences the sharpness of the JONSWAP spectrum's peak. Where increasing the value will give a sharper peak, and where decreasing it will have the opposite effect. The factor may be determined by observed data, or if no such data is available one may use the following definition [2] to establish it:

$$\gamma = \begin{cases} 5, & \frac{T_p}{\sqrt{H_s}} \leq 3.6 \\ \exp\left(5.75 - 1.15\frac{T_p}{\sqrt{H_s}}\right), & 3.6 < \frac{T_p}{\sqrt{H_s}} < 5 \\ 1, & 5 \leq \frac{T_p}{\sqrt{H_s}} \end{cases} \tag{2.23}$$

The JONSWAP spectrum is assumed to be best suited for cases where $3.6 < T_p/\sqrt{H_s} < 5$. If one finds oneself outside of this interval the JONSWAP spectrum should be applied with care.

TMA spectrum

The PM and JONSWAP spectra assume deep water conditions. In order to account for depth Bouws et al. proposed the TMA spectrum [10]. This spectrum is a modified JONSWAP spectrum, which assumes non breaking waves. The depth dependency is obtained by multiplying the spectrum with a depth and frequency dependent function, giving this expression:

$$S_{TMA}(\omega) = S_j(\omega)\phi(\omega) \tag{2.24}$$

where

$$\phi(\omega) = \frac{\omega^5 \frac{\partial k}{\partial \omega}}{2g^2k^3} \tag{2.25}$$

Inserting the dispersion relation

$$\omega^2 = gk \cdot tanh(kd) \tag{2.26}$$

gives:

$$\phi(\omega) = \frac{cosh^2(kd)}{sinh^2(kd) + \frac{\omega^2 d}{g}} \tag{2.27}$$

where k is the wave number and d is the water depth.

A concern with the PM, JONSWAP and TMA spectra is that their high frequency tail is described by ω^{-5}, whereas empirical evidence indicates that it should be closer to ω^{-4}. This could yield a smaller dynamic response for high frequencies than what one would realistically observe [2].

2.1.4 Wave elevation

The wave elevation is obtained from a wave spectrum $S(\omega)$. This allows one to describe an irregular sea state by summing several regular waves with different periods [11], amplitudes and phase angles. The wave elevation ζ of a short crested wave is described by the following expression:

$$\zeta(x, y, t) = \zeta_A cos(\omega t - kx \cdot cos(\theta) - ky \cdot sin(\theta) + \epsilon) \tag{2.28}$$

where k is the wave number, θ is the angle between a defined x-axis and the wave propagation direction and ϵ is the phase angle. From the above expression one may express the sum of several wave elevations with different frequencies and different directions.

$$\zeta(x, y, t) = \sum_{i=1}^{I} \sum_{j=1}^{J} \zeta_{A_{ij}} cos(\omega_i t - k_i x \cdot cos(\theta_j) - k_i y \cdot sin(\theta_j) + \epsilon_{ij}) \tag{2.29}$$

In order to solve the above equation one may use a wave spectrum. The relation between the wave amplitude ζ_{ij} and a directional wave spectrum is given by:

$$\zeta_{A_{ij}} = \sqrt{2S(\omega_i, \theta_j)\Delta\omega\Delta\theta} \tag{2.30}$$

Inserting equation (2.30) into equation (2.29) gives the final expression which allows one to calculate the wave elevation based on a wave spectrum.

$$\zeta(x,y,t) = \sum_{i=1}^{I}\sum_{j=1}^{J}\sqrt{2S(\omega_i,\theta_j)\Delta\omega\Delta\theta}cos(\omega_i t - k_i x\cdot cos(\theta_j) - k_i y\cdot sin(\theta_j) + \epsilon_{ij}) \tag{2.31}$$

2.1.5 Wind

The wind may be modeled as two dimensional field, meaning that it propagates parallel to the horizontal plane. The wind will vary with its distance to the ground. This wind profile may be expressed as a function of the considered height. The following function may be used to describe this [12]:

$$\bar{u}(z) = \bar{u}_r\left(\frac{z}{z_r}\right)^{\alpha} \tag{2.32}$$

where:

z is the height above the water level

z_r is the reference height, typically 10 meters

$\bar{u}_r$ is the average velocity at height z_r

α is a height coefficient

The varying wind speed may be modeled by a wind spectrum. There are several alternatives, including the Davenport spectrum, the Harris spectrum or the ISO 19901-1 NPD spectrum. These spectra are based on the assumption of wind acting freely over a sufficiently large land surface. They may however still be applied to marine structure [2]. The main difference between the spectra occurs for low frequencies. If low frequency are important some care should be taken in the choice of wave spectrum. In the following, the NPD spectrum is presented. First, the design wind speed $u(z,t)$ at a height z is defined:

$$u(z,t) = U(z)\left[1 - 0.41\cdot I_u(z)\cdot ln\left(\frac{t}{t_0}\right)\right] \tag{2.33}$$

where $U(z)$ is the 1 hour mean wind speed, and it is defined as:

$$U(z) = U_0\left[1 + 5.73\cdot 10^{-2}(1 + 0.15\cdot U_0)^{0.5}\cdot ln\left(\frac{t}{t_0}\right)\right] \tag{2.34}$$

and $I_u(z)$ is the turbulence intensity factor expressed by:

$$I_u(z) = 0.061 + 0.043 \cdot U_0 \left(\frac{z}{10}\right)^{-0.22} \tag{2.35}$$

where U_0 is the 1 hour mean wind speed at 10 meters.The NPD wind spectrum may now be written as:

$$S(f) = \frac{320 \cdot \left(\frac{U_0}{10}\right)^2 \cdot \left(\frac{z}{10}\right)^{0.45}}{(1 + f_m^n)^{5/3n}} \tag{2.36}$$

$$f_m = 172 \cdot f \cdot \left(\frac{z}{10}^{\frac{2}{3}}\right) \cdot \left(\frac{U_0}{10}\right)^{-0.75} \tag{2.37}$$

where $S(f)$ $[m^2/s]$ is the spectral density at frequency f, and $n = 0.468$. Note that the NPD spectrum can only be used for the one hour mean wind speed measured at 10 meters over z=0. Finally, the fluctuating wind speed may be determined by the use of a state space model [12].

2.1.6 Current

Ocean currents may be separated into different categories, where the most relevant ones, in this case, are the wind generated currents and the tidal currents. The wind currents are created by wind stress, and the tidal currents are regular currents occurring as the shift between high and low tides occurs. The tidal currents are of particular interest in coastal waters, especially in inlets and straights [2]. Generally, the current velocity may be taken as a sum of all current contributions. Here, this translates in the following manner:

$$V_c(z) = V_{c,wind}(z) + V_{c,tide}(z) \tag{2.38}$$

where z is the depth.

Currents may be modeled by design current profiles if sufficient field measurements are not available. The tidal current velocity in shallow waters may be modeled by a power law. Accordingly, the following profile is obtained:

$$V_{c,tide}(z) = V_{c,tide}(0)\left(\frac{d+z}{d}\right)^{\alpha} \tag{2.39}$$

where:

d is the water depth to the still water depth

$v_{c,tide}$ is the tidal current velocity at the still water level

z is the distance from the still water level

α is a chosen exponent, commonly $\alpha = 1/7$

The wind generated current velocity may be described by a linear current design profile:

$$V_{c,wind}(z) = V_{c,wind}(0)\left(\frac{d_0+z}{d_0}\right) \tag{2.40}$$

where d_0 is the reference depth for wind generated current, set as $d_0 = 50m$.

In shallow coastal waters the tidal profiles will likely be inaccurate as the tidal currents will vary greatly from location to location. The only way to be certain of the current velocity is to measure it.

2.1.7 Estimation of significant wave height and peak period

When detailed measurements are lacking it is necessary to estimate a significant wave height H_s and peak period T_P based on local conditions and wind statistics. In this case, the method for calculating the parameters will be a method detailed in Norwegian standard for marine fish farms [5]. The method assumes that the waves are wind generated, and that the waves vary with fetch length and the 10 minute mean wind measured 10 meters over the water surface. The 50 year wind speed gives the 50 year wave conditions. The procedure is expressed as:

$$H_s = 5.112 \cdot 10^{-4} U_A F^{1/2} \tag{2.41}$$

$$T_P = 6.238 \cdot 10^{-2} (U_A F)^{1/3} \tag{2.42}$$

where:

F [m] is the fetch length

U_A is the adjusted wind speed defined by:

$$U_A = 0.71U^{1.23} \tag{2.43}$$

The fetch length will vary based on the local environment. Thorsen's Port Designer's Handbook [6] presents a simple method for estimating the fetch length in coastal waters. It consists of weighting the different possible fetch lengths with their angles. The end result is an effective fetch length, which may be used as a general fetch length for the area. This is illustrated in the following figure taken from the Port Designer's Handbook:

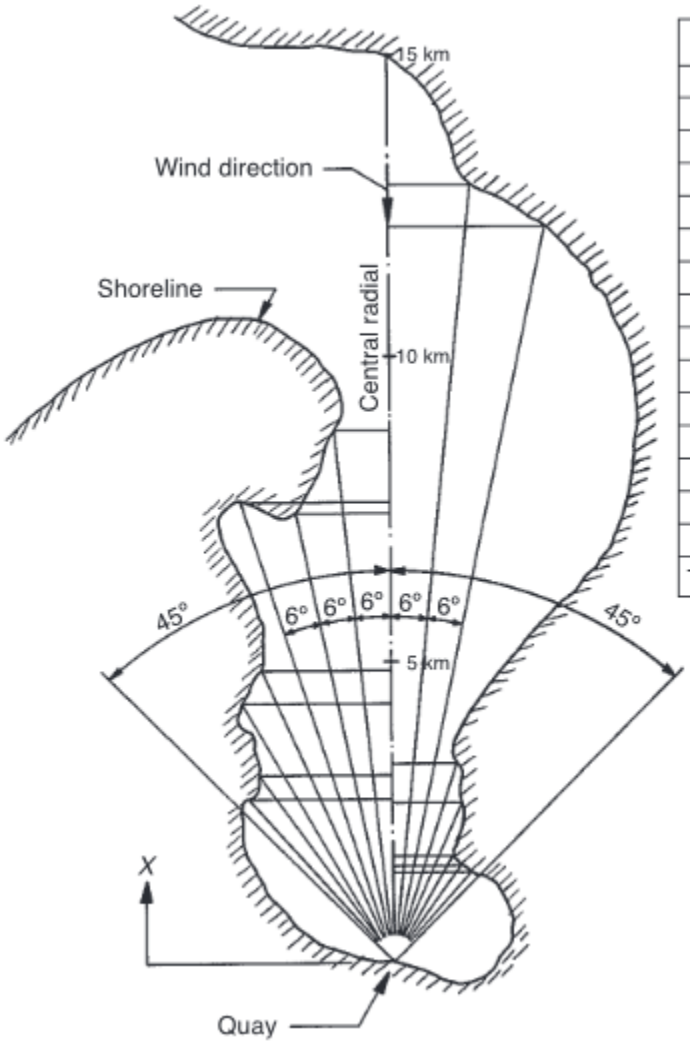

α	cos α	X	X cos α
42°	.743	2.7	2.0
36°	.809	2.9	2.3
30°	.866	4.2	3.6
24°	.914	4.8	4.4
18°	.951	7.6	7.3
12°	.978	7.4	7.2
6°	.995	9.8	9.8
0°	1.000	15.0	15.0
6°	.995	12.7	12.6
12°	.978	12.0	11.7
18°	.951	3.3	3.2
24°	.914	2.6	2.4
30°	.866	1.7	1.5
36°	.809	1.5	1.3
42°	.743	1.5	1.1
Total	13.512		85.4

$$F_{\text{eff}} = \frac{\Sigma X \cos \alpha}{\Sigma \cos \alpha}$$

$$\frac{85.4}{13.512} = 6.3 \text{ km}$$

Figure 2.1: Calculation of effective fetch for an irregular shoreline. Here, X is the fetch length

It is recommended that the calculated values be checked against wave maps or against others with knowledge of the area. This should be done because these general methods may not necessarily be completely accurate for all coastal waters, as such waters may have vast variation based on location.

If the calculated significant wave height and peak period are to be used in a JONSWAP wave spectrum, the following peakedness factor γ is recommended [5]:

$$\gamma = 44\left(\frac{H_s}{F}\right)^{2/7} \tag{2.44}$$

This is a smaller peakedness factor than the standard one. This modification is meant to take into account the fact that one is considering wind waves generated in coastal waters, where the expected peak shape of the wave spectrum will be smaller [5].

2.1.8 Design wave method

The design wave method is a method for estimating the largest forces acting on a structure subjected to waves [5]. It involves defining a regular wave, commonly a Stokes 5^{th} order wave, and stepping it through the studied structure. In order to account for the lack of dynamic effects the following modification is made:

$$H_{max} = 1.9 \times H_s \tag{2.45}$$

where H_s is the significant wave height and H_{max} is supposed to be the the wave height of the largest wave. A problem which arises is that the largest forces are not necessarily generated by the wave with the largest wave height. Additionally, the method is not suited for cases where there are important dynamic effects occurring.

2.2 Mooring

2.2.1 General

A spread mooring system is composed of a floating body, that has its motions inhibited by a set of anchor lines that are attached to the body and the sea surface [1]. The anchor lines are pretensioned, and are either chains or ropes. The tension in the lines is generated by the anchor lines' weight and by the elastic properties of the lines. The latter means that the tension will increase if the span of a anchor line increases, which creates the force that impedes the motion of the body. It is also important that the anchors retain their positions in the mooring system in order to maintain the desired position of the floating body. A shift in anchor position could also create slack in the anchor lines, which could give snapping forces in the system. These forces can be greater than the anticipated loading on the anchor lines, and may cause lines to fail.

Mooring lines may be model with the catenary equations. In the following these equations will be presented.

2.2.2 Catenary equations

A catenary is defined as the curve an idealized hanging line follows when it hags subjected only to its own weight between two points. In the case of anchor lines the two points are: the connection point of the line to the floating body and the sea surface. An example of a catenary anchor line may be seen in the figure 2.2 taken from Faltisen's *Sea Loads on Ships and Offshore Structures* [1].

Consider the line shown in figure 2.2. In this model dynamic effect and bending stiffness is neglected. The hydrodynamic forces from the environment acting on the anchor line may be described by two forces F and D, where F is a force acting tangential to the line and D is a force acting normal to the line. Additionally, the line is subjected to its own weight. One may define the following: w is submerged weight per unit length of the line in water, T is the line tension, A is the cross-sectional area of the line and E is the elastic modulus. Using this, the expressions describing the relation between the forces acting on a given part of the line may be written as:

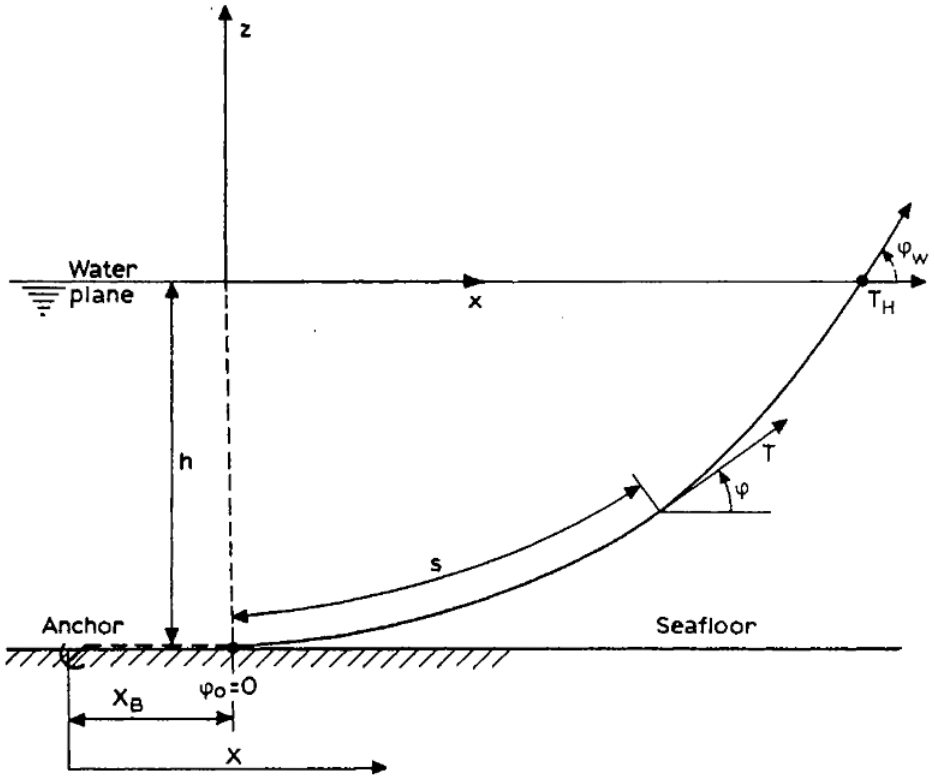

Figure 2.2: Example of an anchor line with symbols [1].

$$dT - \rho g A\, dz = [w\, sin\phi - F(1 + T/(AE))]ds \tag{2.46}$$

and:

$$T\, d\phi - \rho g A z\, d\phi = [w\, cos\phi + D(1 + T/(AE))]ds \tag{2.47}$$

where s, z and ϕ are defined as seen in figure 2.2. These expression are typically unsolvable, therefore it is necessary to neglect the current forces F and D. The elasticity of the line is also neglected. T' is given by:

$$T' = T\rho g z A \tag{2.48}$$

Using this, and the assumptions made previously one obtains:

$$dT' = w\, sin\phi\, ds \tag{2.49}$$

and:

$$T' d\phi = w \cos\phi \, ds \tag{2.50}$$

Integrating equation (2.50) gives:

$$s - s_0 = \frac{1}{w} \int_{\phi_0}^{\phi} \frac{T'_0}{\cos\theta} \frac{\cos\phi_0}{\cos\theta} d\theta = \frac{T'_0 \cos\phi_0}{w} [\tan\phi - \tan\phi_0] \tag{2.51}$$

where:

$$T' \cos\phi = T'_0 \cos\phi_0 \tag{2.52}$$

The relative x and z positions of the line may now be found because $dx = \cos\phi \, ds$ and $dz = \sin\phi \, ds$. The result is seen below:

$$x - x_0 = \frac{T'_0 \cos\phi_0}{w} \left(\log\left(\frac{1}{\cos\phi} + \tan\phi \right) - \log\left(\frac{1}{\cos\phi_0} + \tan\phi_0 \right) \right) \tag{2.53}$$

$$z - z_0 = \frac{T'_0 \cos\phi_0}{w} \left[\frac{1}{\cos\phi} - \frac{1}{\cos\phi_0} \right] \tag{2.54}$$

Horizontal tension

The horizontal tension T_H at the water plane is defined as:

$$T_H = T \cos\phi_w = T'_0 \tag{2.55}$$

Additionally, T_H may be expressed as:

$$\frac{xw}{T_H} = \log\left(\frac{1 + \sin\phi}{\cos\phi} \right) \tag{2.56}$$

Now, let $x_0 = 0$ and $z_0 = -h$. Using these assumptions and equations (2.51), (2.53) and (2.54), s and z may be expressed as a function of the horizontal tension, as seen here:

$$s = \frac{T_H}{w} \sinh\left(\frac{w}{T_H} x \right) \tag{2.57}$$

and:

$$z + h = \frac{T_H}{w}\left[cosh\left(\frac{w}{T_H} - 1\right)\right] \tag{2.58}$$

Vertical tension

The vertical line tension is found simply by this manner:

$$dT'_z = dT'\,sin\phi + T'\,cos\,phi\,d\phi = w^2\,sin^2\phi\,ds + w^2\,cos^2\phi\,ds \tag{2.59}$$

$$T'_z = ws \tag{2.60}$$

Total tension

The total tension in the anchor line may be written as:

$$T - \rho g z A = T_H + w(z + h) \tag{2.61}$$

$$T = T_H + wh + (w + \rho g A)z \tag{2.62}$$

From this one can note that the maximum tension in the line is given for $z = 0$.

$$T_{max} = T_H + wh \tag{2.63}$$

Horizontal tension plot

It is common to plot the horizontal tension as a function of the horizontal distance X between the anchor and the connection point of the line. This relation may be established by firstly defining X.

$$X = l - l_s + x \tag{2.64}$$

where:

l is the length of the anchor line.

l_s is the length of the anchor line which does not touch the sea surface.

x is the horizontal distance between the point where the line touches the sea surface and the

connection point of the line.

a is defined by:

$$a = \frac{T_H}{w} \tag{2.65}$$

Now, l_s is given by:

$$l_s = h\sqrt{1+2\frac{a}{h}} \tag{2.66}$$

and x is obtained from:

$$h = a\left[cosh\left(\frac{x}{a}\right)-1\right] \tag{2.67}$$

where h is the distance from the connection point to the sea surface. This yields:

$$x = a\,cosh^{-1}\left(1+\frac{h}{a}\right) \tag{2.68}$$

The final expression for the horizontal distance X then becomes:

$$X = l - h\sqrt{1+2\frac{a}{h}} + a\,cosh^{-1}\left(1+\frac{h}{a}\right) \tag{2.69}$$

Using this one can now plot the distance X together with the horizontal tension.

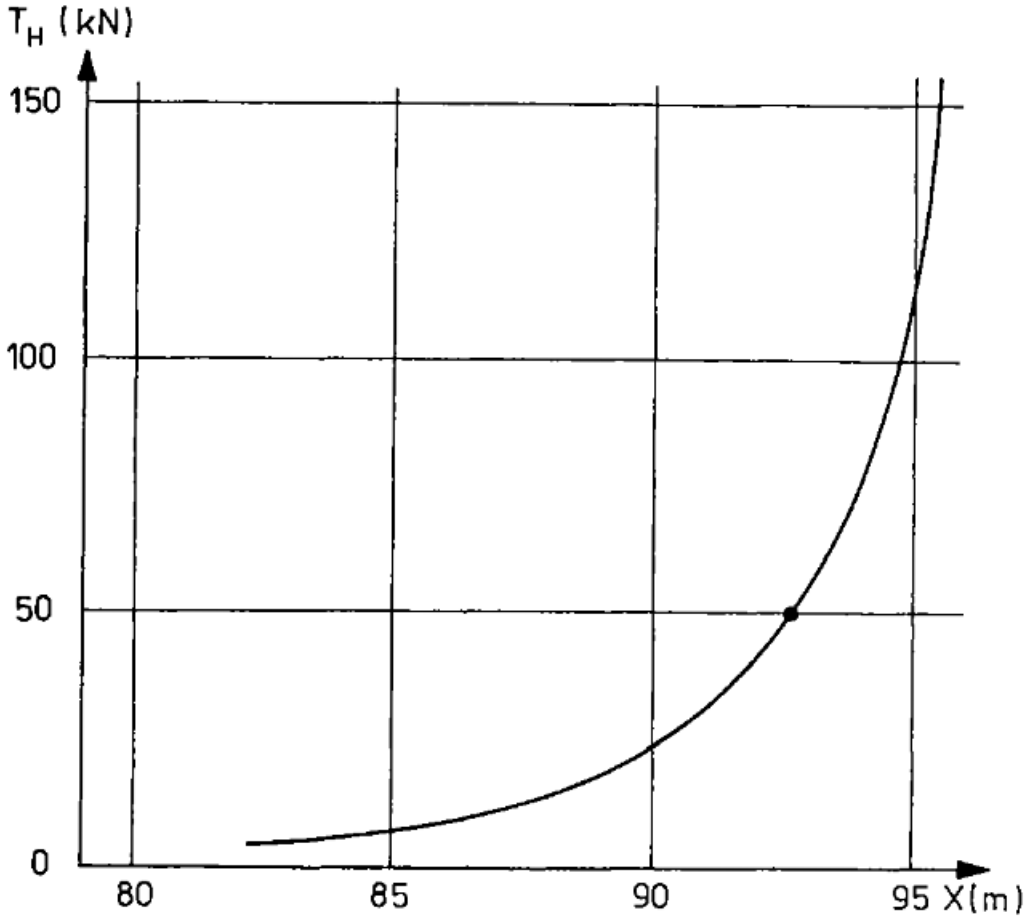

Figure 2.3: Example of a plot of the horizontal force in an anchor line as a function of the horizontal distance X [1].

2.2.3 Elastic anchor line equations

In extreme conditions the effect of elasticity can not be neglected. It is possible to modify the catenary equations for this purpose [1]. The following expressions are taken from the last part, as they are not influenced by the elasticity. Here, it is assumed that $\phi_0 = s_0 = 0$.

$$T' = \frac{T'_0}{cos\,\phi} \tag{2.70}$$

$$s = \frac{T'_0}{w} tan\,\phi \tag{2.71}$$

In order to determine the expressions for the x- and z-coordinates it is necessary to establish the relation between the stretched length dp and the unstretched length ds of a line element.

$$dp = ds\left(1 + \frac{T}{AE}\right) \tag{2.72}$$

Accordingly, it follows that:

$$\frac{dx}{ds} = cos\,\phi\left(1 + \frac{T}{AE}\right) = cos\,\phi + \frac{T'_0}{AE} \tag{2.73}$$

and:

$$\frac{dz}{ds} = sin\,\phi\left(1 + \frac{T}{AE}\right) = sin\,\phi + \frac{w}{AE}s \tag{2.74}$$

Let the unstretched anchor line length l_s be defined as:

$$l_s = \frac{T_z}{w} \tag{2.75}$$

Integrating equation (2.74) and solving for h then yields the following:

$$h = \frac{T_H}{w}\left[\frac{1}{cos\,\phi_w} - 1\right] + \frac{1}{2}\frac{w}{AE}l_s^2 \tag{2.76}$$

Solving for the horizontal tension T_H gives:

$$T_H = \frac{T_z^2 - \left(wh - \frac{1}{2}\frac{w^2}{AE}l_s^2\right)^2}{2\left(wh - \frac{1}{2}\frac{w^2}{AE}l_s^2\right)} \tag{2.77}$$

The total tension T may be expressed as:

$$T = (T_H^2 + T_z^2)^{\frac{1}{2}} \tag{2.78}$$

Finally, the distance x may be given by integrating equation (2.73).

$$x = \frac{T_H}{w} log\left(\frac{(T_H^2 + T_z^2)^{\frac{1}{2}} + T_z}{T_H}\right)\frac{T_H}{AE} l_s \tag{2.79}$$

If one wishes to use these equations to calculate x it is necessary to assume values for T_z, and then calculate l_s. Knowing l_s one may obtain T_H from equation (2.77). which then gives x from equation (2.79). If one already has a given T_H, the above calculation should be done with several assumed values for T_z. Then the results should be obtained by interpolation.

2.2.4 Snapping

Snapping occurs when a mooring line goes slack due to a lack of tension, and then the tension suddenly increases causing the line to go taut very rapidly. This creates a significant impact force in the line which can far exceed the expected extreme static and dynamic load values on a line. This effect may be seen by considering a set of simplified dynamic equations [13]. First, consider a line with zero tension. In this case the line will be subjected to a drag force and its own weight. The following expression may be written:

$$M\frac{\partial^2 q}{\partial t^2} = F_q - T_0\frac{d\phi_0}{ds} \tag{2.80}$$

where:

T_0 is the static effective tension

q is the normal displacement based on the static configuration

s is the Lagrangian coordinate

ϕ_0 is the static angle

F_q is the drag force acting on the line

Now, a dynamic tension is applied to the line giving the following:

$$M\frac{\partial^2 q}{\partial t^2} = (T_0 + T_1)\left(\frac{\partial^2 q}{\partial s^2} + \frac{d\phi_0}{ds}\right) + F_q - T_0\frac{d\phi_0}{ds} \tag{2.81}$$

where the dynamic tension T_1 is given by:

$$T_1 = \frac{EA}{L}\left[p(L) - \int_0^L q\frac{d\phi}{ds}ds + \frac{1}{2}\int_0^L \left(\frac{\partial q}{\partial s}\right)^2 ds\right] \tag{2.82}$$

where:

E is the Young's modulus

A is the line cross-sectional area

$p(L)$ is the tangential displacement imposed at the end of the cable

Snapping occurs when the line goes from the slack state to the taut state. From the expressions above, one can see that the dynamic tension is the factor which causes the dramatic increase in tension. Particularly, the velocity of the line contributes significantly to the increase in tension. One may also note that:

$$\frac{\partial q}{\partial t} = v_{ff} \tag{2.83}$$

where:

v_{ff} is the free fall velocity of the line

This implies that the snapping force is dependent on the free fall velocity of the line.

A simple way to estimate the snapping force is detailed in DNV's recommened practice H103 Modelling and analysis of marine operations [14]. It consists of expressing the snapping force as a function of the characteristic snap velocity v_{snap}.

$$F_{snap} = v_{snap}\sqrt{K \cdot (M + A_{33})}[N] \tag{2.84}$$

where:

K is the stiffness of the system

M is the mass of the system

A_{33} is the added mass in heave of the system

and v_{snap} is defined by:

$$v_{snap} = v_{ff} + C \cdot v_r [m/s] \tag{2.85}$$

where:

v_r is the vertical relative velocity between object andwater particles

C is a correction factor

This model is similar to the simplified model presented earlier in that depends on the free fall velocity.

2.3 Dynamic equation of motion

2.3.1 General

The dynamic equation of motion may be expressed as follows:

$$M\ddot{x} + C\dot{x} + D_1\dot{x} + D_2 f(\dot{x}) + K(x)x = q(t, x, \dot{x}) \tag{2.86}$$

$$M = m + A(\omega)$$

where:

M is the frequency-dependent mass matrix

m is the body mass matrix

A is the frequency dependent added-mass

C is the frequency dependent potential damping matrix

D_1 is the linear damping matrix

D_2 is the quadric damping matrix

f is the vector function where each element is given by $f_i = \dot{x}_i |x|$

K is the hydrostatic stiffness matrix

x is the position vector

q is the excitation force

The excitation force is composed by several different components as seen below:

$$q(t,x,\dot{x}) = q_{WI} + q^1_{WA} + q^2_{WA} + q_{CU} + q_{ext} \tag{2.87}$$

where:

q_{WI} is the wind drag force

q^1_{WA} is the first order wave excitation force

q^2_{WA} is the second order wave excitation force

q_{CU} is the current drag force

q_{ext} are any additional forces like specified forces, coupling forces or station-keeping forces

2.3.2 Mass

General

In the dynamic equation of motion the mass term describes the inertial forces acting on the system. This term is typically a mass matrix, which distributes the mass of the studied body for all considered degrees of freedom. The rotational degrees of freedom are expressed as mass moments of inertia in the matrix. Included in this matrix are also forces created by the interaction between the water and the body. These forces are modeled by adding additional mass to the mass matrix. This mass is called hydrodynamic mass or added mass. This is done because the forces in question are proportional to the acceleration of the body [15]. Added mass may be determined by potential theory, or one may use already calculated values for certain cross-sections.

Added mass:

Strip-theory can be used to calculate forces created by added mass. This method involves separating the studied body into several smaller "strips" along the main axis. For each strip the added mass is calculated with the help of tabular values and then it is multiplied with the length of the strip. Finally, all the strips are added together giving the total added mass. An other alternative involves applying the Morison's equation on the strip:

$$F = \rho C_m V a + \frac{1}{2}\rho C_d A v|v| \tag{2.88}$$

where ρ is the density of the water, V is the volume of the body, C_m is the added mass coefficient and a is the acceleration of the system.

It is clear that the first term of the Morison equation calculates the inertial forces. Here the added mass coefficient will typically be between 1 or 2, and may be found in literature. When the force on all strips has been calculated they are added together giving the total inertial force acting on the studied body. This is the method used in SIMO when slender elements are used to calculate the forces acting on a body.

In shallow waters the added mass coefficient may be influenced by wall interaction effects. The effects may be explained by interaction between the boundary layers of the sea surface and the body [16]. The added mass coefficient may in this case be found in figure 2.4.

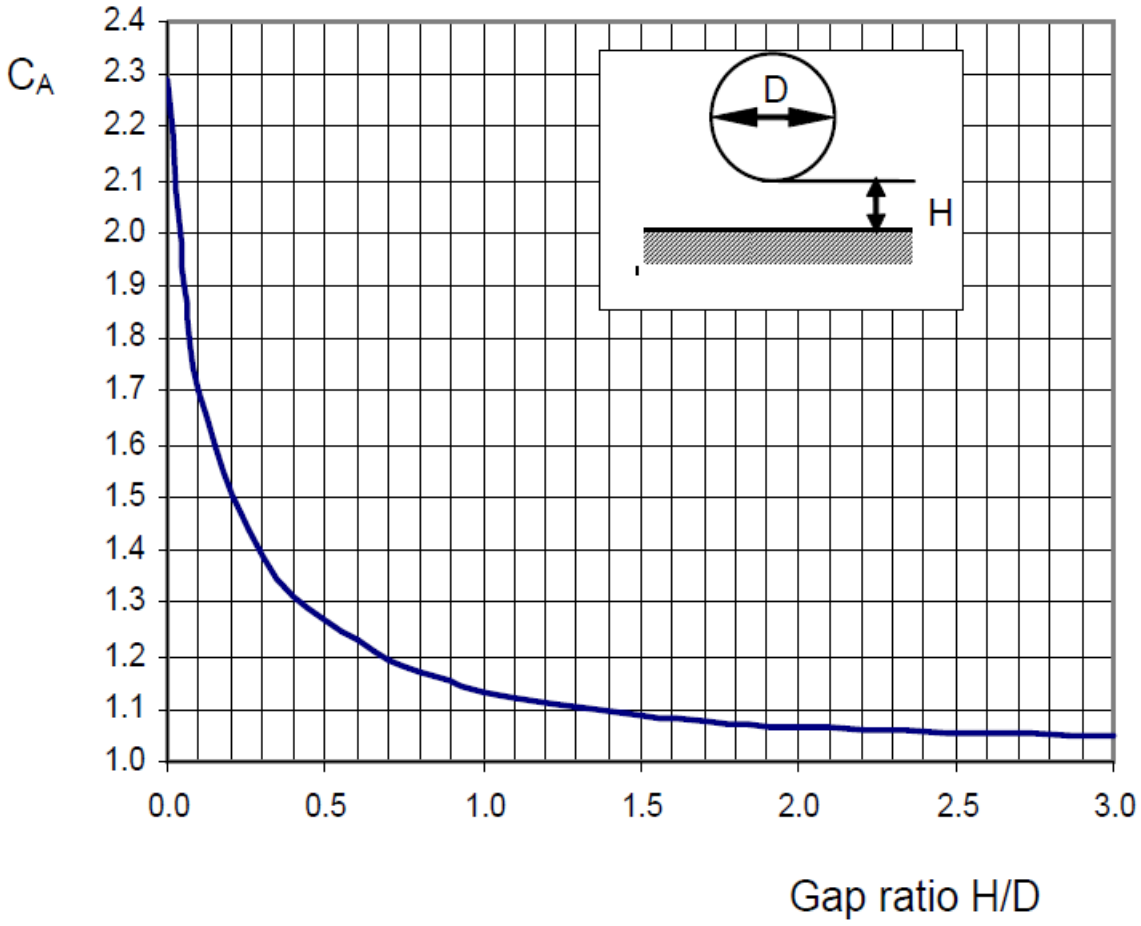

Figure 2.4: Added mass coefficient C_A of a circular cylinder in the vicinity of a fixed boundary.

Mass moment of inertia

The mass moment of inertia determines how difficult it is to rotate a body about an axis. In this case, the mass moment of inertia about the origin of a barge is of main interest. These moments show, in this case, how susceptible a barge is to roll, pitch and yaw motions. The mentioned motions correspond to respectively the mass moment of inertia about the x-axis, the y-axis and the z-axis. Generally, the mass moment of inertia is defined as:

$$I = mR^2 \tag{2.89}$$

where I is the mass moment of inertia, m is the mass of the body and R is the distance between the axis and the rotation mass. For a rectangular plane this becomes:

$$I = \frac{1}{12} m(a^2 + b^2) \tag{2.90}$$

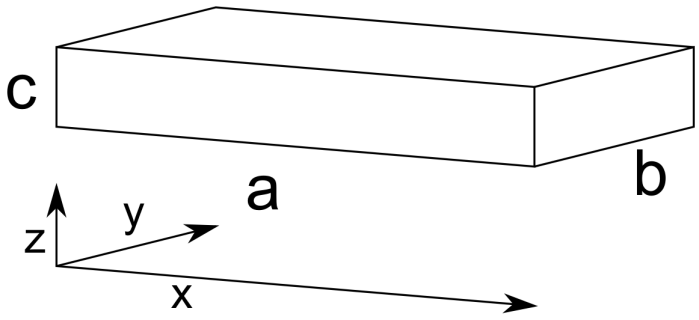

Figure 2.5: Barge

By considering figure 2.5, the specific mass moment of inertia equations are given as:

$$I_{xx} = \frac{1}{12} m(b^2 + c^2) \tag{2.91}$$

$$I_{yy} = \frac{1}{12} m(a^2 + c^2) \tag{2.92}$$

$$I_{zz} = \frac{1}{12} m(a^2 + b^2) \tag{2.93}$$

As a barge is symmetrical, the coupled mass moments of inertia I_{yx}, I_{zx} and I_{zy} will be zero.

2.3.3 Damping

General

Damping is created by processes which dissipate the energy stored in the oscillations of a dynamic system. The importance of the accuracy of the damping varies with the system in question. In particular, damping becomes very relevant for the total response when the system is close to resonance. It is very hard to calculate the exact damping of a system, due to all the different contributors. In practice, it is necessary to rely on approximations based on both theoretical knowledge and empirical knowledge.

A simple way to model the damping C of a system, is to assume that it may be expressed as a percentage of the critical damping [17]. In this case the percentage x is chosen based on experience. The model itself, assumes that one is considering a mass M suspended by a spring K, this is then yields the following expression for the eigenfrequncy of the system:

$$\omega_0 = \sqrt{\frac{K}{M}} \tag{2.94}$$

From this one gets:

$$C_{crit} = 2M\omega_0 = 2\sqrt{MK} \tag{2.95}$$

$$C = x \cdot C_{crit} \tag{2.96}$$

When using this model, one is also recommended to preform a sensitivity test by varying the chosen percentage.

For a moored floating body there are several different processes which contributes to the damping of the system [15]. They may be divided into two different categories: structural damping and hydrodynamic damping. In addition, one must consider any damping effects created by drag on the mooring lines. This type of damping will be dependent on water particle velocity

and the mooring lines diameter and drag coefficient.

Structural damping

Structural damping is caused by the material composition of the studied system, and by the couplings between elements in the system. The damping is mainly derived from the internal frictions and displacements in the material, when the material is elastic. The magnitude of this damping may be expressed as a percent of the critical damping. For steel one can expect the percentage to be between 0.5 % and 0.8 %, whereas for concrete the ratio may approach 1.2 % of critical damping. Note also that this kind of damping may vary with temperature, load size, load frequency and load amplitude, due to its dependency on the internal nature of the body's material.

Hydrodynamic damping

Hydrodynamic damping can be described by three different contributions: viscous damping, potential damping and skin friction due to shear forces [17].

1. Viscous damping is caused by vortices created by the body as it moves in water. This damping force may be said to vary proportionally with the squared oscillation speed of the system. This may be calculated with the drag term in Morison's equation.

2. Potential damping is a result of the waves created by the oscillation of the body. This process transfers the motion energy of the body into wave energy.

3. Skin friction due to shear forces between the body and the water. This damping source is negligible for large structures, as the former sources are a magnitude larger.

Hydrodynamic damping varies with the geometry of the body in question, and with the frequency of the oscillation in the system. If the cross section of the body is small compared to the wave length, the damping will be dominated by the drag damping, whereas if the cross section is large compared to the wave length the potential damping will dominate. In more specific terms, this may be defined as a cylinder with the diameter D. It is considered large when:

$$\frac{\lambda}{D} > 5 \tag{2.97}$$

Additionally, the damping is largest for a body which floats in the surface. Figure 2.6 shows different damping coefficients for a barge as a function of wave frequency [15].

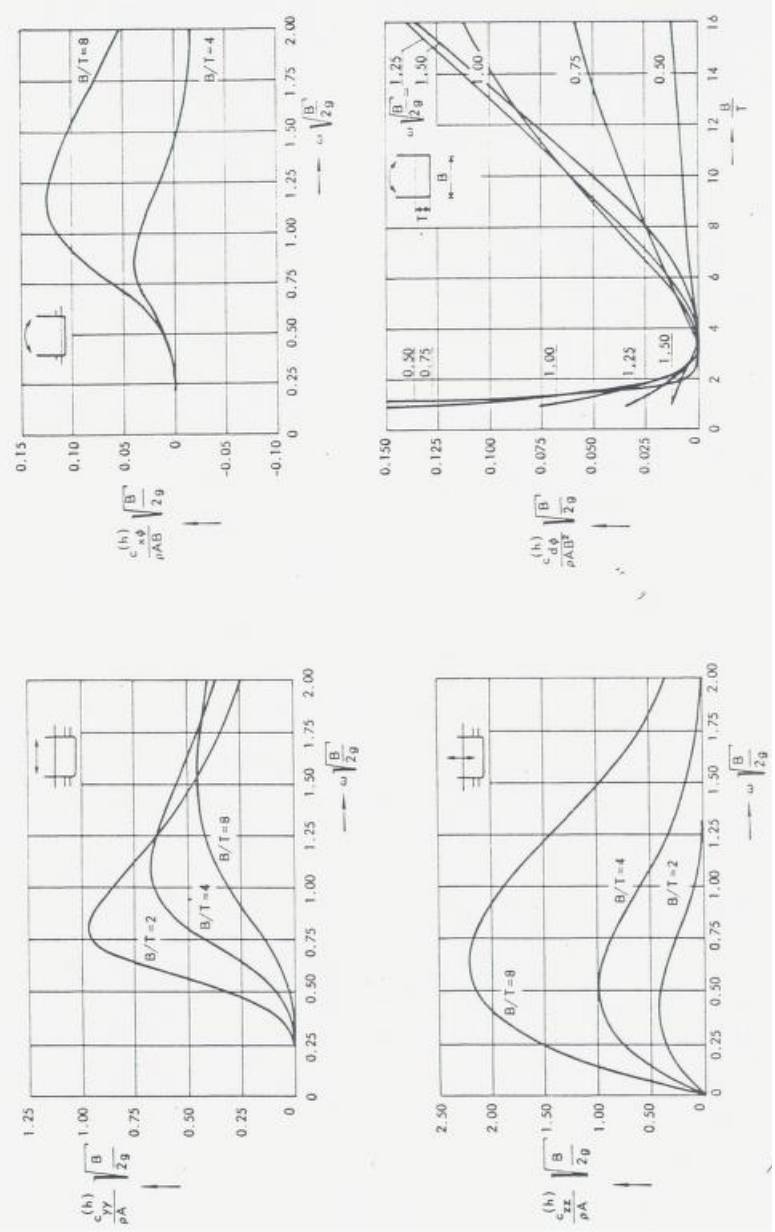

Figure 2.6: Hydrodynamic damping for a rectangular floating cylinder. A = wet cross section area, B = width, T = draft, ρ = density of water.

2.3.4 Hydrostatic stiffness

If one considers a freely floating body, the hydrostatic stiffness will translate into restoring forces acting on this body [1]. These force and moment components are defined as:

$$F_k = -C_{kj}\eta_j \tag{2.98}$$

Here C_{kj} represents the restoring coefficients. A barge is symmetrical in the x-z plane and y-z plane, in this case there are no coupling effects and the only non zero coefficients are the following:

$$C_{33} = \rho g A_{WP} \tag{2.99}$$

where A_{WP} is the water plane area,

$$C_{44} = \rho g V(z_B - z_G) + \rho g \int\int_{A_{WP}} y^2 ds = \rho g V \overline{GM}_T \tag{2.100}$$

$$C_{55} = \rho g V(z_B - z_G) + \rho g \int\int_{A_{WP}} x^2 ds = \rho g V \overline{GM}_L \tag{2.101}$$

where V is the displaced volume of water, z_G is the center of gravity and z_B is the center of buoyancy. $\overline{GM}_T$ is the transverse meta-centric height and $\overline{GM}_L$ is the longitudinal meta-centric height.

Moored floating body

When considering a moored floating barge, one must take into account the restoring contributions from the mooring system [1]. Assuming relatively small horizontal motions one may write:

$$T_H = (T_H)_M + C_{11}\eta_1 \tag{2.102}$$

$(T_H)_M$ is the average horizontal force in a mooring line and η_1 is the motion in the horizontal direction. The restoring coefficient in surge is defined by:

$$C_{11} = \frac{dT_H}{dX} = \omega \left[\frac{-2}{\left(1 + 2\frac{(T_H)_M}{h\omega}\right)} + cosh^{-1}\left(1 + \frac{h\omega}{(T_H)_M}\right) \right]^{-1} \tag{2.103}$$

where h is the height from the sea surface to the mooring attachment point. C_{11} may be found either through solving the analytical expression above, or through the consideration of a plot of the horizontal force T_H as it varies with the length X between the mooring attachment point projected down on the sea surface and the point where the mooring line is anchored. An example of this plot may be seen in figure 2.3. The above expression shows the spring effect caused by a mooring line on a moored body. A normal mooring system will have several mooring line, and one will therefore have several spring effects that must be taken into consideration. The effects may be grouped into surge and sway forces and yaw moment. They may be expressed as:

$$\begin{aligned} F_1^M &= \sum_{i=1}^{n} T_{Hi} cos(\psi_i) \\ F_2^M &= \sum_{i=1}^{n} T_{Hi} sin(\psi_i) \\ F_6^M &= \sum_{i=1}^{n} T_{Hi}[x_i sin(\psi i) - y_i cos(\psi_i)] \end{aligned} \tag{2.104}$$

where T_{Hi} is the horizontal force from mooring line i. x_i and y_i are the coordinates of the attachment point of the mooring line i. Finally, ψ_i is the angle between the mooring line i and the x-axis. The above mooring forces and moments must be balanced by the excitation forces, this allows one to calculate the restoring coefficients by determining the equilibrium position. This problem can be quite complex, as such it is often solved by iteration.

The linear restoring effects may be found in a simpler manner, by utilizing the relation from equation (2.103), which gives:

$$\begin{aligned} C_{11} &= \sum_{i=1}^{n} k_i cos^2 \psi_i \\ C_{22} &= \sum_{i=1}^{n} k_i sin^2 \psi_i \end{aligned} \tag{2.105}$$

$$C_{66} = \sum_{i=1}^{n} k_i (x_i sin\psi_i - y_i cos\psi_i)^2$$

$$C_{62} = C_{26} = \sum_{i=1}^{n} k_i (x_i sin\psi_i - y_i cos\psi_i) sin\psi_i$$

Where, k_i is the restoring coefficient for mooring line i determined by equation (2.103). The coupling coefficients C_{16}, C_{61}, C_{12} and C_{21} are zero if one assumes a symmetric mooring system about the x-z plane.

2.4 Excitation forces

2.4.1 General

The excitation forces which may act on a floating body include first and second order wave forces, wind forces and current forces. Additionally, station-keeping forces, specified forces and coupling forces are considered as excitation forces. This may be expressed as seen earlier in equation (2.87).

2.4.2 Wave excitation forces

Wave excitation forces can be separated into three. First order forces varying with wave frequency, second order mean, rapidly or slowly varying wave drift forces, and higher-order ringing forces. This may be expressed in this manner [12]:

$$q(t) = q^{(1)}(t) + q^{(2)}(t) + q^{(R)}(t)$$

$$q(t) = \frac{1}{2\pi} \int_{-\infty}^{\infty} h^{(1)}(\tau_1)\zeta(t-\tau_1)d\tau_1 + \frac{1}{4\pi^2} \int_{-\infty}^{\infty}\int_{-\infty}^{\infty} h^{(2)}(\tau_1,\tau_2)\zeta(t-\tau_2)\zeta(t-\tau_1)d\tau_1 d\tau_2 + q^{(R)}(t) \tag{2.106}$$

where:

$q^{(1)}(t)$ is the time-dependent first-order wave force.

$q^{(2)}(t)$ is the time-dependent second-order wave force.

$q^{(R)}(t)$ is the time-dependent third-order ringing force.

$h^{(1)}$ is the linear impulse response function.

$h^{(2)}$ is the second-order impulse response function.

$\zeta(t)$ is a wave elevation function.

$h^{(1)}$ and $h^{(2)}$ may be Fourier transformed as follows:

$$h^{(1)}(\tau) = \frac{1}{2\pi}\int_{-\infty}^{\infty} H^{(1)}(\omega)e^{i\omega\tau}d\omega \tag{2.107}$$

$$H^{(1)}(\omega) = \int_{-\infty}^{\infty} h^{(1)}(\tau)e^{-i\omega\tau}d\tau \tag{2.108}$$

$$h^{(2)}(\tau_1,\tau_2) = \int_{-\infty}^{\infty}\int_{-\infty}^{\infty} H^{(2)}(\omega_1,\omega_2)e^{i(\omega_1\tau_1+\omega_2\tau_2)}d\omega_1 d\omega_2 \tag{2.109}$$

$$H^{(2)}(\omega_1,\omega_2) = \frac{1}{4\pi^2}\int_{-\infty}^{\infty}\int_{-\infty}^{\infty} h^{(2)}(\tau_1,\tau_2)e^{-i(\omega_1\tau_1+\omega_2\tau_2)}d\tau_1 d\tau_2 \tag{2.110}$$

where:

$H^{(1)}$ is the first-order transfer function.

$H^{(2)}$ is the second-order transfer function.

The force contribution from the ringing forces will not be covered in this text.

First order wave excitation force

The first order wave forces are calculated as a function of the wave frequency ω. The forces are a product of the wave elevation and the first order transfer function.

The first order wave excitation force is now expressed as follows:

$$q^{(1)}_{WA}(\omega) = H^{(1)}(\omega)\zeta(\omega) \tag{2.111}$$

where $H^{(1)}$ is the complex first order transfer function.

Second order wave excitation force

The second order wave excitation force is caused by the second order wave forces. When the first order wave forces are calculated with potential theory it is assumed that the free surface condition and the body boundary condition are solved for the mean position of the submerged body surface and the mean position of the free surface. For the second order wave forces the instantaneous position of the body is taken into account. However, the second order wave forces are not a completely accurate representation of the total wave forces, as the terms in the velocity potential which are linear or quadratic with the wave amplitude are the same as the ones used in the calculation of first order wave forces. Solving the second order forces problem yields mean forces, and forces that oscillate with difference frequency and sum frequencies in addition to the forces obtained from the linear solution [1]. The second order wave excitation force may be expressed in the following manner [12]:

$$q_2 = \int_{-\pi}^{\pi}\int_{-\pi}^{\pi}\int_{-\infty}^{\infty}\int_{-\infty}^{\infty}\sum_{i=1}^{n} Z(\omega_1,\beta_1)Z^*(\omega_2,\beta_2)H^{(2)}(\omega_1,\omega_2,\beta_1,\beta_2)d\omega_1 d\omega_2 d\beta_1 d\beta_2 \tag{2.112}$$

where:
$Z(\omega)$ is a function taking into account the instantaneous positions of the studied body
$H^{(2)}$ is the full second order transfer function

The second order wave forces must be considered for large volume structures, as the motion of the large body may create significant mean wave forces. Additionally, one must check whether or not the difference frequency force and the sum frequency forces may induce resonance effects. DNV's recommended practices c205 [2] propose the following figure to be used to determine the nature of a structure:

A structure is considered to have large volume if it falls within sector II or IV. The border between large and small volume may be expressed in this manner:

$$\frac{\pi D}{\lambda} = 0.5 \tag{2.113}$$

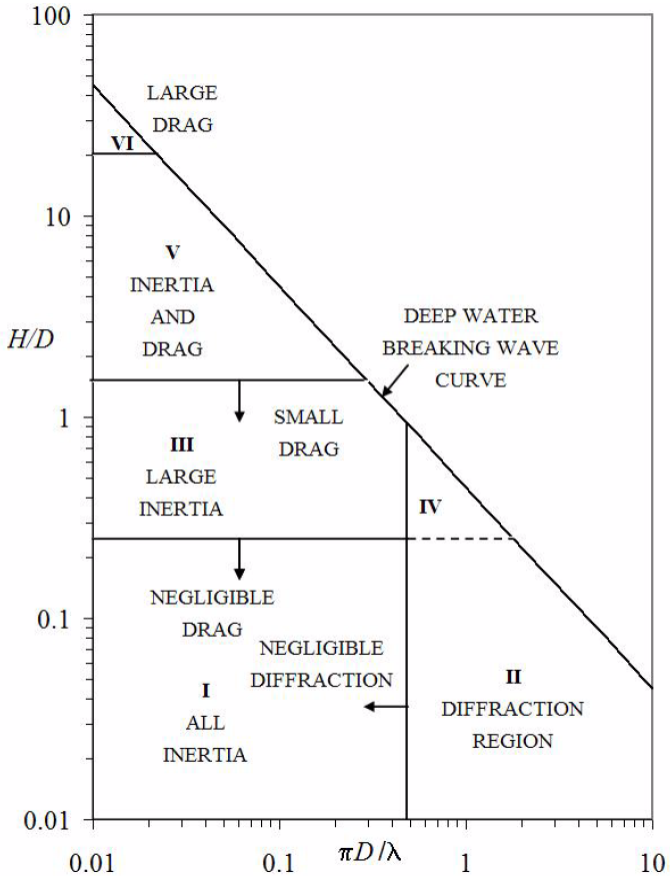

Figure 2.7: Different wave force regimes [2]. Here: D is a characteristic dimension, H is the wave height and λ is the wave length.

2.4.3 Wind forces

The wind excitation force acting on a moored floating body may be calculated based on instantaneous wind and body velocities. The simplest method is shown here:

$$q_{WI} = \frac{1}{2}\rho C_d A V^2 \tag{2.114}$$

where:

ρ is the density of the air

C_d is a drag coefficient

A is the projected area of the body subjected to the wind force

V is the wind speed

Here C_d may be found in literature depending on composition of the body.

In SIMO the following expression gives the relation between the wind speed and the wind force acting on the considered body [12]:

$$q_j = C_j(\alpha)\, v^2 \tag{2.115}$$

where:

j is the degree of freedom

C is the wind force coefficient for the instantaneous relative direction

v is the relative velocity between body and wind

α is the direction relative velocity in the local coordinate system

One may note that the two expressions are relatively similar in that they are both proportional with respect to V^2.

2.4.4 Current forces

General

The current force acting on a moored floating body may be described as a drag force, and it may be expressed similarly to the wind force [7]:

$$q_{CU} = \frac{1}{2}\rho C_d A U^2 \tag{2.116}$$

where:

ρ is the density of the water

C_d is a drag coefficient

A is the projected area of the body subjected to the current drag force

U is the current speed

In SIMO the current force is handled differently based on what is being studied. The current forces for all bodies are calculated using the current velocity at the surface, whereas the varying

current velocities may be used for mooring lines. The expression used for the current force is the following [12]:

$$q_{CU} = C_1(\alpha)\,|u(t)| + C_2(\alpha)\,|u(t)|^2 \tag{2.117}$$

where:

C_1 is the linear current force coefficient

C_2 is the quadratic current force coefficient

u is the relative velocity between the body and the current velocity

α is the angle between the direction of the body and the current velocity

In this expression the linear term is seldom used, because as seen above the current drag force may be relatively well described by the quadratic term alone.

Drag coefficients

The current drag coefficient depends mainly on the Reynolds number and on the material roughness of the body. The surface roughness k of concrete can be taken as 3×10^{-3} meters. Assuming a high Reynolds number ($R_e > 10^6$) and a large Keulegan Carpenter number, the drag coefficient may be found as [2]:

$$C_d = \begin{cases} 0.65 & ;\frac{k}{D} < 10^{-4}(\text{smooth}) \\ \left(29 + 4 \cdot log_{10}\left(\frac{k}{D}\right)\right)/20 & ;10^{-4} < \frac{k}{D} < 10^{-2} \\ 1.05 & \frac{k}{D} > 10^{-2}(\text{rough}) \end{cases} \tag{2.118}$$

where:

k is the surface roughness

D is the diameter of the body

In shallow waters, one might expect some interaction between the sea bottom and the body. These interactions depend on the relative size of the body's diameter D and the distance between the body and the sea surface H. The larger the diameter is in comparison to the distance,

the larger the effect becomes on the current drag force. This is due to the fact that the water will be forced to flow in between the body and the sea surface, where there will be interaction between the respective boundary layers [16]. The effect may be summed up by the following figure:

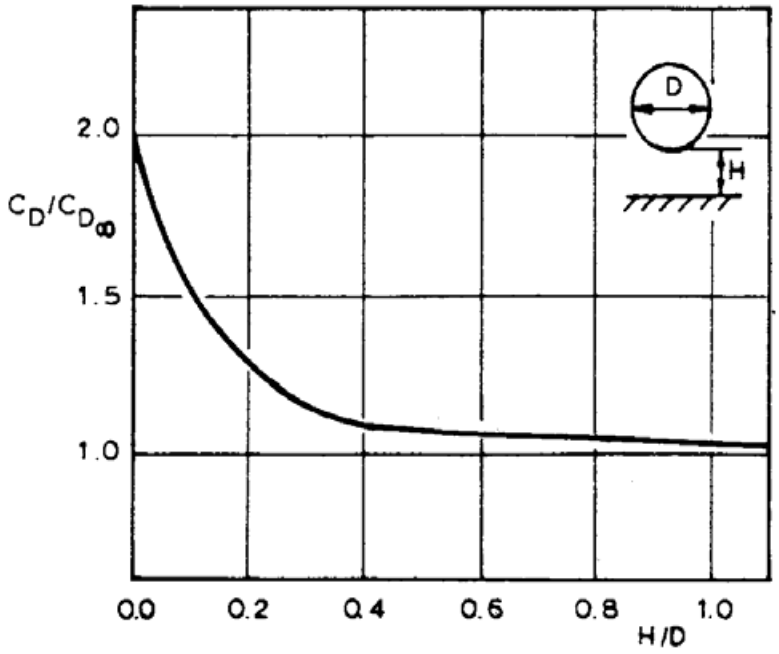

Figure 2.8: Influence of a fixed boundary on the drag coefficient of a circular cylinder in oscillatory supercritical flow [2]. Here, $C_{D\infty}$ is the drag coefficient for infinite depth.

As one can note, this effect is not noticeable before we approach an H equal to 20 % or less of the diameter of the body.

Drag on chains

Chains have a larger surface area than a line, and it is therefore necessary to use a larger drag coefficient in order to take into account the increase in drag force. DNV recommends the following drag coefficients for a normal chain [18]:

$$C_{d(Transverse)} = 2.4 \tag{2.119}$$

$$C_{d(Longitudinal)} = 1.15 \tag{2.120}$$

2.4.5 Station-keeping forces

The mooring lines in SIMO are modeled by catenary expressions. These expressions include a quasi static analysis and a simplified dynamic model. The lines are modeled by any number of line segments. A shooting method is used to calculate the line characteristics. This means that the boundary conditions of one end of the line is calculated by iterations based on the boundary conditions of the other end. The model also takes into account the velocity and the acceleration of the line, and by doing so it also takes into account the elasticity of the line. The following quasi-static expression is established [12]:

$$m\ddot{u} + c\dot{u} + (k_G + k_E)u = k_E X_t \tag{2.121}$$

where:

m is the mass of the line

c is the damping of the line

k_G is the geometrical stiffness

k_E is the elastic stiffness

x_T is the tangential motion excitation of the line end

u is the displacement of the line

Here, the quasi-static shape is assumed to be an approximation to the true shape of the velocity and the acceleration of all points of the mooring line. The mass m and the damping c are calculated using quasi-static shape of the line. The damping coefficient also takes into account a linearisation of the quadratic drag force. This means that the drag contributes to the total damping of the mooring line. Additionally, the quasi-static shape allows the calculation of u, this then gives the dynamic tension T_D.

$$T_D = K_E(x_t - u) \tag{2.122}$$

This allows SIMO to calculate dynamic effects such as snapping.

The actual iterative process used to solve the mooring line equations is presented in the

following. First the relation between x and u is the axial stretching of the line, and is given by:

$$c_i \dot{u}_i |\dot{u}_i| + k_i u_i = k_E x_i \tag{2.123}$$

After the time step Δt the expression becomes:

$$c_{i+1} \dot{u_{i+1}} |\dot{u_{i+1}}| + k_{i+1} u_{i+1} = k_E x_{i+1} \tag{2.124}$$

Now the total force for a time step is given by:

$$\Delta F_i^D + \Delta F_i^S = \Delta Q_i \tag{2.125}$$

where:

$$\Delta F_i^D = F_{i+1}^D - F_i^D = \frac{1}{2}(c_{i+1} + c_i)(\dot{u_{i+1}} |\dot{u_{i+1}}| - \dot{u}_i |\dot{u}_i|) \tag{2.126}$$

$$\Delta F_i^S = F_{i+1}^s - F_i^s = \frac{1}{2}(k_{i+1} + k_i)(u_{i+1} - u_i) \tag{2.127}$$

$$\Delta Q_i = Q_{i+1} - Q_i = k_E(x_{i+1} - x_i) \tag{2.128}$$

The above expression can now be used to calculate the line forces by iteration. Finally, the line forces are added to the global excitation forces and from there they are included in the global dynamic equation of motions.

2.5 Solving the dynamic equation of motion

2.5.1 General

This section will give an outline of how the dynamic equation is solved in SIMO [12]. First of all the position vector of a body is defined as:

$$x = (x, y, z, \phi, \theta, \psi)^T \tag{2.129}$$

where x, y, are the coordinates of the body origin in the global coordinate system. One may now define the dynamic model as:

$$\ddot{x} = f(x, \dot{x}, \xi) \tag{2.130}$$

where ξ is vector containing all inputs which are independent of x and $\dot{x}$. In this vector, one will also find the positions and velocities of any bodies coupled to the considered body. Additionally, the velocity $\dot{x}$ of the body origin and the acceleration $\ddot{x}$ of the body origin are defined as:

$$\dot{x} = (\dot{x}, \dot{y}, \dot{z}, \dot{\phi}, \dot{\theta}, \dot{\psi})^T \tag{2.131}$$

$$\ddot{x} = (\ddot{x}, \ddot{y}, \ddot{z}, \ddot{\phi}, \ddot{\theta}, \ddot{\psi})^T \tag{2.132}$$

A body moving in water will be subjected to linear momentum P_B due to the external forces F and angular momentum L_B due to external moments M. This is expressed as:

$$P_B = m(v + \omega \times r_c)$$

$$L_B = I\omega + mr_c \times v \tag{2.133}$$

where:
m is the body's mass
v is the velocity of the body origin
ω is the angular velocity of the body
r_c is the position of the center of gravity relative to the bodt origin
I is the body's inertia tensor with respect to the body origin.

We have:

$$\dot{P}_B = F$$

$$\dot{L}_B = M \tag{2.134}$$

This gives:

$$\dot{P}_B + \omega \times P_B = F$$

$$\dot{L}_B + \omega \times L_B + v \times P_B = M \tag{2.135}$$

The body mass matrix B is derived from the mass and coordinates of the body, and may be written as:

$$B = \begin{bmatrix} B_{11} & B_{12} \\ B_{21} & B_{22} \end{bmatrix} \tag{2.136}$$

Inserted into equation (2.133) it gives:

$$P_B = B_{11} v + B_{12} \omega$$

$$L_B = B_{21} v + B_{22} \omega \tag{2.137}$$

And from this one may derive:

$$B_{11} \dot{v} + B_{12} \dot{\omega} + \omega \times P_B = F$$

$$B_{21} \dot{v} + B_{22} \omega + \omega \times L_B + v \times P_B = M \tag{2.138}$$

Finally, the equation of motion may be written as:

$$V = \begin{bmatrix} \dot{v} \\ \dot{\omega} \end{bmatrix} + \begin{bmatrix} \omega \times P \\ \omega \times L + v \times P \end{bmatrix} = \begin{bmatrix} F_1 \\ M_1 \end{bmatrix} \tag{2.139}$$

where:

V is the virtual mass matrix, which contains the body mass and any defined added mass.

Fixing the frame of reference yields the following expression for the equation of motion:

$$\begin{bmatrix} \dot{v} \\ \dot{\omega} \end{bmatrix} = V^{-1} \begin{bmatrix} -\omega \times P + F_1 \\ -\omega \times L - v \times P + M_1 \end{bmatrix} + \begin{bmatrix} \omega \times v \\ 0 \end{bmatrix} \tag{2.140}$$

Knowing the equation of motion, one can now detail the steps taken when solving it. The initial values of x, $\dot{x}$ and ξ are assumed to be known.

1. The velocity $(\dot{x}, \dot{y}, \dot{z})^T$ is transformed to body-coordinate representation v.

2. ω is obtained from the relation:

$$\omega = \frac{\dot{\gamma}}{M^{-1}(\gamma)} \tag{2.141}$$

where:

$$\gamma = (\phi, \theta, \psi)^T \tag{2.142}$$

and:

$$M = \begin{bmatrix} 1 & sin\phi tan\theta & cos\phi tan\theta \\ 0 & cos\phi & -sin\phi \\ 0 & sin\phi sec\theta & cos\phi sec\theta \end{bmatrix} \tag{2.143}$$

3. Using x, v, ω and ξ the external force F_1 and moment M_1 are calculated using the equation of motion (2.139).

4. The former step then yields the accelerations $\dot{v}$ and $\dot{\omega}$ from equation (2.139).

5. v is transformed from the local system to the global one.

6. $\ddot{\gamma}$ is obtained from:

$$\ddot{\gamma} = \begin{bmatrix} \ddot{\phi} \\ \ddot{\theta} \\ \ddot{\psi} \end{bmatrix} = \frac{\partial f}{\partial \gamma} M\omega + M\dot{\omega} \tag{2.144}$$

where:

$$\frac{\partial f}{\partial \gamma} = \begin{bmatrix} (qcos\phi - rsin\phi)tan\theta & (qsin\phi + rcos\phi)sec^2\theta & 0 \\ -qsin\phi - rcos\phi & 0 & 0 \\ (qcos\phi - rsin\phi)sec\theta & (qcos\phi + rsin\phi)tan\theta sec\theta & 0 \end{bmatrix} \tag{2.145}$$

and p, q and r are defined by:

$$\omega = (p, q, r)^T \tag{2.146}$$

such that:

$$\dot{\phi} = p + qsin\phi tan\theta + rcos\phi tan\theta$$

$$\dot{\theta} = qcos\phi - rsin\phi \tag{2.147}$$

$$\dot{\psi} = qsin\phi sec\theta + rcos\phi sec\theta$$

Finally a simple combination gives:

$$\ddot{x} = (\dot{\nu}^T, \ddot{\gamma}^T)^T \tag{2.148}$$

The next step values for x, $\dot{x}$ and ξ are now determined by numerical integration. SIMO offers different ways of preforming these calculations. In the following the Runge-Kutta-like method for numerical integration will be presented.

2.5.2 Runge-Kutta-like method

The third-order Runge-Kutta-like numerical integration method used in SIMO is the following [12]:

$$\begin{aligned}
\Delta\dot{x}_1 &= Tf(x(t_k), \dot{x}(t_k), \xi_k) \quad (1)\\
\Delta x_1 &= T\dot{x}(t_k) + \frac{1}{4}T^2 f(x(t_k), \dot{x}(t_k), \xi_k) \quad (2)\\
f'_{k+1} &= f(x(t_k) + \Delta x_1, \dot{x}(t_k) + \Delta\dot{x}_1, \xi_{k+1}) \quad (3)\\
\Delta\dot{x}_2 &= Tf'_{k+1} \quad (4)\\
\Delta x_2 &= T\left(x(t_k) + \frac{5}{12}\Delta x_1\right) + \frac{1}{3}T^2 f'_{k+1} \quad (5)\\
\dot{x}_{k+1} &= \dot{x}(t_k) + \frac{1}{2}b(\Delta\dot{x}_1 + \Delta\dot{x}_2) \quad (6)\\
x_{k+1} &= x(t_k) + \frac{1}{2}(\Delta x_1 + \Delta x_2) \quad (7)
\end{aligned} \tag{2.149}$$

where:

t_k is the the time step

T is the time step size

2.6 Statistics

2.6.1 Long term statistics

The long term variability of a random variable may most easily be described by measuring the its variation over a sufficiently long time period. This will give a data sample, which can then be studied in order to allow one to make long term predictions of the probability of occurrence of certain events. This is done by fitting a probability distribution to the data sample. In the following probability distributions will be explained and the Weibull and Gumbel probability distribution will be presented. Additionally, the procedure for predicting long term values based on a data sample will be shown.

2.6.2 Probability distributions

General

A probability distribution is a statistical function which describes all possible values that a random variable can take within a given range together with the probability that each possible value is associated with. The probability distribution of a random variable x is said to be continuous if it can be described by the following [19]:

1. The probability of an event x between two points a and b is:

$$p[a \leq x \leq b] = \int_a^b f(x)\,dx \tag{2.150}$$

2. f(x) is non-negative.

3. The integral of f(x) is one.

$$\int_{-\infty}^{\infty} f(x) = 1 \tag{2.151}$$

Integrating f(x) gives the cumulative distribution function F(x) which describes the probability that a random variable X will have a value less than or equal to x.

$$F_X(x) = \int_{-\infty}^{x} f_X(t)\,dt \tag{2.152}$$

and the cumulative distribution function is defined by:

$$F_X(x) = P(X \leq x) \tag{2.153}$$

From these equations one may derive a final important property:

$$P(X > x) = 1 - P(X \leq x) \tag{2.154}$$

In statistics the cumulative distribution functions may be fitted to observed data. This allows one to obtain relatively accurate long term statistics based on empirical observations, assuming that the distribution used is a good fit to the data. For example, one may fit a Weibull distribution to a set of wind speeds measured over ten years, in order to calculate the wind speed which a return rate of 100 years. Obviously, this is very useful in the design of structures. Similarly, a Gumbel distribution can be used to predict the peak wave heights [2].

The exact procedure involves calculating the cumulative probability of the observed data, defined by:

$$F(k) = \frac{k}{n+1} \tag{2.155}$$

where k is the number of observation at step k, and n is the total number of observations. An example may be seen in the table below:

Table 2.1: Example of how to obtain the cumulative probabilities associated with a data sample.

x [m/s]	Obsv.	k	F(k)
5	5	5	0.28
6	10	15	0,83
7	2	17	0,94

The observed cumulative probabilities may now be transformed according to the chosen probability function. The transformed probabilities are then plotted against the observed x values. If the distribution is a good fit the data points should appear approximately linear. This graphical representation is called a probability paper. From this paper, it is possible to derive the parameters of the cumulative distribution function, and with this one may calculate the x values with given return rates, such as 100 year waves [2]. Roughly, the procedure may be expressed by:

$$x = F^{-1}(p(x)) \tag{2.156}$$

where F the chosen cumulative distribution function and p(x) is the probability of the considered event, and p(x) is given by:

$$p(x) = 1 - P(X \leq x) \tag{2.157}$$

The accuracy of the calculated values depends on how well the cumulative distribution function fits the data sample, and it depends on the quality and quantity of the data. In the case, where one is lacking sufficient data one may run Monte Carlo simulations to investigate the accuracy of the distribution. The fit of the distribution function may also be studied with the help other methods, such as R^2 and χ^2 tests. In the following, two probability distribution function shall be described.

Weibull distribution

The Weibull probability distribution is a versatile function which is applied in a wide variety of different fields. It is often useful in cases where a lot of data is available over a relatively long time period. In the case of floating structures it may be employed to describe the probability of different wind speeds [2]. The function is mainly governed by two factors; a shape parameter k and a scale parameter λ. The cumulative distribution function for the Weibull distribution is given by [20]:

$$F(x) = 1 - e^{-(\frac{x}{\lambda})^k} \tag{2.158}$$

The above expression may be used to fit a Weibull distribution to a data sample as shown in

the previous part. Inversing the function yields:

$$ln(-ln(1-F(x))) = k \cdot ln\left(\frac{x}{\lambda}\right) = k \cdot ln(x) - k \cdot ln(\lambda) \tag{2.159}$$

The right hand of the equation shows that if one plots the observed data in a Weibull paper, the data will form a straight line if it is Weibull distributed. It is therefore acceptable to fit a linear trend line to the plotted data, in order to determine the Weibull parameters. Below an example of a such a Weibull probability paper is shown.

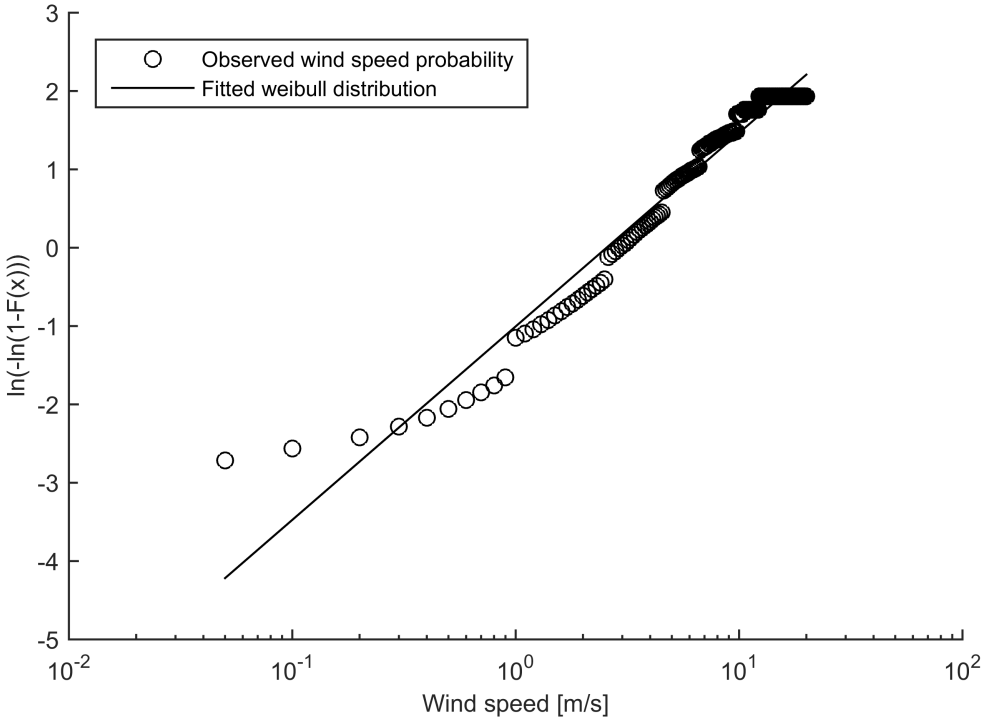

Figure 2.9: Example of a Weibull probability paper.

The shape parameter k may be determined from figure 2.9 as the slope of the trend line. The scale parameter λ is found from equation (2.159), where the final term is the equivalent of the constant term of a linear function:

$$C = k \cdot ln(\lambda)$$

$$\lambda = exp\left(-\left(\frac{C}{k}\right)\right) \tag{2.160}$$

From this it follows that C is the value the trend line takes for x = 0. It is also possible to use other methods to determine these parameters such as the maximum likelihood estimation or the method of moments, however these methods will not be discussed here.

Gumbel distribution

The Gumbel distribution is an extreme value distribution. It is tailored to model the distribution of the maxima of a number of samples. The distribution is commonly used to represent such things as the yearly maxima of the level of a river measured over ten years. In marine constructions it may represent the distribution of the maximum response values calculated with waves with different phase angles. The Gumbel distribution itself is a double exponential distribution, governed by a scale parameter β and a location parameter μ. Its cumulative distribution function takes the following form [20]:

$$F(x) = exp\left(-exp\left(-\frac{x-\alpha}{\beta}\right)\right) \tag{2.161}$$

As with the Weibull distribution, a probability paper may be created with the Gumbel distribution. It is similarly done by inversing the cumulative distribution function.

$$-ln[-ln(F(x))] = \frac{x-\alpha}{\beta} \tag{2.162}$$

When this function is plotted in a paper with a logarithmic x- axis and a linear y-axis, it should give a distribution which may be fitted to a straight line, as seen in the figure 2.10.

Using the probability paper one may determine the parameters of the Gumbel distribution. The slope of the fitted line is equal to $1/\beta$, which is the inverse of the scale parameter. One could also use the method of moments to determine the parameters.Accordingly, we have:

$$\mu = \alpha + 0.57722\beta \tag{2.163}$$

$$\sigma_{std} = 1.28255\beta \tag{2.164}$$

If one calculates the mean value μ and the standard deviation σ_{std} from the data sample the parameters can now be obtained with the use of these expressions:

$$\beta = \frac{1.23255}{\sigma_{std}} \tag{2.165}$$

$$\alpha = \mu - 0.57722\beta \tag{2.166}$$

The two aforementioned methods can be used on the same data sample in order to assess the accuracy of the fitted Gumbel distribution.

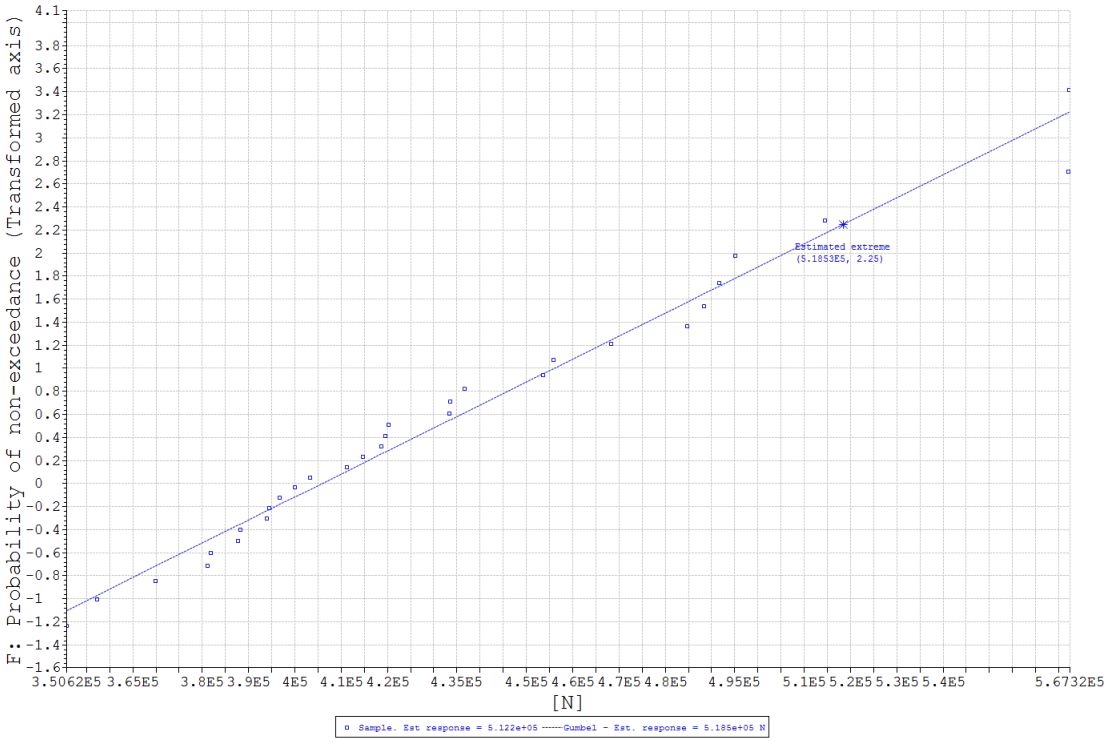

Figure 2.10: Example of a Gumbel distribution.

2.6.3 Fitting probability distributions

General

Probability distribution fitting is the fitting of a probability distribution to a set of data. This is done to allow one to predict the probability of occurrence of the magnitude of a phenomenon in an interval. The distributions are chosen based on the nature of the data sample. Assuming that one has a good data sample, the better the distribution fits to the data the better the probability predictions will be.

The nature of the data sample may be assessed based on its mean. If the data is symmetrically distributed around the mean, one can use the normal distribution. If the data skews to the right of the mean, one can use exponential distributions such as the Weibull distribution or the Gumbel distribution. It is then necessary to preform the fit. This may be done in several different ways, some examples are the method of moments, the maximum likelihood method and the regression method. The regression method is the formerly described method, which consists of transforming the axes of the cumulative distribution.

The accuracy of the predictions made with a fitted distribution function varies with the quality and quantity of the data sample. This gives some uncertainty to the fitted probability distribution. Assuming that one can not improve the quality of the data sample. If the data sample is too small, one may use Monte Carlo simulations to investigate the quality of the fit. If one has a sufficiently large data sample, one may check the quality of the fit by using certain methods, such as the R^2 test or the χ^2 test.

R^2 test

The R^2 is a number which describes the how well a given probability distribution fits a data sample. In particular it should be applied to fits done with the regression method. The test is done in the following manner [21]:

First $\bar{y}$ is the mean of the data sample defined by:

$$\bar{y} = \frac{1}{n}\sum_{i=1}^{n} y_i \tag{2.167}$$

Now the total sum of squares is given by:

$$SS_{tot} = \sum_i (y_i - \bar{y})^2 \tag{2.168}$$

And the residual sum of squares is:

$$SS_{res} = \sum_i (y_i - f_i)^2 \tag{2.169}$$

where f_i is the predicted value associated with y_i.

Finally, the expression for R^2 becomes:

$$R^2 \equiv 1 - \frac{SS_{res}}{SS_{tot}} \tag{2.170}$$

This number will vary between 0 and 1. The closer to one comes to 1 the better the fit, as SS_{res} becomes zero for a perfect fit.

Chapter 3

Modeling basis

3.1 General

The model used in this paper will be based on a floating dock system installed by Bi-Brygga AS in Sande, Vestfold. The system is composed of two main floating concrete docks, and a connecting steel dock. The concrete docks are composed of several smaller concrete elements. The larger dock is intended to serve as a wave breaker, and is therefore wider than the other concrete dock. For the same reason boats may only tie up on the inside of the larger dock. The larger dock is composed of four 17.5 meter long concrete elements, and the smaller dock is composed of one 15 meter long element and two 14 long meter elements. The system may be seen in the plane photography in figure 3.1. In the following the connecting steel dock will be neglected as it is of secondary concern.

3.1.1 Orientation

The docks are oriented south-west to north-east along the long sides of the floating docks. This means that the larger dock is positioned the furthest towards the south.

Figure 3.1: Floating dock system in Sande, Vestfold. PHOTO: NORKART AS

3.2 Dock specifications

3.2.1 General

The concrete docks are composed of smaller concrete elements connected by pretensioned steel wires. The wires are greased in order to protect them from rust and corrosion, and to limit the transfer of tension from the wire to the concrete surrounding it. In between the concrete elements a dampening material protects the wire. The mooring lines are attached to the docks in mooring wells. This gives easy access to the mooring lines from the top of the docks. A figure of one concrete element is shown in figure 3.2.

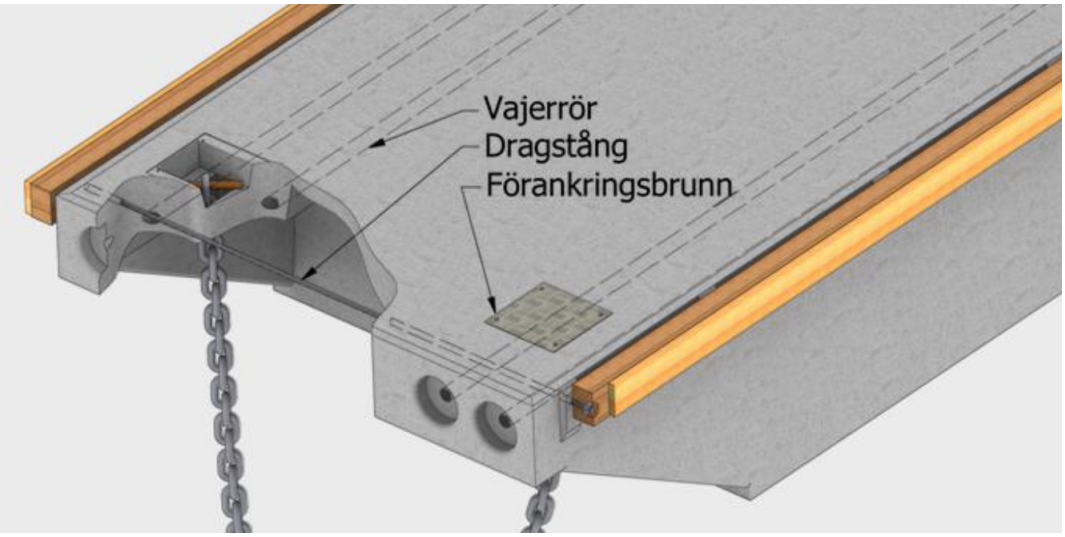

Figure 3.2: Concrete element. PHOTO: RIXÖ-bryggan

In figure 3.2 one can note that there are four pretensioned steel wires connecting the concrete elements. Additionally, one can see that the mooring lines are placed relatively high up in the concrete element. Below, a photo of the end of a concrete element may be seen.

Figure 3.3: Floating dock element end. PHOTO: Bi-Brygga AS

3.2.2 Outriggers

The outriggers are connected to the floating docks by hinges. This means that it is quite difficult to assess the effect they may or may not have on the whole system. One would primarily expect the outriggers to reduce the roll motion to some degree by increasing the mass moment of inertia about the roll-axis. Video footage of the dock suggests that it is possible to neglect the effect. As such, the influence of the outriggers will be neglected in this paper.

Figure 3.4: Hinged outriggers PHOTO: Bi-Brygga AS

3.3 Mooring specifications

The mooring of the dock system may be seen in the following figure:

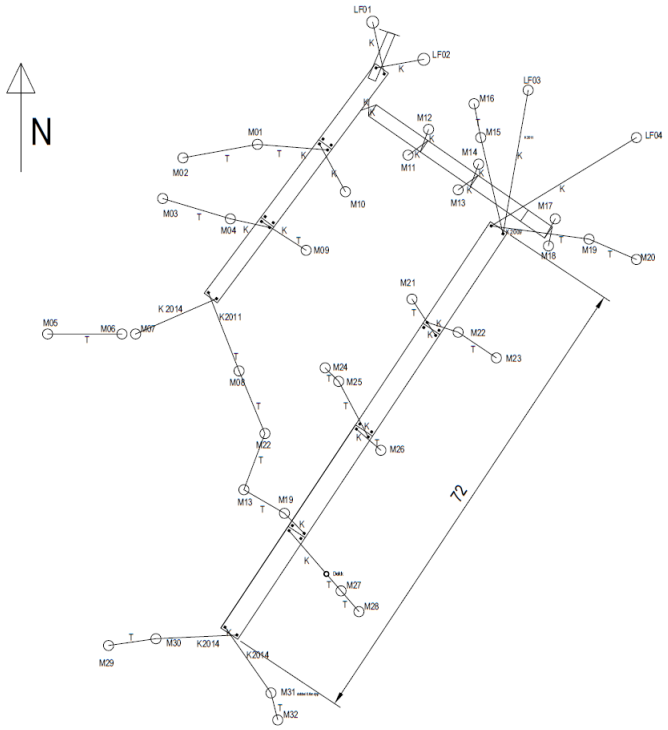

Figure 3.5: Mooring plan. PHOTO: Bi-Brygga AS

The mooring lines are steel chains, and the anchors are so called plow-anchors made of concrete.

3.4 Storm damage

In late December 2013 the floating dock system sustained substantial damage in a winter storm. In this paper only the most important damages will be considered. A damage assessment done in January revealed that four mooring lines had failed. This had then led to a 1-2 meter translation of the system to the north. The failed mooring lines were identified in figure 3.6.

Several failed chain links were also recovered during the damage assessment. A photo of one such link is found in figure 3.7.

This implies that the damage done to the floating dock system was mainly caused by the failure of the mooring chains.

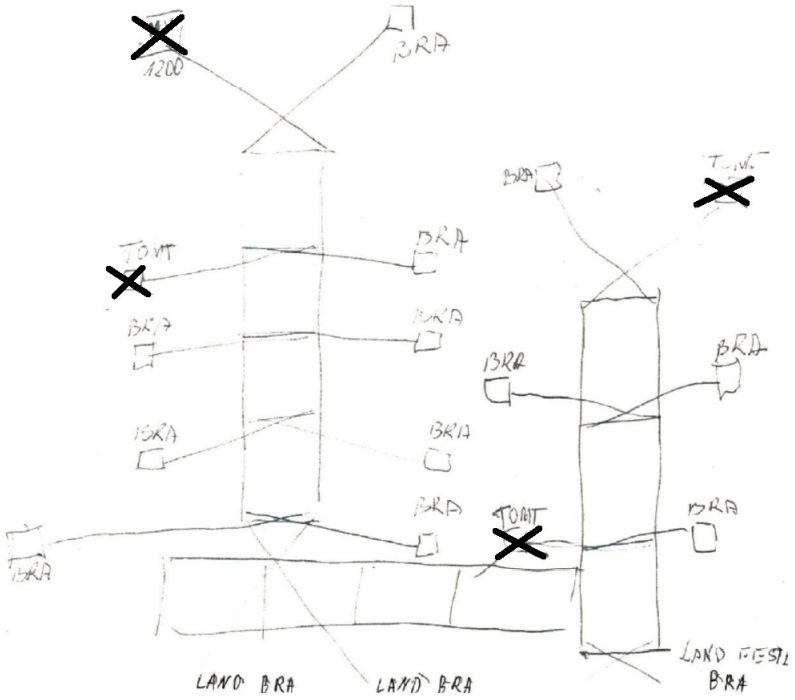

Figure 3.6: Failed mooring lines. PHOTO: Bi-Brygga AS

Figure 3.7: Failed chain link. PHOTO: Bi-Brygga AS

3.5 Design basis

A computer model will be established in SIMA, which will study the dynamic behaviour of the previously presented floating dock system. SIMA is a program developed by Marintek that provides a graphical user interface to the programs SIMO and RIFLEX, as well as a post-processing

tool. As such this paper will use SIMO in SIMA to preform the dynamic analysis. SIMA version 3.1.0.10464 for Windows is used in the analyses. The model will be based on theoretical calculations and recommended practices. In particular, *DNV's recommended practices c205 Environmental conditions and environmental loads* [2]. Additionally, the Norwegian standard for floating fish farms *NS 9415* [5] will be used, and some of its recommendations will be evaluated. A short video clip of the dynamic behaviour of the floating dock has been provided by Bi-Brygga AS. This clip will be used to compare the motion of the model with the motion of the real structure.

Chapter 4

Model description

4.1 General

4.1.1 Computer model

A model of the two concrete docks was established in SIMA. The connecting steel dock was neglected. The model is composed of seven barge shaped bodies, where four bodies make up the longest dock, and the remaining docks make up the smaller dock. The forces acting on the bodies are calculated with the help of slender elements. The mooring system of the structure is model with catenary lines, which can account for drag and dynamic effects such as snapping. The model is also subjected to uni-directional waves, wind and current. The response of the structure is then calculated by SIMO. The model may be seen in figure 4.1.

Units

The basic SI units have been used in the analysis model, they are defined in table 4.1.

Coordinate system

The computer model is created such that the length of the docks follow the x-axis. The width follows the y-axis, and the z-axis is pointing vetrically upwards. The angles used in the model are measured from the x-axis. The origo is placed in the center of gravity of the first concrete element of the smaller dock.

Table 4.1: Units

Property:	**SI unit:**
Length	m
Time	s
Mass	kg
Force	N
Stress	Pa (N/m^2)

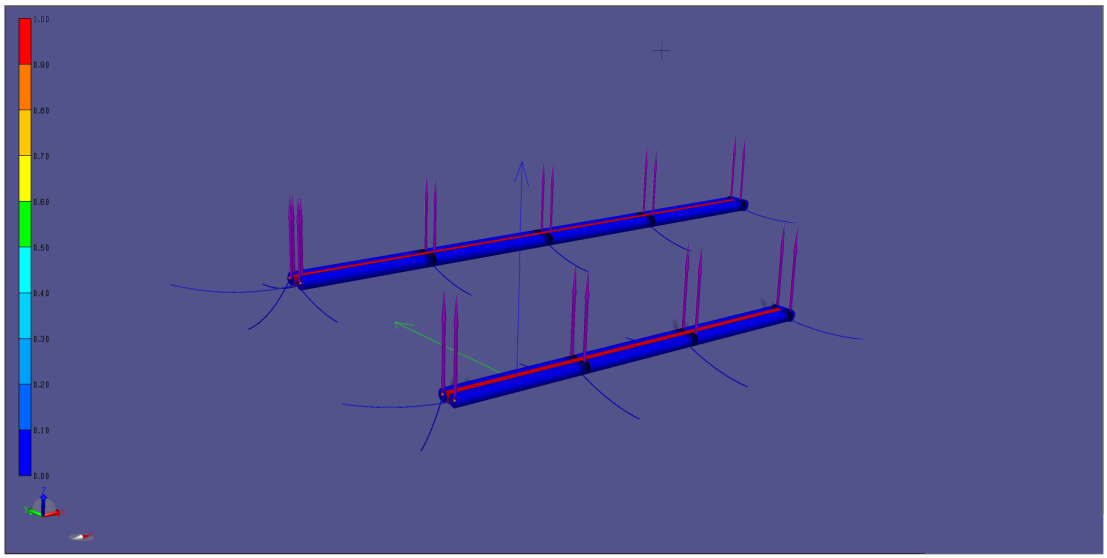

Figure 4.1: Floating dock SIMA model

4.1.2 Nomenclature

There is a need to establish a naming scheme for the components which make up the structure. The different concrete elements are given a number according to which dock they are a part of, as can be seen in figure 4.2.

The mooring lines must also be named. The following scheme is used: the lines are numbered from 1-4, where 1 is the north-western line and 4 is the south-eastern line. Now, body is shortened to B. An example of the nomenclature may now be written as: $BS1L1$. Here, the second letter references the dock in question, where N indicates the north dock and S indicates the south dock. The first number indicates the number of the body in question. The third letter L is short for line. Finally, the last number indicates the line number. The landlines are identified by a double L. The final nomenclature may be found in figure 4.3

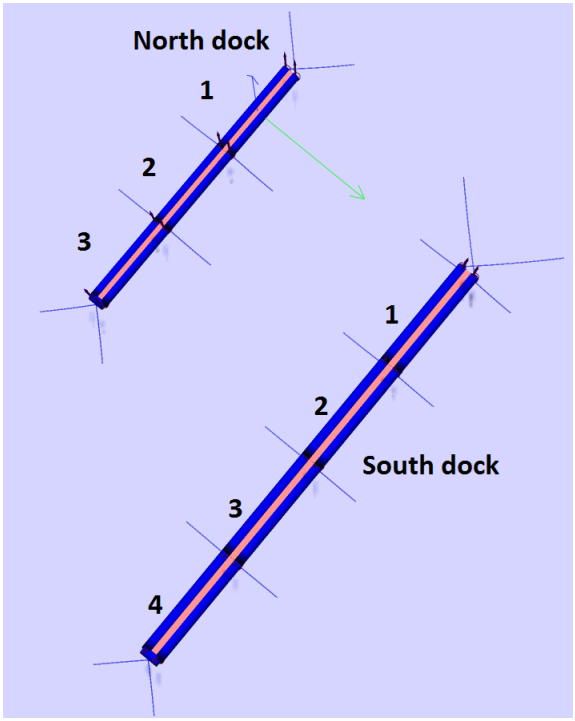

Figure 4.2: Dock nomenclature

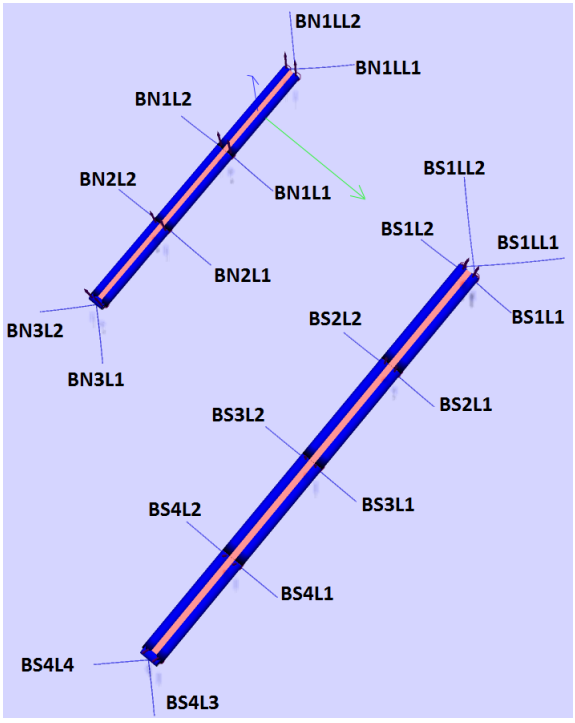

Figure 4.3: Dock mooring nomenclature

4.2 Kinetics

4.2.1 General

The concrete elements which make up the floating docks are modeled as barges. Their dimension are shown in in table 4.4.

Table 4.2: Body dimensions

Body:	Length [m]:	Width [m]:	Height [m]:
BN1	15.0	2.4	1.05
BN2	14.0	2.4	1.05
BN3	14.0	2.4	1.05
BS1	17.5	3.0	1.2
BS2	17.5	3.0	1.2
BS3	17.5	3.0	1.2
BS4	17.5	3.0	1.2

4.2.2 Mass

General

The real shape of the floating concrete elements is different from a barge. This means that there will be some inconsistency in the mass calculated from the draft and the actual mass. The mass of the bodies are obtained from Bi-Brygga AS. The north dock has a distributed mass of 1000 kg/m, and the south dock has a distributed mass of 1800 kg/m. This gives:

Table 4.3: Body mass

Body:	Mass [kg]:
BN1	15000.0
BN2	14000.0
BN3	14000.0
BS1	32400.0
BS2	32400.0
BS3	32400.0
BS4	32400.0

Consider the following equation:

$$\Delta = \rho\nabla = \rho LBT \tag{4.1}$$

where T is the draft of the body. The draft of the system is estimated to about 50 cm. Using the draft one finds the total approximated mass of the north dock as 58179 kg, and the total approximated mass of the south dock as 150675 kg. The total values for the real docks are respectively 43000 kg and 129600 kg. This over estimates the mass by respectively 35 % and 16 %. One can conclude that the barge shape is not an ideal approximation of the shape of the dock elements. The values obtained from Bi-Brygga AS were used for the model.

Mass moment of intertia

The mass moment of inertia are found according to section 2.3.2 by assuming that the bodies are barge shaped. The calculated values are given in the following table:

Table 4.4: Body mass moment of inertia

Body:	I_{xx} $[kgm^2]$**:**	I_{yy} $[kgm^2]$**:**	I_{zz} $[kgm^2]$**:**
BN1	8.58E+03	2.83E+05	2.88E+05
BN2-3	8.01E+03	2.30E+05	2.35E+05
BS1-4	2.82E+04	8.31E+05	8.51E+05

4.2.3 Damping

The damping is found using figure 2.6. The peak frequency of the wave spectrum is used as the wave frequency ω. This assumption will make the damping somewhat too large for lower wave periods. However, as damping is most important at resonance the assumption should be satisfactory. The following values are calculated.

The barge geometry is symmetrical so there are no coupled damping effects. The damping in pitch may not by found in figure 2.6, it is therefore taken as ten times the damping in roll.

Table 4.5: Body damping

Body:	$Sway\ [kg/s]$**:**	$Heave\ [kg/s]$**:**	$Roll\ [kg/s]$**:**	$Pitch\ [kg/s]$**:**
BN1	1.62E+04	7.29E+04	1.95E+06	1.95E+07
BN2-3	1.62E+04	7.29E+04	1.95E+06	1.95E+07
BS1-4	1.62E+04	7.29E+04	1.95E+06	1.95E+07

4.2.4 Hydrostatic stiffness

The hydrostatic stiffness is calculated according to section 2.3.4. Again there are no coupled effects. The results are:

Table 4.6: Body hydrostatic stiffness

Body:	$Heave\ [kg/s]$**:**	$Roll\ [kg/s]$**:**	$Pitch\ [kg/s]$**:**
BN1	3.62E+05	1.24E+05	6.74E+06
BN2-3	3.38E+05	1.16E+05	5.47E+06
BS1-4	5.28E+05	3.23E+05	1.34E+07

The hydrostatic stiffness in surge, sway and yaw are derived from the mooring system. These values are calculated by SIMO.

4.3 Coupling elements

4.3.1 General

The concrete elements are connected by steel wires. This is modeled by fixed elongation coupling elements. These elements essentially allows one to define a linear relationship between the distance between bodies and the force in the coupling. This means that the coupling gradually increases its resistance to the elongation it suffers because of the body motions. Additionally, the damping of the coupling material may be added. In this case the couplings are assumed to be pretensioned steel. The stiffness of one steel wire is found with the following expression:

$$k = \frac{EA}{L} \tag{4.2}$$

where k is the stiffness of the wire, E is the Young's modulus, A is the cross-sectional area of the wire and L is the total length of the wire. Now, the linear relation between elongation x and force F is defined by:

$$F = kx \tag{4.3}$$

There are four wires connecting each of the floating docks. One coupling element is used to model two steel wires. The resulting graph is:

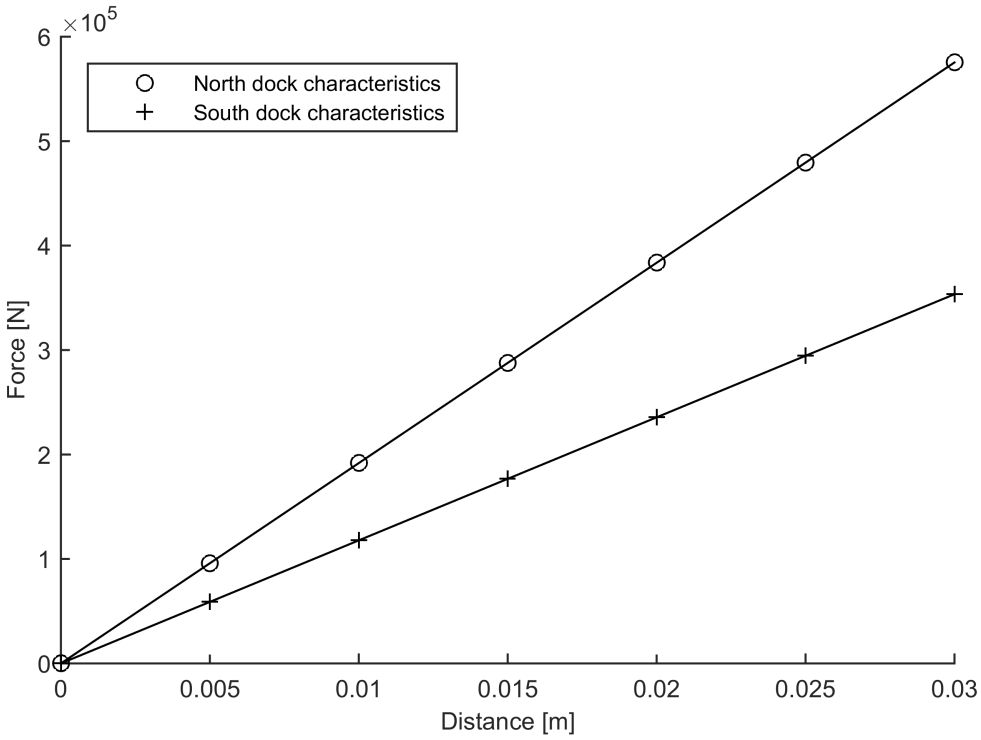

Figure 4.4: Fixed elongation coupling characteristics

4.3.2 Coupling damping

The damping values for the steel wires are obtained by the use of equation (2.95). The damping is taken as 2% of the critical damping. The mass is taken as half the mass of the connected body, and the stiffness is found as seen in the previous. Thus the damping values of the couplings are given as:

Table 4.7: Damping of fixed elongation couplings

Body:	**Damping [kg/s]:**
BN1	8.82E+03
BN2-3	8.52E+03
BS1-4	9.29E+03

The assumption of the damping being 2% of the critical damping seems reasonable, as the steel wires are not expected to contribute significantly to the damping of the whole structure.

4.4 Slender element modeling

The forces acting on the floating docks are calculated with Morison's equation. This is done by applying slender elements to the bodies. The slender elements are assigned a specific volume and mass. Additionally, a drag coefficient and a added mass coefficient are defined. The drag coefficient is calculated using equation (2.118) In this case, the water is shallow. This means that the sea bottom must be taken into account. Figures 2.4 and 2.8 give these coefficients as a function of the gap ratio. The gap ratio H/D for the slender elements are found as:

Table 4.8: Slender element gap ratios

Body:	**Gap ratio H/D [-]:**
BN1	2,08
BN2-3	2,08
BS1-4	1,67

Each body has two longitudinal slender elements, this is done in an attempt to adequately model the roll motion of the floating docks. As slender elements may only calculate forces in one direction, two smaller slender elements are applied in the transverse direction in order to calculate the transverse force contribution. Table 4.9 summarizes the slender element values.

Table 4.9: Slender element properties

Body:	**Specific volume** $[m^2]$**:**	**Distributed mass** $[kg/m]$**:**	**Drag coeff.** $[-]$**:**	**Added mass coeff.** $[-]$**:**
BN1	1.26	500	0.93	1.07
BN2-3	1.26	500	0.93	1.07
BS1-4	1.8	900	0.91	1.09

In SIMA the slender element strips are taken as either dry or fully submerged. This works decently for vertical elements, however for horizontal elements it is necessary to define the drag and added mass coefficients as depth dependent. This is done by defining a relative submerged volumes for different vertical displacements of a slender element strip. In this case, the coefficients are kept unchanged for all the relative submerged volumes. This is not a perfect approximation as the added mass coefficients will vary with the water depth, however the differences are negligible. For example, a 20% decrease in water depth would make the added mass coefficient increase with 0.01.

4.5 Mooring

4.5.1 General

The mooring lines are all modeled with the same characteristics. The mooring forces are obtained according to section 2.4.5. The layout of the mooring lines can be seen in figure 4.3. The chains are characterized by the following:

Table 4.10: Chain mooring line characteristics

Diameter [mm]:	**Length [m]:**	**Breaking strength [kg]:**	**Young's modulus [MPa]:**
25	10	3.0E+04	2.1e+11

Here the diameter is the diameter of one chain link. The chain is modeled by a line in the model. The diameter of the line is chosen such that the breaking strength remains the same. The increased drag force is taken into account by larger drag coefficients. The mooring line length is

determined as four times the water depth. This is a design principle used by Bi-Brygga AS. The following characteristics were calculated for the modeled lines:

Table 4.11: Mooring line model characteristics

Diameter [mm]:	**Length [m]:**	**Unit weight in air [-]:**	**Ratio of weight in water to weight in air [-]:**
35	10	73.62	0.87

The drag coefficients are taken according to section 2.4.4.

Table 4.12: Mooring line drag coefficients

Transverse drag coefficient [-]:	**Longitudinal drag coefficient [-]:**
2.4	1.15

4.5.2 Mooring line tension

The curve of the mooring line is determined by the tension in the line. Using the parameters detailed in the previous part one may plot the horizontal line tension as a function of the distance between the anchor of the mooring line and its connection point to the floating dock. The graph may be seen in figure 4.5.

The floating docks are supposed to be relatively tightly moored. This is simulated by the means of increasing the line tension. For the default condition a tension of 2000 N is applied to the lines. For the condition with slack in the line the tension is set to 500 N. The difference may be seen in figure 4.6.

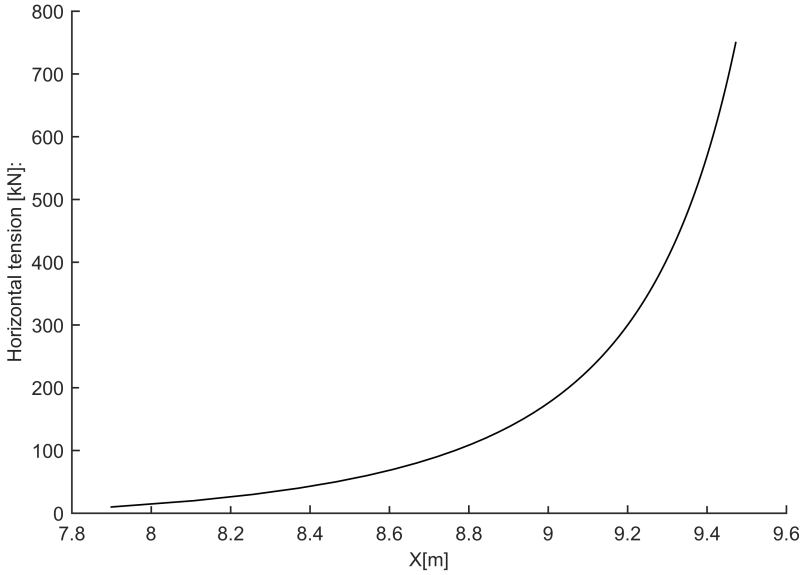

Figure 4.5: Line tension characteristics

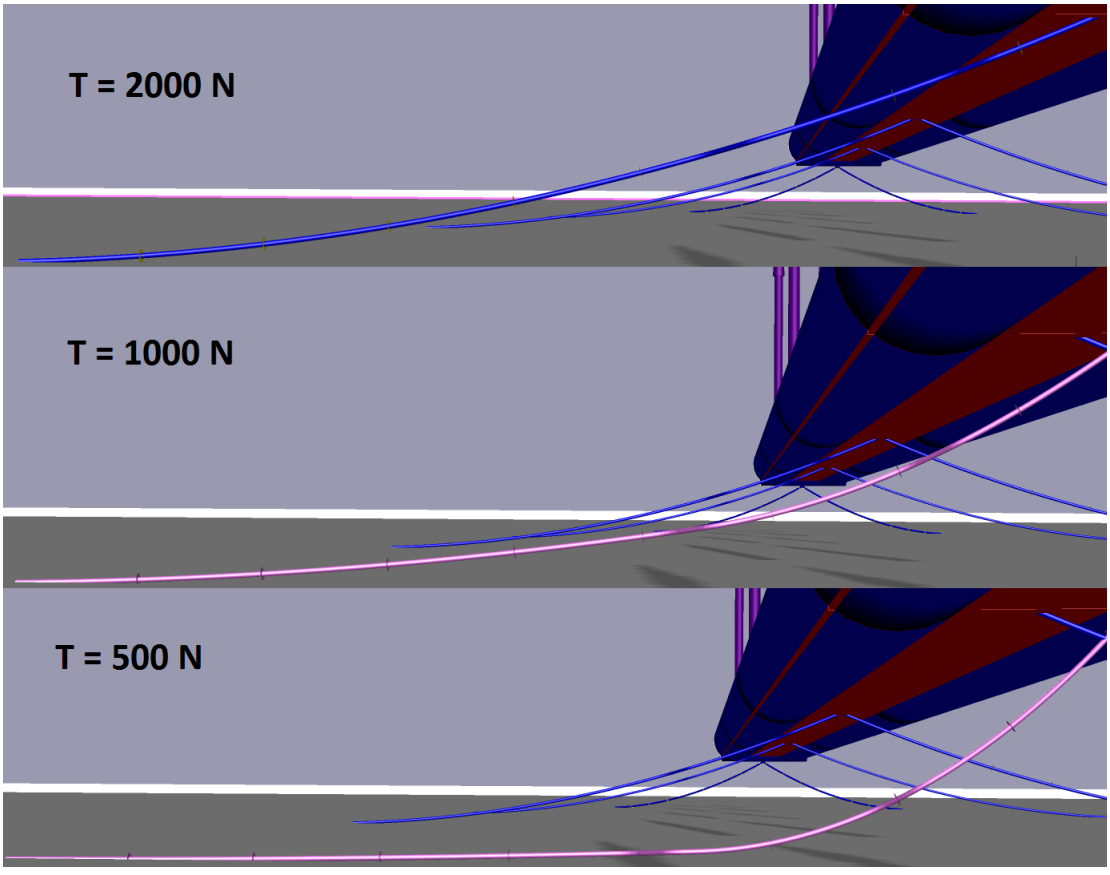

Figure 4.6: Mooring line tautness based on the line tension T

4.5.3 SIMA mooring line characteristics

The SIMA mooring characteristics were obtained by analytical calculation, and some iteration on the practical parameters. The parameters detailed in the previous were implemented directly into the program. The land lines were defined as anchored at 0.5 meters below the sea surface. As they are modeled by catenary lines, the anchor point must be defined below the mooring connection point. The other lines were anchored at the sea bottom. Specified forces were added to the model to maintain the water line of the system as the weight of the mooring lines increased the draft of the model.

4.6 Environment

4.6.1 Wind modeling

General

Meteorologisk institutt provides free wind velocity measurements for several locations in Norway [3]. In this case, the closest weather station is situated in Sande, Vestfold. It is situated about 7 km away from the floating docks. The wind statistics may be used to calculate the expected 50 year wind velocity, which is the recommended design wind velocity for structures according to *Eurocode 1: Actions on structures* [22]. The wind statistics may be summed up in a wind rose diagram. Figure 4.7 shows the wind rose for Sande.

Here, one can note that the wind mostly blows in a northern direction, and that most of the winds are of a relatively small magnitude. Now, it is necessary to consider the geographical location of the floating docks. A map of the general area is shown in figure 4.8.

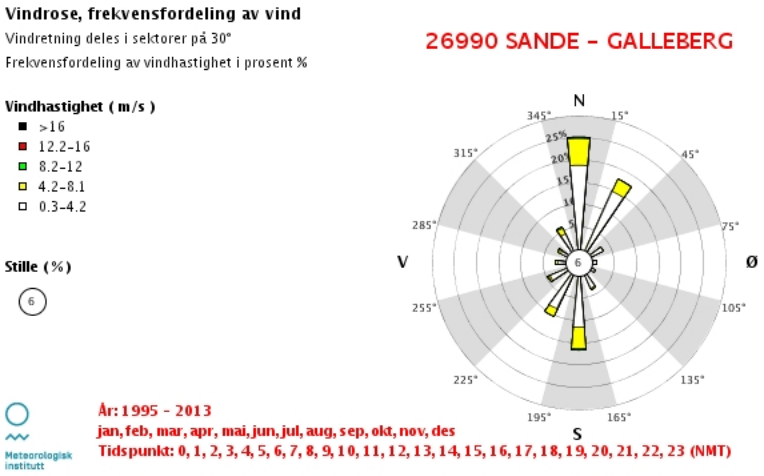

Figure 4.7: Wind rose for Sande, Vestfold. PHOTO: Meteorologisk institutt [3]

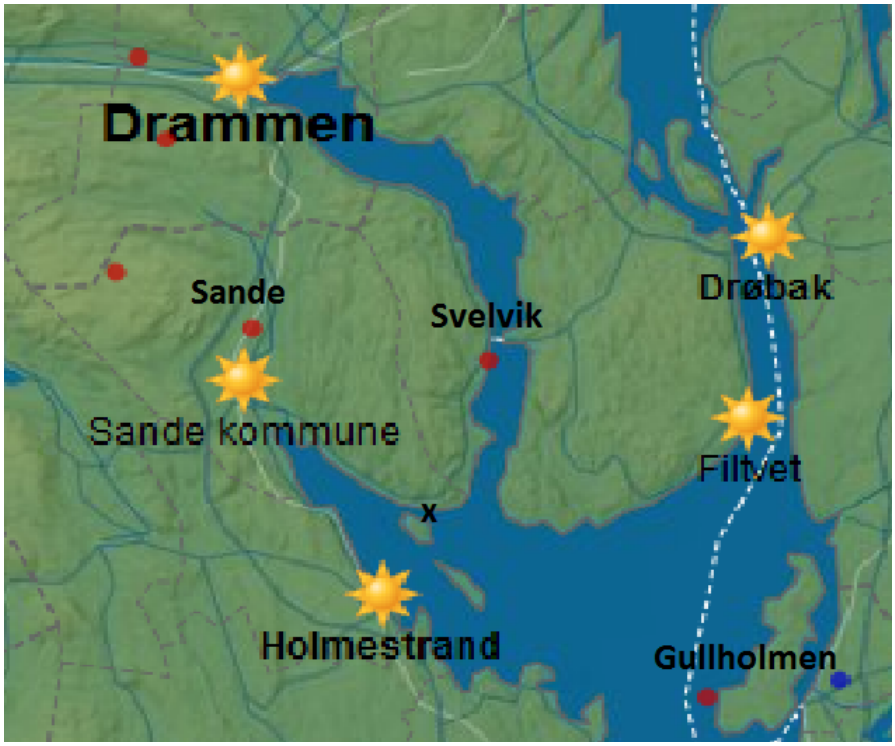

Figure 4.8: Map of weather stations in the Oslo fjord. Here, the black cross shows the location of the floating docks. The red dots show weather stations. PHOTO: Meteorologisk institutt

As one can see Sande has a large land mass to the south of it, this will probably give lower the wind speeds in Sande than at the floating docks. Svelvik would be an interesting location, unfortunately this station does not record hourly wind velocities. In order to obtain a clearer picture of the wind conditions in the area, the wind rose of Gullholmen will be considered.

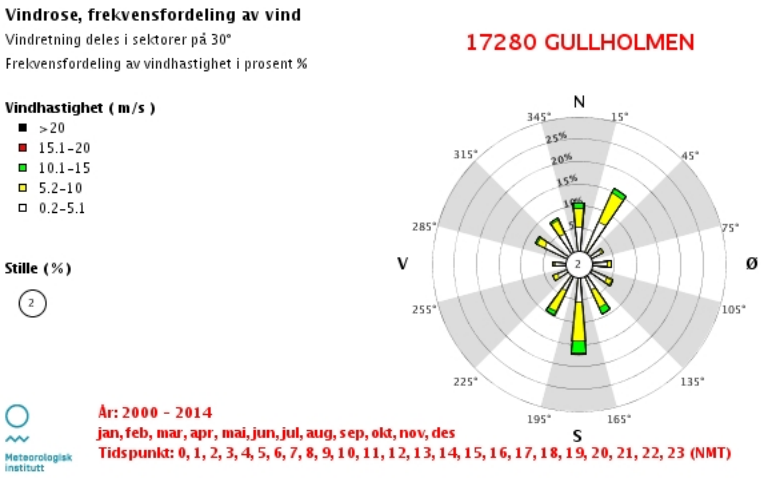

Figure 4.9: Wind rose for Gullholmen, Østfold. PHOTO: Meteorologisk institutt [3]

The wind velocities are clearly significantly higher out in the fjord. The wind directions seem relatively similar. In the following, the 50 year wind velocities will be estimated for both locations.

Wind distributions

The Sande station has measured the wind velocity since 1995, and the Gullholmen station has been in operation since november 2000. This gives a decently sized data sample size. Using the mean wind speed taken from 10 meters above the ground, the data samples are Weibull distributed according to section 2.6.2. The following graphs are obtained:

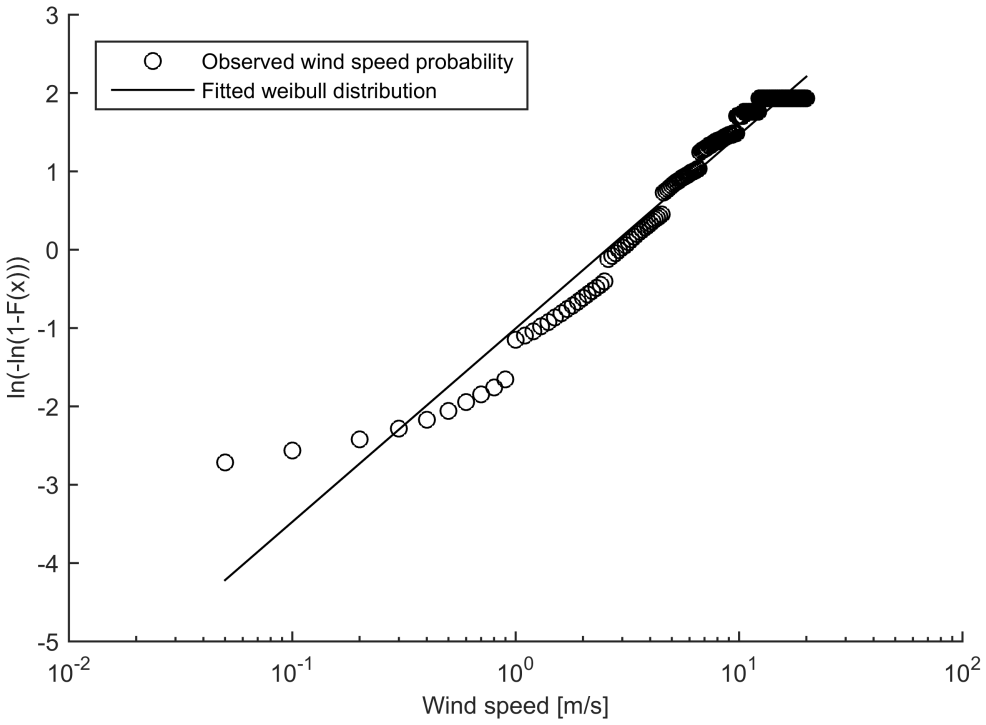

Figure 4.10: Weibull probability paper based on the Sande wind statistics

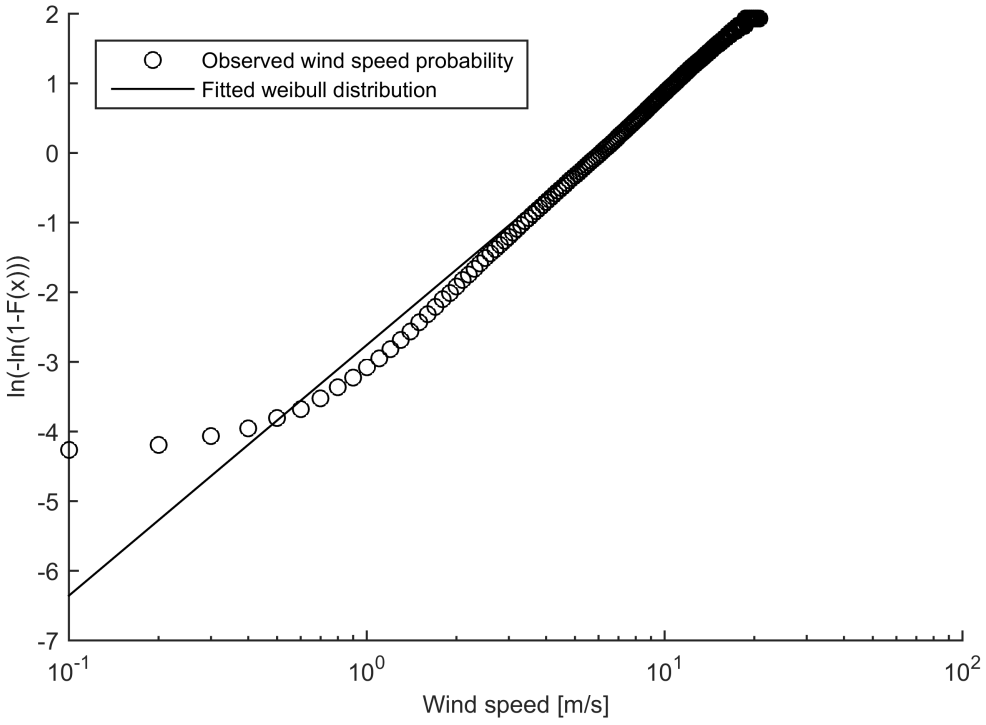

Figure 4.11: Weibull probability paper based on the Gullholmen wind statistics

Certain characteristic wind values may be derived from the Weibull distributions. The expected 50 year wind velocity is calculated.

Table 4.13: 50 year wind velocity for Sande and Gullholmen

Location:	**50 year wind velocity [m/s]:**
Sande	23.3
Gullholmen	30.1

The 2013 late winter storm may also be found in the statistics. The highest mean wind velocities recorded in the storm may be seen in the following table:

Table 4.14: 2013 winter storm wind velocity for Sande and Gullholmen

Location:	**Storm wind velocity [m/s]:**
Sande	14.2
Gullholmen	23.0

Quality evaluation

The accuracy of the probability distribution fitting can be evaluated. This will be done with a R^2 test, according to section 2.6.3. The *Eurocode 1: Actions on structures* [22] also gives design values for Sande, which may be used for comparisons sake. No design wind velocity is given for Gullholmen. The following table shows the results of the quality check:

Table 4.15: Quality evaluation of the expected 50 year wind velocities in Sande and on Gullholmen

Location:	R^2 **test:**	**Eurocode 50 year wind [m/s]:**
Sande	0.96	23
Gullholmen	0.98	-

The distribution fits well to the data, and the calculated expected value for Sande is quite similar to the recommended value. It seems that the results are of a decent quality. The data quality should be good too, as the data points are recorded automatically by a computer every

hour. Note that for the Sande station an automatic weather station was first installed in 2005. This means that for the 10 first years of the operation only two values were recorded per day. This has been accounted for in the probability model, and as the Sande 50 year value correspond with the government recommended value, it is considered to be adequately accurate.

For the 2013 winter storm one can calculate its return period in the two different locations and compare it, as seen here:

Table 4.16: Return period of the 2013 winter storm

Location:	**Return period [days]**
Sande	220
Gullholmen	211

Again the values found seem to reinforce the impression that the Weibull distributions describe the wind velocities with decent accuracy. Additionally, it seems that the 2013 storm might be considered as the yearly winter storm.

Wind force

The wind force acting on the floating docks is considered to be negligible. Assuming that the wind blows from south to north, a fairly small area is exposed to the wind. The exposed area is also situated close to the ground, which means the wind velocity acting on the floating docks is a lot smaller than the 10 meter above ground mean wind velocity. Calculations using equation (2.114) confirms this assumption.

4.6.2 Significant wave height and peak period modeling

Effective fetch length

The fetch length is calculated according to section 2.1.7. Figure 4.12 shows the radials drawn to calculate the effective fetch length.

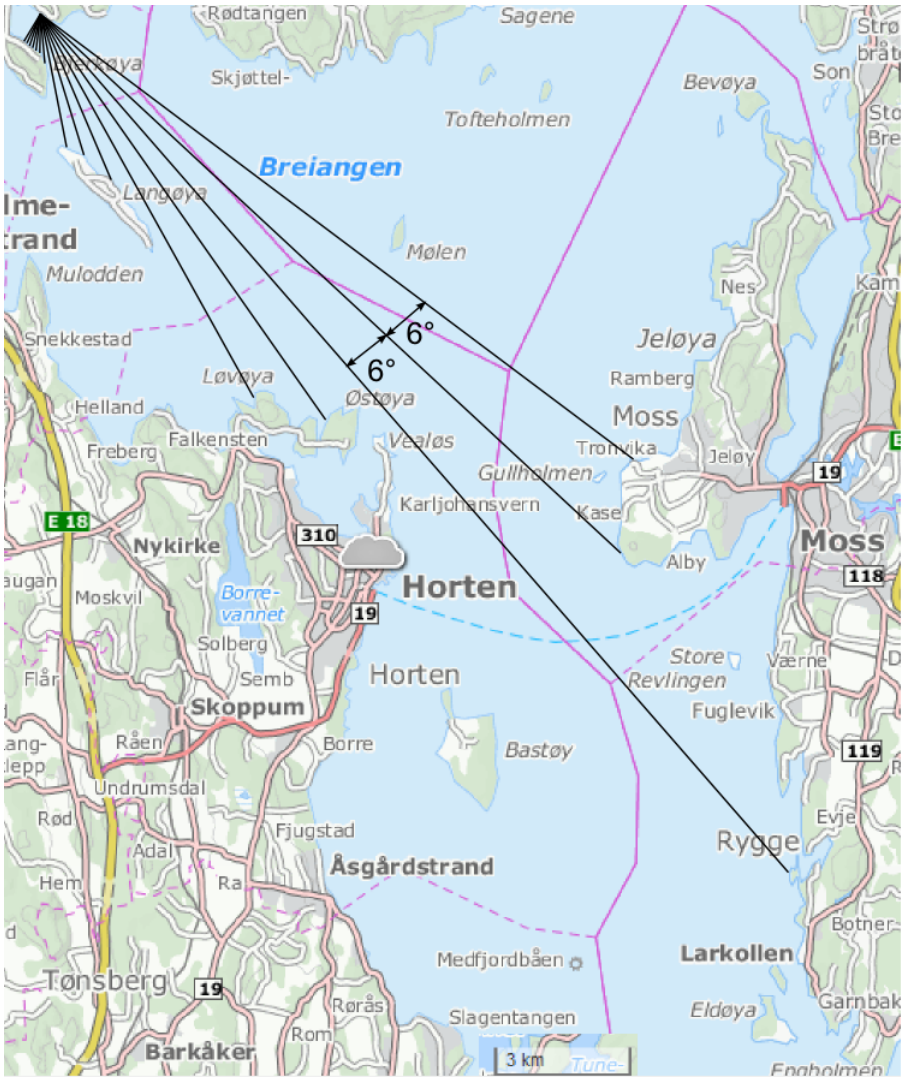

Figure 4.12: Effective fetch length calculation

From this figure the following table is obtained:

Table 4.17: Fetch lengths for the floating docks:

α [degrees]:	Fetch length X[m]:
42	1.64E+04
36	1.75E+04
30	2.51E+04
24	1.09E+04
18	9.60E+03
12	3.91E+03
6	3.26E+03
0	3.01E+03
6	1.10E+03
12	8.61E+02
18	8.07E+02
24	7.67E+02
30	7.60E+02
36	7.49E+02
42	7.13E+02

The effective fetch is obtained by weighting the values in table 4.17, and then is given by:

Table 4.18: Effective fetch length for the floating docks:

Effective fetch length [m]:
6.10E+03

Significant wave heights and peak periods

The significant wave heights and peak periods are calculated for the 50 year expected wind velocities, as well as for the 2013 winter storm values. This is done according to section 2.1.7, and the results are found in table 4.19 and in table 4.20.

The real significant wave height and peak period is likely found somewhere in between of the Sande and Gullholmen values. As Sande is more shielded by land than the floating docks, and Gullholmen is subjected directly to Skagerak, which will give quite high wind velocities. All the calculations were done with the effective fetch length of the floating docks.

Table 4.19: 50 year expected significant wave height H_s and peak period T_p:

Location:	**Significant wave height H_s [m]:**	**Peak period T_p [s]:**
Sande	1.36	3.70
Gullholmen	1.86	4.11

Table 4.20: 2013 winter storm significant wave height H_s and peak period T_p:

Location:	**Significant wave height H_s [m]:**	**Peak period T_p [s]:**
Sande	0.74	3.02
Gullholmen	1.34	3.68

Peakedness factor

In the following wave spectra based on the peakedness factor γ will be presented. The peakedness factor according to DNV [2] may be found in the following table:

Table 4.21: DNV recommended peakedness factors

Wave condition:	$T_p/\sqrt{H_s}$	**Peakedness factor γ [-]:**
Sande 50 year storm	3.17	5
Gullholmen 50 year storm	3.23	5
Sande 2013 storm	3.51	5
Gullholmen 2013 storm	3.18	5

4.6.3 Water depth modeling

The water depth varies from 2-3 meters, decreasing towards the shore. This simply taken as an average depth of 2.5 meters. In this case this is considered shallow waters. As shown in section 2.1.2 one has shallow water when:

$$d < \frac{\lambda}{2} \tag{4.4}$$

where d is the water depth and λ is the wave length. The following table shows that all the considered wave conditions are shallow water conditions:

Table 4.22: Shallow water condtion when $d = 2.5[m]$

Wave condition:	$\frac{\lambda}{2}$ **[m]:**
Sande 50 year storm	10.66
Gullholmen 50 year storm	13.15
Sande 2013 storm	7.10
Gullholmen 2013 storm	10.55

The water depth is however not so shallow that the water partical orbitals are disrupted. This implies that shallow water wave theory will be able adequatly describe the water conditions in the floating dock model.

4.6.4 Wave modeling

General

The waves are modeled as unidirectional wind waves calculated from wave spectra. The waves are assumed to be moving in a north-western direction, which is the most important angle of approach. In SIMA this translates to a directional angle of 247.5°. All the spectra presented in section 2.1.3 have been considered for all the significant wave height and peak periods presented in the previous section. For the Jonswap and TMA spectra the recommended values for the peakedness factor γ from DNV [2] and from the Norwegian standard for fish farms have been evaluated [5]. Respectively, $\gamma = 5$ and $\gamma = 2.5$. Note that all the wave conditions fall slightly outside the optimal area of use for the Jonswap spectrum, and may therefore be influenced by this. However, as the conditions are not significantly outside the optimal area the effects of this are assumed to be negligible. The results may be seen in the following figures:

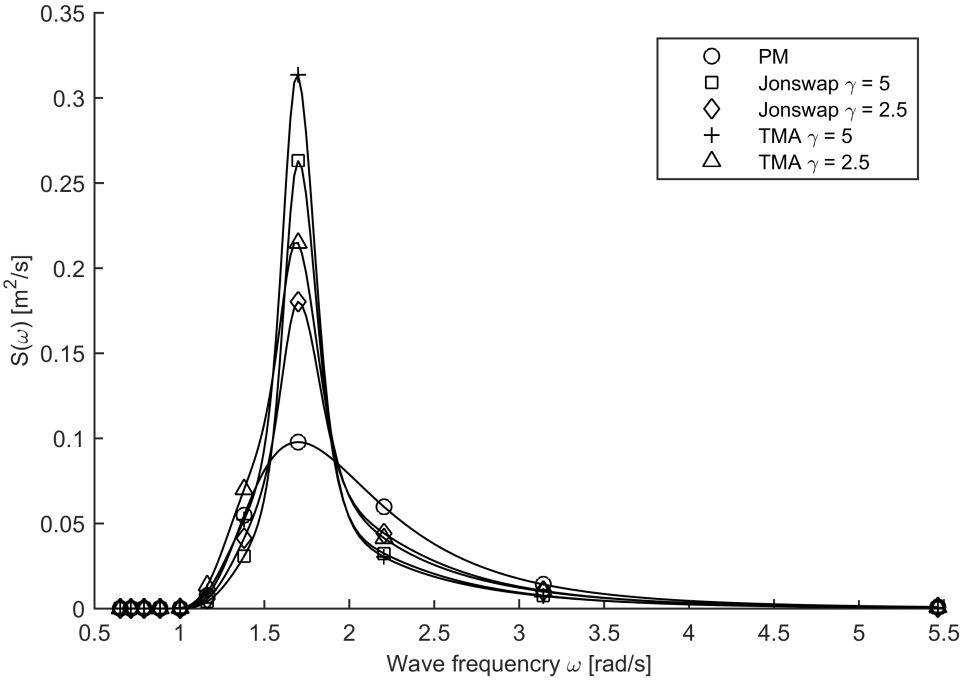

Figure 4.13: Wave spectra for the Sande 50 year storm.

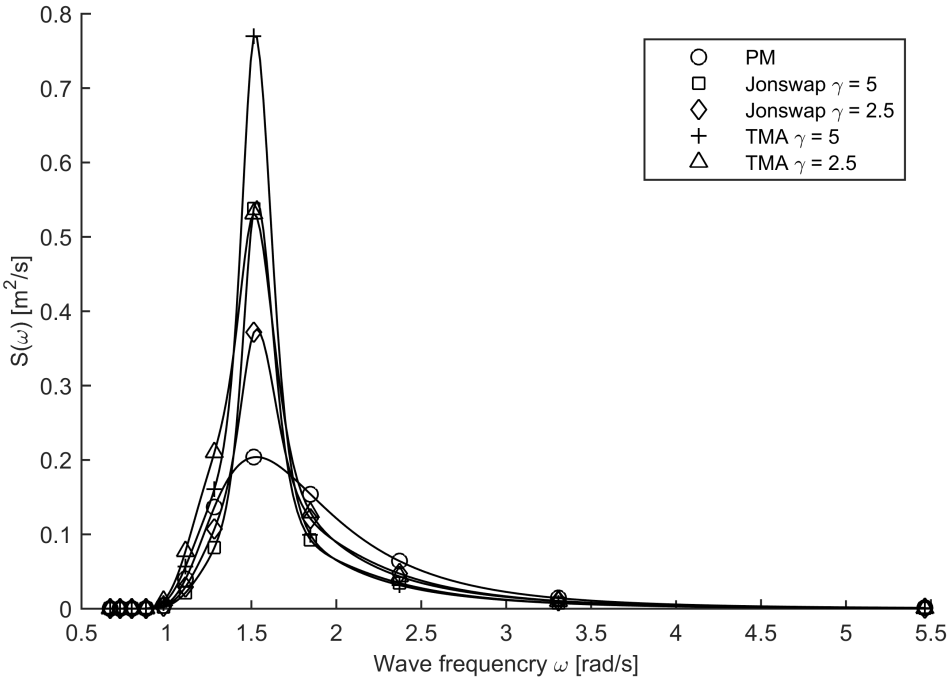

Figure 4.14: Wave spectra for the Gullholmen 50 year storm.

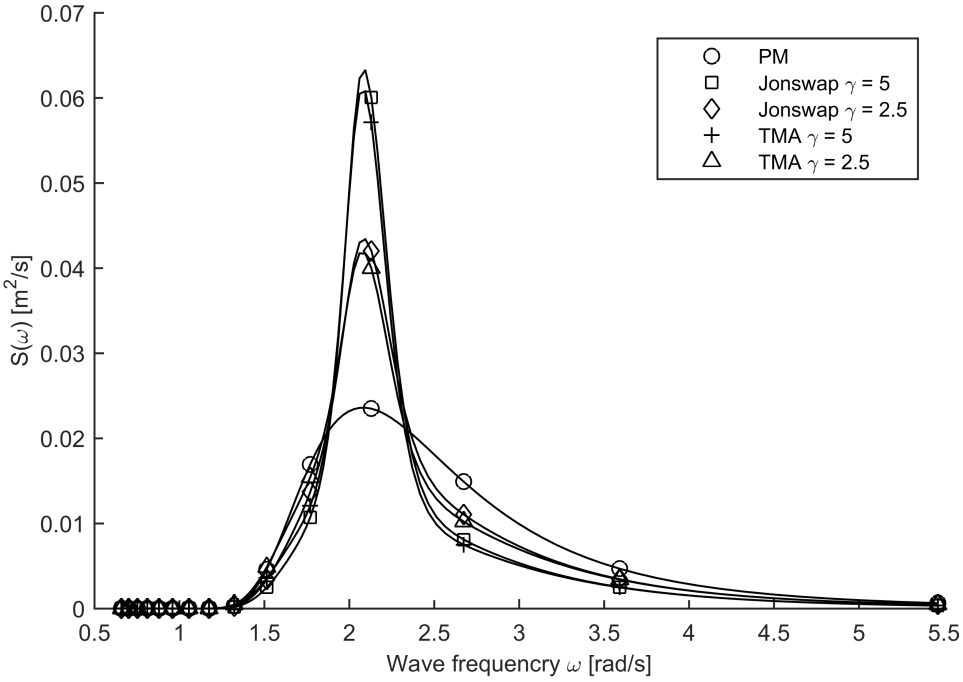

Figure 4.15: Wave spectra for the Sande 2013 winter storm.

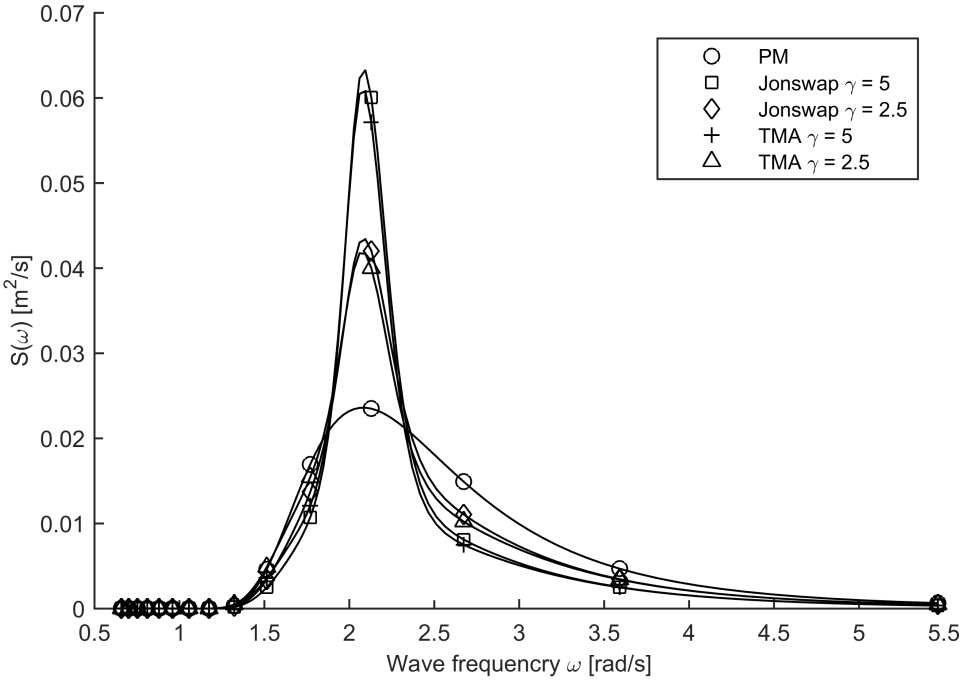

Figure 4.16: Wave spectra for the Gullholmen 2013 winter storm.

The figures show that there is an interaction between the significant wave height and the water depth. The TMA spectrum is smaller than the Jonswap spectrum for the Sande 2013 winter storm, whereas it is larger for the other cases. There is a significant difference in wave height between these cases. In general one can note that the peakedness factor γ, increases the peak when it increases. As expected the PM and Jonswap spectrums have approximately the same area under their curves. The TMA spectrums however have varying area, this is likely explained by the fact that the TMA model attempts to account for shallow water effects. Indeed, this would help to explain why the TMA spectrum is smaller in the case of smaller wave heights and is larger in the case of larger wave heights.

Other wave effects

The wave model used in SIMA is somewhat simplistic, in that it does not take into account wave breaking and second order wave effects. It is not unlikely that wave breaking will occur on account of the shallow water depth. This can give slamming forces, it is quite possible that these forces could be the largest forces acting on the floating docks. This can be somewhat mitigated by selecting a high percentile maximum force from a Gumbel distribution. The second order wave forces are most important for large volume structures. Figure 2.7 shows that the floating docks may be considered to be a small volume structure, and therefore the second order wave forces should be negligible. Finally, the wave model does not consider wave screening. This is a weakness in the model, as the south dock is purposefully larger than the north dock in order to shield the latter dock from the waves. This means that the forces acting on the north dock may be smaller than what the model shows.

Design wave method

The design wave method is also considered, as it is recommended by the Norwegian standard for floating fish farms [5]. Table 4.23 for the maximum wave height is established based on section 2.1.8.

Evidently, the 50 year values are too large as they are greater than the water depth. This mean that the design wave method may only be applied for the 2013 Sande winter storm case.

Table 4.23: Maximum wave heights

Wave condition:	H_{max} **[m]:**
Sande 50 year storm	2.59
Gullholmen 50 year storm	3.55
Sande 2013 storm	1.41
Gullholmen 2013 storm	2.55

4.6.5 Tidal modeling

The tide is not included in the SIMA model. The effect of the tide will instead be considered by investigating the effect of the lines becoming slack. This should be equivalent to a low tide condition. A high tide will increase the tautness of the mooring system, and it is not expected to be critical, as it will make dynamic effects such as snapping smaller. The tidal levels based on the middle sea level for Selvik, Vestfold can be seen in figure 4.17. Selvik lies quite close to the floating docks, as such the tidal values are taken as relatively accurate. The values are collected by Kartverket, and are publicly available [4].

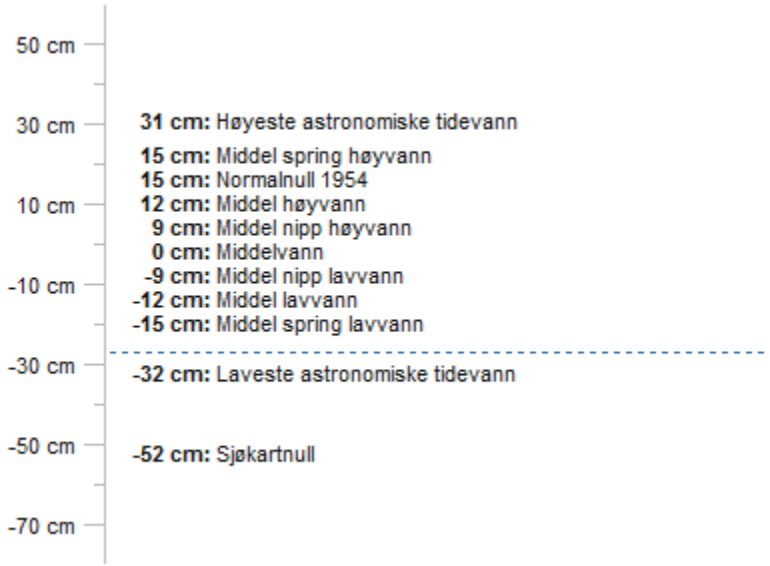

Figure 4.17: Tidal levels in Selvik, Vestfold [4]. Here 0 cm is the mean water level between high and low tide.

The tidal levels do not vary much (+/- 30 cm), it is not likely to be significant. Unless the slackness of the lines causes significant snapping.

4.6.6 Current modeling

Current velocity

The Norwegian standard for floating fish farms [5] allows one to choose design current velocities based on the structure's degree of exposure to the waves. The significant wave height and the wave peak period found for the floating dock system is classified as large exposure. The relevant part of the table is reproduced here:

Table 4.24: Classification of waves based on H_s and T_p

Wave classes:	$H_s[m]$**:**	$T_p[s]$**:**	**Description:**
A	0.0 - 0.5	0.0 - 2.0	Small exposure
B	0.5 - 1.0	1.6 - 3.2	Moderate exposure
C	1.0 - 2.0	2.5 - 5.1	Large exposure

Knowing the wave class, the design current velocity is now chosen accordingly:

Table 4.25: Classification of environments based on current velocity V_c

Current classes:	$V_c[m/s]$**:**	**Description:**
a	0.0 - 0.3	Small exposure
b	0.3 - 0.5	Moderate exposure
c	0.5 - 1.0	Large exposure

Obviously, these values can not be taken as is, as the classifications are not equivalent. As there are no field measurements to help with evaluating the choice of current velocity, it is necessary to consider the importance of the accuracy of the current velocity. Therefore, several current velocities will be considered in the dynamic analysis, and the relative importance of an accurate current velocity will be investigated. The shallow coastal waters makes it hard to estimate a current velocity, as the magnitude of the tide can shift drastically based on local conditions. The following values are proposed for the dynamic analysis:

Table 4.26: Current velocities to be used in the dynamic analysis

Current velocities V_c [m/s]:
0.1
0.3
0.5

Current profile

The current profile is modeled using equations (2.38), (2.39) and (2.40). In order to get the desired sea surface velocity equation (2.38) is divided by two. Figure 4.18 illustrates this procedure:

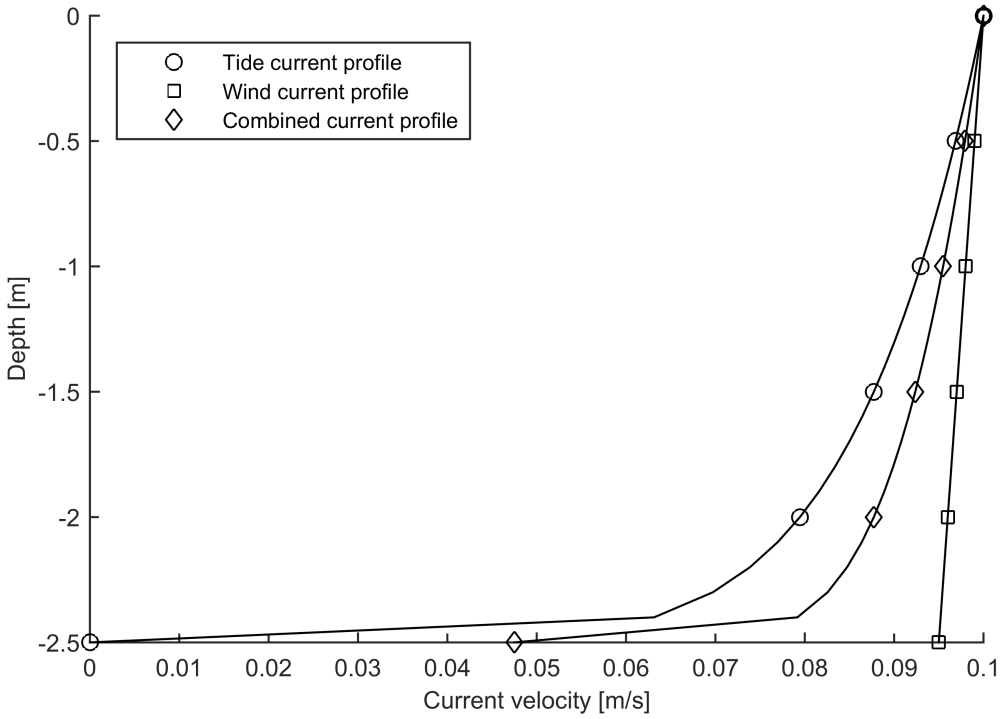

Figure 4.18: Current profiles for current velocity $V_c = 1$ [m/s]

This approach is likely somewhat inaccurate, as the tidal currents are probably larger than the wind currents, both due to the coastal waters and to the fact that the geographical location may lower the wind speeds due to terrain shielding. Nevertheless, the differences should not be too important as the floating dock floats in the sea surface, where the current profiles are still quite similar. The profiles will vary mostly for the mooring lines, which will influence the drag

force on these lines. However, the lines have small diameters and the force difference is therefore assumed to be negligible. The current profiles that will be used in the dynamic analysis may be seen in figure 4.19. Note that these profiles are worst case situations where the tide current acts in the same direction as the wind current. This will only likely to happen when the tide goes from low tide to high tide.

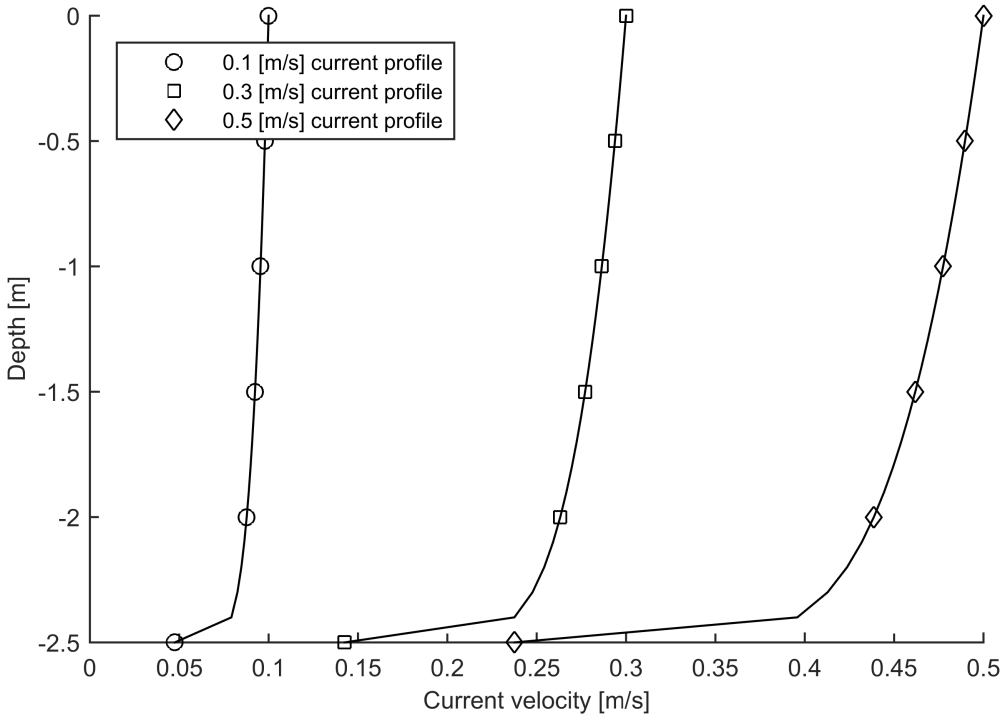

Figure 4.19: Current profiles used in the dynamic analysis

Chapter 5

Analysis description

5.1 General

The dynamic analysis of the floating docks system is carried out in SIMA 3.1. The effect of current, wave spectrum and mooring line tautness will be evaluated. The following conditions will be included in the analysis: the Sande 50 year storm, the 2013 Sande winter storm and the 2013 Gullholmen winter storm. The Gullholmen 50 year storm gives significant wave heights which are too large for the model to handle. In any case the this condition is so extreme that other effects such as wave breaking become important. The analysis consists of simulating a 3 hour storm. A time increment of 0.01 seconds is used. The complete analysis of the system is run with 30 random wave seeds. Each run generates a maximum force value for a considered component. The 30 maximum values are then Gumbel distributed according to section 2.6.2. The 90 percentile value of the Gumbel distribution is taken as a the maximum value. This percentile is quite high and is therefore possibly an overestimation of the wave force. However, this is accepted as this assumption is conservative. Mooring line $BS4L3$ is the line which has to resist the waves acting on the south dock. This line also failed in the 2013 winter storm. It is therefore assumed to be the most critical component. This will be confirmed by the full dynamic analysis. Additionally, the forces acting on the separate concrete elements must be considered. In particular, those acting on the south dock element $BS4$. Similarly on the north docks, $BN3L1$ and $BS3$ are considered critical because of the wave direction. The time step between saved data points is set to 0.5 seconds. This is not optimal, but it has been used to keep down analysis time.

Ideally, a time step of 0.1 seconds or less should have been used.

5.2 Wave spectrum analysis

Firstly, the wave spectra presented in section 4.6.4 will be considered. The relative difference is of primary interest here, as the TMA spectrum is already most suitable to the model by definition. The peakedness difference is also quite important as the analysis will show the impact of the different recommendations given by DNV and the Norwegian standard for fish farms. The PM spectrum will not be included in the analysis as this serves no purpose. In this case the current will be set 0.1 m/s, as it is not the focus here. Only the components mentioned earlier in section 5.1 will be considered here. Additionally, thirty wave seed will be used here.

5.3 Current analysis

The current will be considered according to table 4.26. The current profiles will be the combined profiles established in figure 4.19. Here, the waves generated by the TMA spectrum for the 2013 Sande winter storm will be used, as they are the smallest TMA waves. The DNV peakedness factor is used as it is conservative. This will make the relative impact of the current larger and easier to identify. Again, thirty wave seeds are considered. The components from section 5.1 are used to evaluate the relative difference.

5.4 Dynamic analysis

A complete dynamic analysis is run on the floating docks for the 50 year Sande storm with waves generated by the DNV recommended TMA spectrum. A current velocity of 0.1 m/s is used. 30 wave seeds are used and a Gumbel probability distribution is made for every mooring line and dock element. The 90 percentile value is taken as the maximum force. Additionally, the critical components are considered with the DNV recommended 2013 Sande winter storm TMA spectrum, and the 2013 Gullholmen TMA spectrum.

5.5 Mooring tautness analysis

In the previous analyses the mooring lines are assumed to be taut, i.e. there is a tension of 2000 N in the lines. Now, the effect of snapping is investigated by reducing the tautness in the lines to 1000 N and 500 N. The analysis is done with the DNV recommended Sande 50 year storm TMA spectrum. The focus is put on the 50 year values as this corresponds to likely design values. The current is taken as 0.1 m/s. 30 wave seeds are used as the influence of snapping on the maximum force is of main interest. Here, a special model consisting only of the southern dock is used, as the model is quite sensitive to changes in the mooring lines. The tautness of the lines can be seen in figure 4.6.

5.6 Design wave analysis

Finally, a design wave analysis will be attempted in SIMA. The model will be restricted in its degrees of freedom in order to simulate a static model. Then the time domain simulation will be run for one wave period with a regular wave to simulate the wave stepping through the system. The conditions presented in table 4.23 for the 2013 Sande winter storm will be used. The current will be set to 0.1 m/s and the lines will be kept taut. Only the critical components will be considered. Since the model is restrained SIMA will not be able to calculate the mooring line tensions.

Chapter 6

Results

6.1 Current analysis results

The current analysis results are given in table 6.1 and table 6.2. The results are given for the three translational degrees of freedom of the most critical floating elements. Additionally, the force in the critical lines are noted. The results show that compared to the magnitude of the wave loads the current loads are quite small.

Table 6.1: Current analysis results for BN3

Current velocity [m/s]:	**0.1**	**0.3**	**0.5**
Surge x [N]:	2.07E+05	2.08E+05	2.09E+05
Sway y [N]:	3.09E+05	3.10E+05	3.13E+05
Heave z [N]:	1.23E+05	1.23E+05	1.23E+05
BN3L1 [N]:	3.21E+05	3.22E+05	3.23E+05
BN3L2 [N]:	2.95E+05	2.96E+05	2.97E+05

Table 6.2: Current analysis results for BS4

Current velocity [m/s]:	**0.1**	**0.3**	**0.5**
Surge x [N]:	4.52E+05	4.53E+05	4.55E+05
Sway y [N]:	1.01E+06	1.01E+06	1.02E+06
Heave z [N]:	3.00E+05	3.00E+05	3.00E+05
BS4L3 [N]:	7.78E+05	7.78E+05	7.80E+05
BS4L4 [N]:	5.57E+05	5.57E+05	5.59E+05

6.2 Wave spectrum analysis results

The wave spectrum analysis results are given for the same floating elements as in the previous section. The results are summarized in table 6.3 and table 6.4. There is little variation in the calculated results.

Table 6.3: Wave spectrum analysis results for BN3

Wave spectrum:	**Jonswap**	**Jonswap**	**TMA**	**TMA**
Peakedness factor:	**2.5**	**5**	**2.5**	**5**
Surge x [N]:	5.19E+05	5.19E+05	5.19E+05	5.19E+05
Sway y [N]:	6.05E+05	6.05E+05	6.05E+05	6.05E+05
Heave z [N]:	2.59E+05	2.59E+05	2.58E+05	2.59E+05

Table 6.4: Wave spectrum analysis results for BS4

Wave spectrum:	**Jonswap**	**Jonswap**	**TMA**	**TMA**
Peakedness factor:	**2.5**	**5**	**2.5**	**5**
Surge x [N]:	7.77E+05	8.77E+05	7.77E+05	7.77E+05
Sway y [N]:	1.65E+06	1.65E+06	1.65E+06	1.65E+06
Heave z [N]:	5.69E+05	5.69E+05	5.69E+05	5.69E+05

6.3 Dynamic analysis results

All calculated values may be found in Appendix C.2. There, one may also see some examples of the Gumbel distribution plots which were made for this paper. Here, the critical values are presented in tables 6.5 and B.1. The values found here may be considered as design values on account of that they are 90 percentile values. As one can note the loading in the critical mooring lines is larger than the capacity of the lines.

Table 6.5: Dynamic analysis results for BN3

Condition:	**Sande 50 year storm:**	**Sande 2013 storm:**	**Gullholmen 2013 storm:**
Surge x [N]:	5.19E+05	2.67E+05	4.97E+05
Sway y [N]:	6.05E+05	3.36E+05	5.69E+05
Heave z [N]:	2.59E+05	1.57E+05	2.53E+05
BN3L1 [N]:	6.22E+05	3.62E+05	6.07E+05
BN3L2 [N]:	5.93E+05	3.48E+05	5.90E+05

Table 6.6: Dynamic analysis results for BS4

Condition:	**Sande 50 year storm:**	**Sande 2013 storm:**	**Gullholmen 2013 storm:**
Surge x [N]:	8.77E+05	5.08E+05	9.01E+05
Sway y [N]:	1.65E+06	1.26E+06	1.51E+06
Heave z [N]:	5.69E+05	4.05E+05	5.71E+05
BS4L3 [N]:	1.30E+06	1.03E+06	1.27E+06
BS4L4 [N]:	1.29E+06	8.00E+05	1.28E+06

Figure A.2 showing the tension in all the mooring lines for the Sande 50 year design storm. One can see that all design values exceed the max capacity $3.0E+05$ N of the mooring lines, with the exception of the south dock land lines.

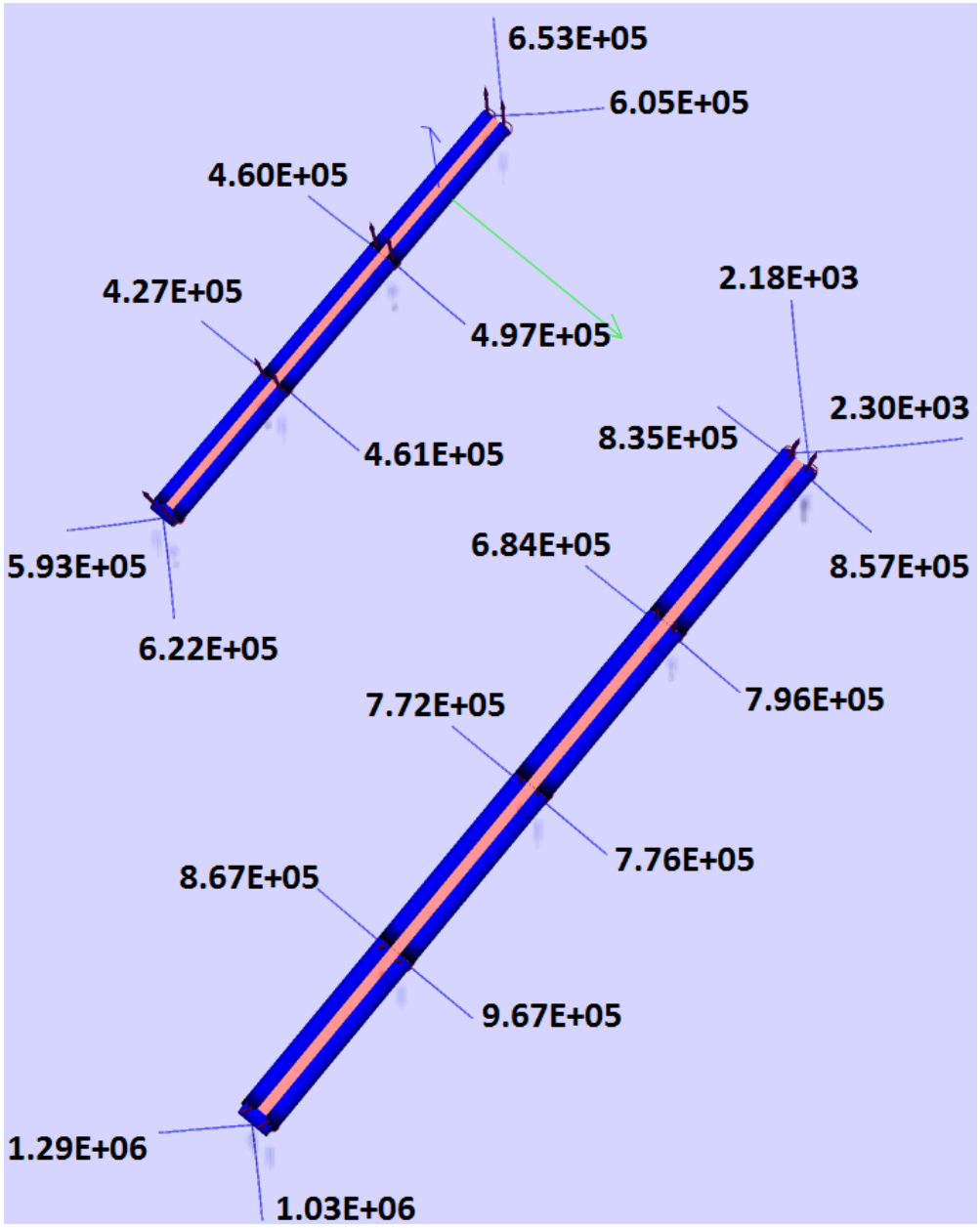

Figure 6.1: Proposed 50 year design values for the mooring lines of the floating docks

6.4 Mooring line analysis results

The results from the mooring line tension analysis are given for the critical elements of the southern floating dock. They are shown in table 6.7. An increase in total force is seen when the line pretension is decreased from 2000 N to 1000 N. When the line pretension is further decreased the forces acting on the floating dock decrease somewhat. However, the force in the critical line BS4L3 remains significantly higher for the 500 N case than for the 2000 N case.

Table 6.7: Mooring line pretension analysis results for BS4

Line tension [N]:	**2000**	**1000**	**500**
Surge x [N]:	3.77E+05	4.95E+05	4.93E+05
Sway y [N]:	7.38E+05	9.93E+05	7.14E+05
Heave z [N]:	4.35E+05	5.02E+05	4.12E+05
BS4L3 [N]:	5.40E+05	7.14E+05	7.04E+05
BS4L4 [N]:	6.60E+05	7.19E+05	6.86E+05

6.5 Design wave analysis results

The results are given in table 6.8. Here, one can see that there is some ambiguity as whether or not these forces are sufficient to cause failure in the mooring lines. The surge force is the only force which exceeds the capacity of the mooring lines. Likely, this would still likely overload the mooring lines.

Table 6.8: Design wave method results for the 2013 Sande winter storm

Element:	**BN3**	**BS4**
Surge x [N]:	7.82E+05	4.92E+05
Sway y [N]:	4.22E+04	5.57E+04
Heave z [N]:	1.38E+05	1.26E+05

6.6 Animation of the results

An animation of the results has been attached to the electronic version master. This motion of the floating docks model is compared with recorded footage of the motion of the floating docks. The footage in question is taken under a smaller storm, however one can see still see that the behaviour of the model is relatively similar to the motion of the floating docks. It is possible that the movement between elements is slightly too stiff in the model. Additionally, one can see that the mooring lines are not as taut in the recording as in the model. This could be due to low tide at the time of the recording, or it could be a result of the damage the floating dock structure suffered in 2013. The animation also shows that there are waves breaking on the southern dock. This could potentially be a source of peak forces acting on the floating dock structure, in the form of slamming forces. These forces are not accounted for in the dynamic analyses.

Chapter 7

Discussion of results

7.1 Current

The results show that the current forces are negligible in this case. This is not necessarily true for all floating docks, as the case studied here is subjected to large wave loads. For a more standard floating docks the current forces could be significant. The main issue here is that the current forces are derived based on current velocity and the structure composition. Therefore, whether or not the current forces are important, depends entirely on the magnitude of the wave forces acting on the structure. Obviously, it is entirely possible that the current velocities used in this report are too small. In order to accurately calculate the current forces it is necessary to measure the current velocities locally. Especially in coastal waters where the tide current can vary greatly from place to place, and the wind current may be influenced by fetch length. The current velocities used here were taken from *Norsk Standard NS 9415 Flytende oppdrettsanlegg Krav til utforming, dimensjonering, utførelse, installasjon og drift* [5] . In this case, one can not comment on the accuracy of these values as there is no observed data on the local current velocities.

7.2 Wave spectra

The wave spectra results give nearly identical total forces. This could be construed as evidence showing that the wave spectra do not need to be chosen very accurately. However, the more likely explanation here is that the time step between saved data points is too large. As the differ-

ence between the spectra is mostly seen in their peaks, it is possible that the highest peak values have been left out. The time step between saved data points is large in order to keep the analysis time down. Choosing the 90 percentile value in the Gumbel distribution of the maximum values should be able to somewhat account for the possible underestimation. Regardless of the results found here, the TMA spectrum should still be used as it is theoretically the best fit for shallow water conditions. No conclusion can be made with respect to the peakedness factor, other than that using the DNV peakedness factor will be more conservative.

7.3 Dynamic analysis

The dynamic analysis shows that the 50 year Sande storm overloads the floating docks completely. The Sande 2013 winter storm also overloads the docks. The latter results indicates that the analysis is likely overestimating the loading on the floating docks. As they imply that nearly all the mooring lines should have failed. This is simply explained by the fact that the 90 percentile Gumbel values have been chosen. These values are quite rare, as can be seen in appendix C.1 where the Gumbel plots show that out of 30 considered storms the 90 percentile values are rarely exceeded more than once. Nevertheless, even a single Sande 2013 winter storm induces failure loads in critical the mooring lines such that one can assume that the model is a reasonable and somewhat conservative representation of reality. The animation attached electronically to this paper, shows that the motion of the floating docks is quite similar to the motion of the floating docks model. The floating docks system appears to be quite under-dimensioned, as the 2013 Sande winter storm corresponds roughly to the yearly winter storm.

Ideally, the mooring lines should be dimensioned after the 50 year design values. This would imply that $BS4L3$ and $BS4L4$ would need a to have a capacity of 130 tons. The other lines could be covered by 90 ton capacity lines. Obviously, this is an extreme upgrade as the old lines only have a capacity of 30 tons. Additionally, the anchors would have to be upgraded to hold the fully loaded mooring lines. The 2013 winter storm corresponded roughly to the yearly winter storm, and this storm was strong enough to exceed the 30 tons capacity of certain lines. As such a three times increase in capacity does not seem unreasonable. The 50 year design storm is naturally a

lot stronger than the 2013 winter storm.

The 2013 Gullholmen results were calculated to investigate the conditions out in the Oslo fjord, as the majority of the fetch length in this case lies across it. It very difficult to tell whether or not the Sande wind conditions or the Gullholmen wind conditions are the most appropriate ones without local significant wave height measurements. The Sande values are taken here as the floating docks system lies within the Sande county. One can note that the Gullholmen values are very similar to the Sande 50 year values, this does make it likely that the Gullholmen values are too large as if the 2013 winter storm were of such a magnitude, the floating docks system would have been torn completely loose from its mooring.

The dynamic analysis and the floating docks model have some limitations which have mostly been discussed in previous parts. The most important sources of error will be briefly discussed here. The main concern is the time step used between saved data points. The wave spectra analysis strongly suggests that the peak values are being underestimated. If similar analyses are to be run one should consider this. The 90 percentile Gumbel extreme values should mitigate this issue. The second greatest concern is the shallow water condition and the coastal waters. The water depth has been accounted for as much as possible. However, factors such as marine growth and sea surface friction have not been considered. There is reason to believe that the water particle orbitals of the waves could be influenced by extensive marine growth, by either the damping of wave force or by a reduction of the effective depth. This is a concern because of the relative size of the significant wave height when compared to the water depth. The former phenomenon would be conservative, whereas the latter would increase the wave loads. One must also comment on the estimation of the significant wave height and the peak period. The calculated values have not been substantiated by observed values. It is therefore somewhat difficult to assess their accuracy. The dynamic analysis results do, however indicate that the values should be somewhat trustworthy. Finally, the lack of accurate mooring line data is a significant cause for concern, but this point will be elaborated on in the next section.

7.4 Mooring line tension

The main purpose of this analysis was to check the effect of snapping. To this end the mooring line tensions are varied. This could simulate the loss of tension in a line due to low tide or due to movement of the mooring line anchor. The important thing to note here is that the most important factor is not the mooring line tension, but rather the geometrical shape of the mooring line. In this case the mooring line is taut for a pretension of 2000 N, whereas it is not for pretensions of 1000 N and 500 N. The results reflects this affirmation. A significant increase in mooring line tension is seen when the pretension is lowered to a 1000 N. The increase is equivalent of a 16 ton load increase on the critical lines. This corresponds to the line going from taut to slack. Indeed, when the mooring line pretension is further reduced to 500 N, the load on the mooring lines remains quite similar, as the lines have just become somewhat slacker. The results show that great care should be taken to the configuration of the mooring line. If the mooring lines are designed to be taut, it is very important that they remain that way, or are strong enough to with stand any potential snapping forces.

Mooring lines in shallow waters are very dependent on accurate modeling, as small inaccuracies will be relatively more important for shorter lines. This is a concern in this case, as Bi-Brygga AS did not have accurate data for the mooring lines in this case. Rather, a rule of thumb was used to determine the length of the lines. This is a source of inaccuracies as the length of the mooring line directly influences the tension in the mooring line. It is not possible to say whether or not the chosen mooring line length is conservative or nonconservative. The relatively extreme conditions considered in this paper, leave little room for experimentation with the mooring line length, as several parameters must be changed when ever the mooring line length is changed in order for the model to function. A case with less extreme conditions would be better suited for this particular investigation.

7.5 Design wave method

The design wave method is investigated as a possible simplified method for calculating the extreme wave forces acting on the floating docks system. The first thing to note is that only the

2013 Sande winter storm is used due to the required wave height. For the other cases the wave height becomes larger than the water depth. The results found are a smaller than the results obtained from the dynamic analysis. This is not too surprising as the design wave method does not account for shallow water effects. It is unlikely that the design wave method can be used to estimate design wave forces. One could consider increasing the wave height in order to increase the forces obtained by the design wave method, however this is not likely to be a good solution as the local conditions are quite important for floating docks. A general method would have to be very conservative in order to be applicable for all conditions.

7.6 Simplified wave model

The model established in SIMA is essentially a slender element model. This means that the wave forces are calculated with Morison's equation. Using this approach one can obtain the wave forces acting on the floating dock elements. These forces must then be transferred to the mooring lines, and to the coupling elements connecting the floating dock elements. Clearly, the system is quite complicated. In the previous the design wave method was shown to be unreliable. Therefore it seems necessary to use the dynamic analysis approach used in this paper or a similar method. A static analysis will not properly account for the dynamic effects.

7.7 Further work

The work done in this paper should if possible be substantiated by another analysis done on a another floating docks system. This system should not be an extreme case, as the mooring line modeling in SIMA is very sensitive for shallow water depths. Ideally, the environmental data should be based on observations rather than calculated values based on wind velocities. One should also consider whether or not a 50 year design lifetime is appropriate for a floating docks system. More analyses would then help to determine which of the methods used in this paper are fit to be used in a potential standard for the design of floating docks.

The mooring line tautness was found to be quite important, with this in mind one could con-

sider designing a mooring line system which can maintain the tautness of the line despite of for example low tide. This could be achieved with an additional anchor attached between the main anchor and the mooring line connection point. The anchor would be light enough to float at high tide and yet heavy enough to rest on the sea bottom at low tide, thusly maintaining line tautness. Certainly, such a system would be worth employing for the case considered in this paper as it could potentially remove up to 16 tons of extra loading on the mooring lines.

Finally, the importance of wave breaking should be investigated, as this phenomenon could easily create the largest loads acting on the floating dock system, in the form of slamming loads.

Chapter 8

Conclusion

The design of floating docks is not yet standardized in Norway. In this paper a study of relevant literature and methods was done in order to establish a model of a floating docks system. Case data was supplied by Bi-Brygga AS. Marintek's program SIMA was used to establish a SIMO model. The model was subjected to varying current forces, different wave spectra and varying mooring line pretensions. Full dynamic analyses were run based on a 50 year design storm in Sande county. Additionally, a 2013 winter storm in Sande county and a 2013 winter storm on Gullholmen were considered. Finally, the design wave method was applied to the model and evaluated.

The results showed that the current forces were not important for the studied floating docks system. The wave spectra were found to be very similar. This was likely explained by sub-optimally chosen analysis parameters. The dynamic analysis showed that the 50 year design values all exceeded the capacity of the floating docks mooring line system. For the 2013 Sande winter storm several lines were found to be inadequate. The dynamic analysis indicated that the floating docks system is under-dimensioned. Indeed, the storm which caused the floating docks to fail corresponds to a yearly winter storm. The capacity of the mooring lines must be three times greater than what they currently are if the mooring line system is to survive the 50 year design storm.

The mooring line pretension analysis revealed that the geometrical tautness of the line is im-

portant. When the mooring lines slacken the peak forces in the lines drastically increases due to snapping forces. The design wave method was found to be underestimating the forces acting on the system. This was explained to be due to the fact that the design wave method does not accurately account for the dynamic effects acting on the floating docks system. The complex nature of the floating docks system makes it relatively hard to establish an accurate simplified wave model for floating docks. The SIMO model approach is considered to be the simplest accurate method for the estimation of wave forces acting on a floating dock system.

In conclusion, one can say that this paper has presented a possible method for estimating extreme wave loads acting on a floating dock system. The accuracy of the proposed method needs to be substantiated with other case studies done on different floating docks systems.

Appendix A

Wind statistics

In this appendix the wind data used when establishing the Weibull distributions will be presented. The table is somewhat truncated in order to fit it into the paper. The actual tables are more detailed for the higher wind velocity values.

Sande wind statistics

26990 observasjoner for alle tilgjengelige måneder. 1995-2014

FF	<=	0.1	1.1	2.1	3.1	4.1	5.1	6.1	7.1	8.1	9.1	10.1	11.1	12.1	13.1	14.1	15.1	16.1	17.1	18.1	19.1	>	Sum	Rel.fr.	Kum.fr.
(NMT)	0.0	1.0	2.0	3.0	4.0	5.0	6.0	7.0	8.0	9.0	10.0	11.0	12.0	13.0	14.0	15.0	16.0	17.0	18.0	19.0	20.0	20.0			
24	97	801	822	573	412	226	124	72	26	21	10	8										4	3196	3.8	3.8
01	102	801	833	570	461	246	115	53	37	18	11	6		1								3	3257	3.9	7.7
02	99	805	744	587	441	256	127	73	25	18	6	6							1		1	3	3192	3.8	11.6
03	111	758	789	573	463	257	121	61	25	17	8	2		2	1			1				2	3191	3.8	15.4
04	106	778	821	601	445	264	126	56	29	15	4	6		2			1					4	3258	3.9	19.3
05	110	769	751	611	439	278	115	68	18	22	8	4	1			1	1					2	3198	3.8	23.1
06	108	709	754	639	478	262	129	64	23	15	5	1	2	1			1					4	3195	3.8	27.0
07	562	1181	722	1143	488	705	147	192	33	22	55	4		12			1	1				3	5271	6.3	33.3
08	89	650	653	648	533	330	145	73	40	20	7	3	2	2								3	3198	3.8	37.1
09	67	571	640	695	566	333	171	85	44	21	10	3	3	1								2	3212	3.9	41.0
10	62	513	639	718	573	373	208	88	37	27	15	5	1									3	3262	3.9	44.9
11	38	419	597	708	619	399	220	112	60	20	12	3	1	2						1		4	3215	3.9	48.7
12	47	371	574	679	662	432	219	135	47	25	10	7	3	1								4	3216	3.9	52.6
13	226	746	576	1286	666	1018	229	362	54	33	63	2	2	11								4	5278	6.3	58.9
14	45	344	527	688	689	461	242	111	68	27	8	7	2	2								3	3224	3.9	62.8
15	40	316	547	731	648	438	282	118	62	22	10	3	2	1	2				1			2	3225	3.9	66.7
16	39	379	562	765	673	396	228	107	65	26	6	7	2	1								3	3259	3.9	70.6
17	53	420	609	686	682	369	205	106	46	22	2	4	2	1						1		3	3211	3.9	74.4
18	66	488	660	728	589	350	155	92	34	26	10	5		1	1					1		3	3209	3.8	78.3
19	381	1207	756	1242	526	702	145	195	48	14	41	3	1	9	3					1		2	5276	6.3	84.6
20	98	644	749	685	470	261	134	75	43	13	9	7	1	1		1					1	4	3196	3.8	88.4
21	112	702	795	611	451	253	128	67	37	17	8	3	1	2							1	4	3192	3.8	92.3
22	96	779	834	616	443	248	119	67	26	15	9	3		1	1		2					3	3262	3.9	96.2
23	102	777	804	614	391	235	138	73	30	17	5	2	5	1	1							3	3198	3.8	100.0
Sum	2856	15928	16758	17397	12808	9092	3972	2505	957	493	332	104	31	55	9	2	6	2	2	4	3	75	83391		
Rel.fr.	3.4	19.1	20.1	20.9	15.4	10.9	4.8	3.0	1.1	0.6	0.4	0.1	0.0	0.1	0.0	0.0	0.0	0.0	0.0	0.0	0.0	0.1		100.0	
Kum.fr.	3.4	22.5	42.6	63.5	78.8	89.7	94.5	97.5	98.7	99.3	99.6	99.8	99.8	99.9	99.9	99.9	99.9	99.9	99.9	99.9	99.9	100.0			
Middel	0.0	0.6	1.6	2.5	3.5	4.5	5.5	6.5	7.5	8.5	9.6	10.5	11.3	12.4	13.5	14.4	15.5	16.6	17.4	18.8	19.7	53.8			
St.av.	0.0	0.3	0.3	0.3	0.3	0.3	0.3	0.3	0.3	0.3	0.3	0.3	0.3	0.3	0.3	0.2	0.2	0.1	0.4	0.4	0.3	13.4			

Figure A.1: Gullholmen recorded 10 meter wind height velocities [m/s]

Gullholmen wind statistics

17280 observasjoner for alle tilgjengelige måneder. 2000-2014

FF	<=	0.1	1.1	2.1	3.1	4.1	5.1	6.1	7.1	8.1	9.1	10.1	11.1	12.1	13.1	14.1	15.1	16.1	17.1	18.1	19.1	>	Sum	Rel.fr.	Kum.fr.
(NMT)	0.0	1.0	2.0	3.0	4.0	5.0	6.0	7.0	8.0	9.0	10.0	11.0	12.0	13.0	14.0	15.0	16.0	17.0	18.0	19.0	20.0	20.0			
24	77	178	508	705	710	660	567	470	348	263	169	139	98	57	33	25	12	6	5	5	3	4	5042	4.2	4.2
01	81	217	463	692	769	669	542	455	360	254	178	130	86	49	41	18	14	8	3	3	6	4	5042	4.2	8.3
02	77	197	487	698	758	667	566	444	339	262	194	122	89	50	29	26	13	7	4	3	3	7	5042	4.2	12.5
03	76	205	521	685	775	630	555	452	336	250	178	132	85	60	33	26	16	9	7	3	2	6	5042	4.2	16.7
04	80	205	503	727	748	647	505	453	361	247	183	139	81	60	37	25	14	10	5	3	2	5	5040	4.2	20.8
05	73	210	489	725	738	665	519	429	319	293	182	149	87	57	39	25	18	8	4	3	3	5	5040	4.2	25.0
06	78	202	511	742	699	655	535	443	346	272	168	130	84	67	48	26	15	8	2	3	4	3	5041	4.2	29.2
07	62	215	521	721	721	636	539	449	361	256	162	128	88	68	55	20	18	7	4	3	6	2	5042	4.2	33.3
08	53	220	558	719	689	609	536	467	335	266	185	134	86	72	35	35	18	8	5	3	5	3	5041	4.2	37.5
09	64	210	617	669	664	589	527	472	356	287	167	129	107	60	51	24	22	12	4	6	3	1	5041	4.2	41.7
10	66	207	623	637	658	566	477	476	400	290	214	148	87	68	43	33	21	14	5	2	2	4	5041	4.2	45.8
11	69	198	606	618	626	493	522	506	377	295	229	207	102	65	47	34	19	15	4	4	2	3	5041	4.2	50.0
12	60	196	593	579	552	556	491	463	414	315	262	206	132	79	59	35	24	15	5	2	1	3	5042	4.2	54.2
13	67	205	518	539	538	552	539	444	401	346	297	221	151	87	53	32	19	17	3	9	3	1	5042	4.2	58.3
14	65	178	455	518	533	543	523	521	415	377	309	221	166	83	57	29	22	14	7	2	2	3	5043	4.2	62.5
15	62	174	438	475	526	520	555	518	442	393	312	242	166	95	50	25	17	17	9	3	2	3	5044	4.2	66.7
16	60	143	390	487	535	536	572	519	482	393	344	226	134	95	48	32	20	12	5	4	4	2	5043	4.2	70.8
17	64	149	355	509	529	568	605	514	484	392	325	210	136	83	46	28	15	15	4	6	2	4	5043	4.2	75.0
18	58	161	382	552	562	590	567	508	505	401	281	181	117	65	35	39	13	8	5	5	2	6	5043	4.2	79.2
19	64	155	398	556	626	622	571	535	451	375	251	157	101	67	49	30	12	7	7	3		5	5042	4.2	83.3
20	68	161	440	568	665	650	599	474	440	335	236	139	91	66	42	27	18	7	9	2	2	3	5042	4.2	87.5
21	67	167	459	646	720	619	548	511	395	277	231	135	95	67	52	24	11	7	4	3	1	3	5042	4.2	91.7
22	75	186	465	678	687	668	565	457	385	291	203	139	79	59	38	26	15	7	6	7	3	2	5041	4.2	95.8
23	72	196	501	674	693	696	562	450	374	285	163	121	89	57	42	26	14	10	2	5	5	4	5041	4.2	100.0
Sum	1638	4535	11801	15119	15721	14606	13087	11430	9426	7415	5423	3885	2537	1636	1062	670	400	248	118	92	68	86	121003		
Rel.fr.	1.4	3.7	9.8	12.5	13.0	12.1	10.8	9.4	7.8	6.1	4.5	3.2	2.1	1.4	0.9	0.6	0.3	0.2	0.1	0.1	0.1	0.1		100.0	
Kum.fr.	1.4	5.1	14.9	27.3	40.3	52.4	63.2	72.7	80.5	86.6	91.1	94.3	96.4	97.7	98.6	99.2	99.5	99.7	99.8	99.9	99.9	100.0			
Middel	0.0	0.7	1.6	2.6	3.5	4.5	5.5	6.5	7.5	8.5	9.5	10.5	11.5	12.5	13.5	14.5	15.5	16.5	17.5	18.5	19.5	22.8			
St.av.	0.0	0.3	0.3	0.3	0.3	0.3	0.3	0.3	0.3	0.3	0.3	0.3	0.3	0.3	0.3	0.3	0.3	0.3	0.3	0.3	0.3	2.9			

Figure A.2: Gullholmen recorded 10 meter wind height velocities [m/s]

Appendix B

Wave seeds

Here, the random wave seeds used in the dynamic analyses are presented:

Table B.1: Wave seeds used in the dynamic analyses

Seed number:	**Wave seed:**	**Seed number:**	**Wave seed:**
1	6	**16**	161
2	28	**17**	211
3	49	**18**	230
4	76	**19**	235
5	83	**20**	244
6	85	**21**	248
7	104	**22**	249
8	110	**23**	252
9	122	**24**	257
10	123	**25**	270
11	138	**26**	304
12	140	**27**	313
13	147	**28**	337
14	158	**29**	348
15	159	**30**	355

Appendix C

Additional dynamic analysis results

C.1 Critical Gumbel distributions:

The Gumbel distributions are given for elements BN3 and BS4.

Sande 50 year storm

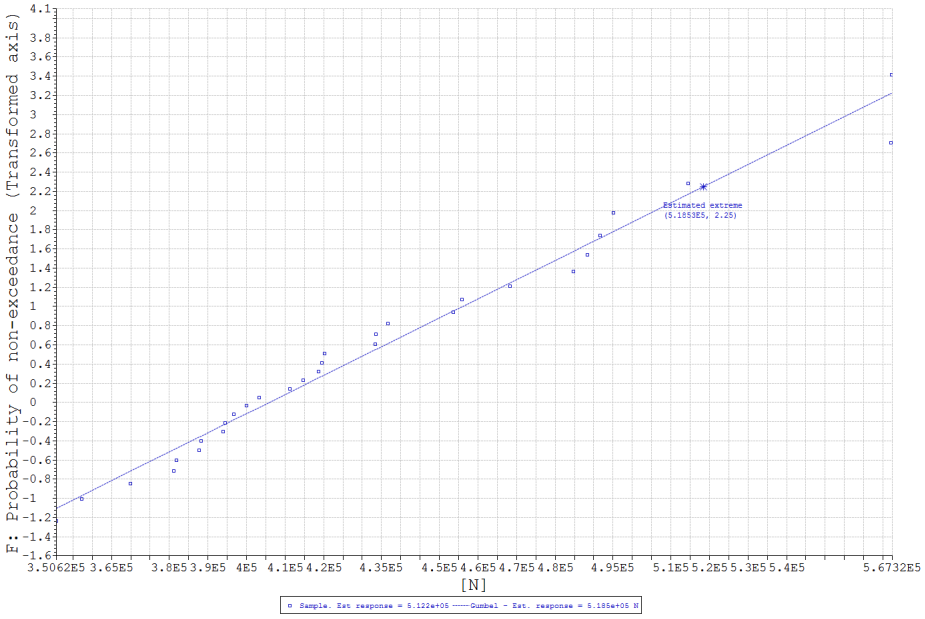

Figure C.1: Gumbel distribution for the BN3 surge force.

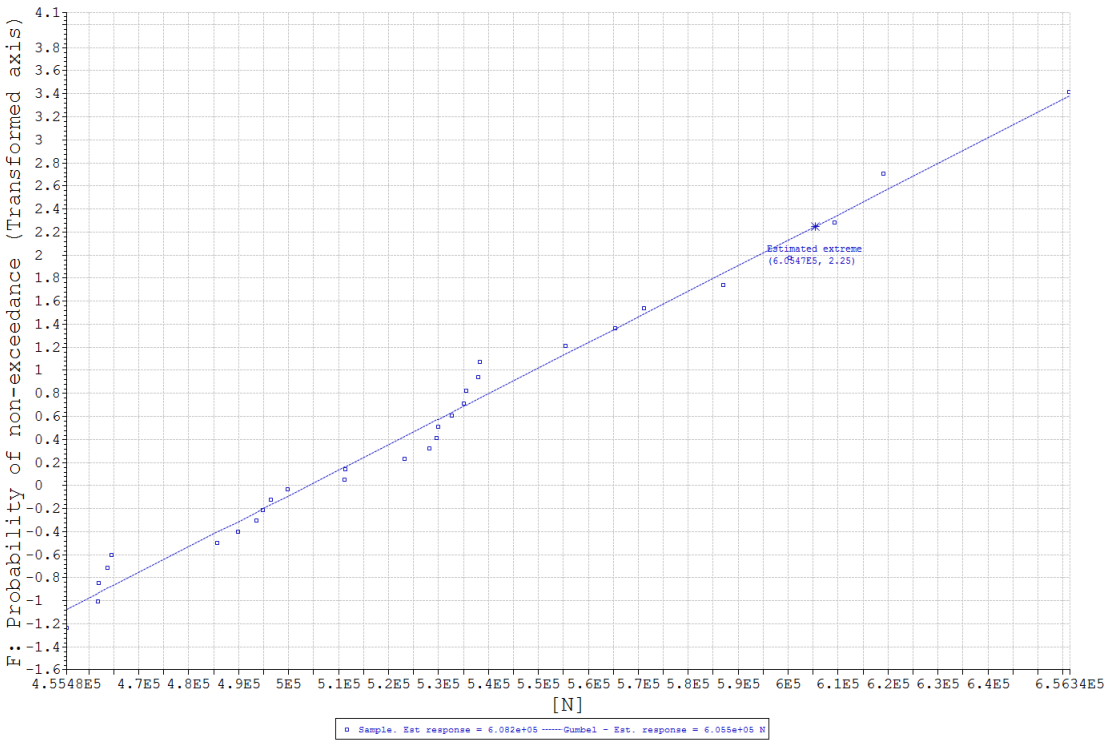

Figure C.2: Gumbel distribution for the BN3 sway force

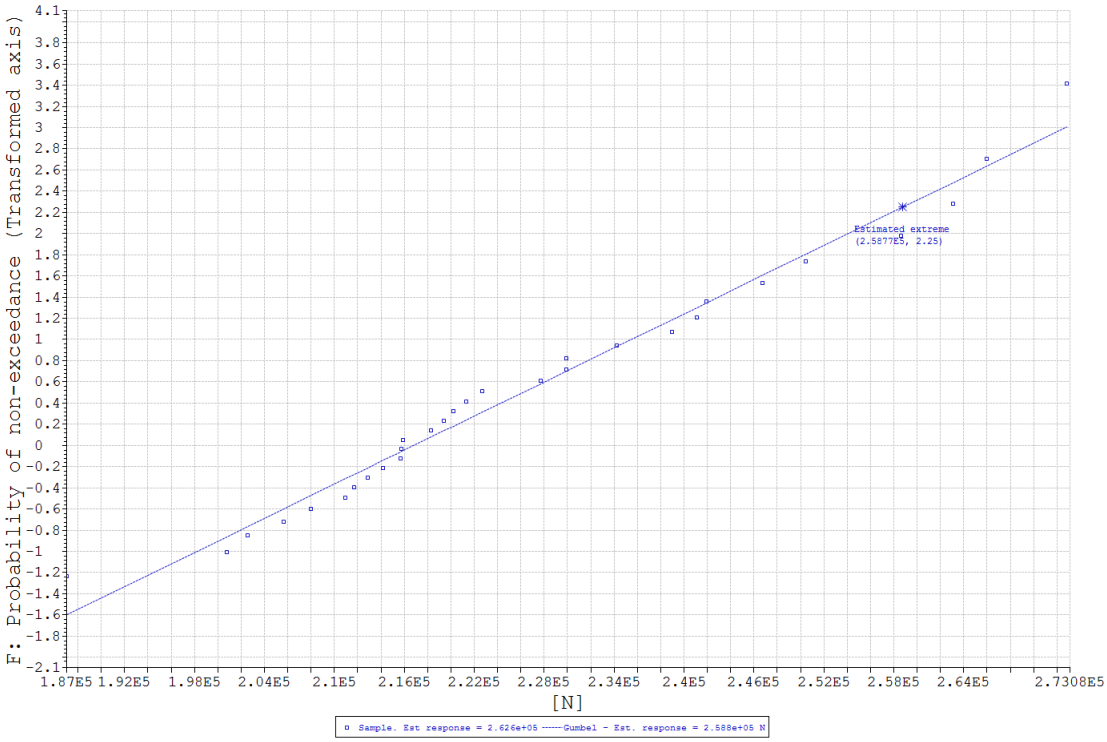

Figure C.3: Gumbel distribution for the BN3 heave force

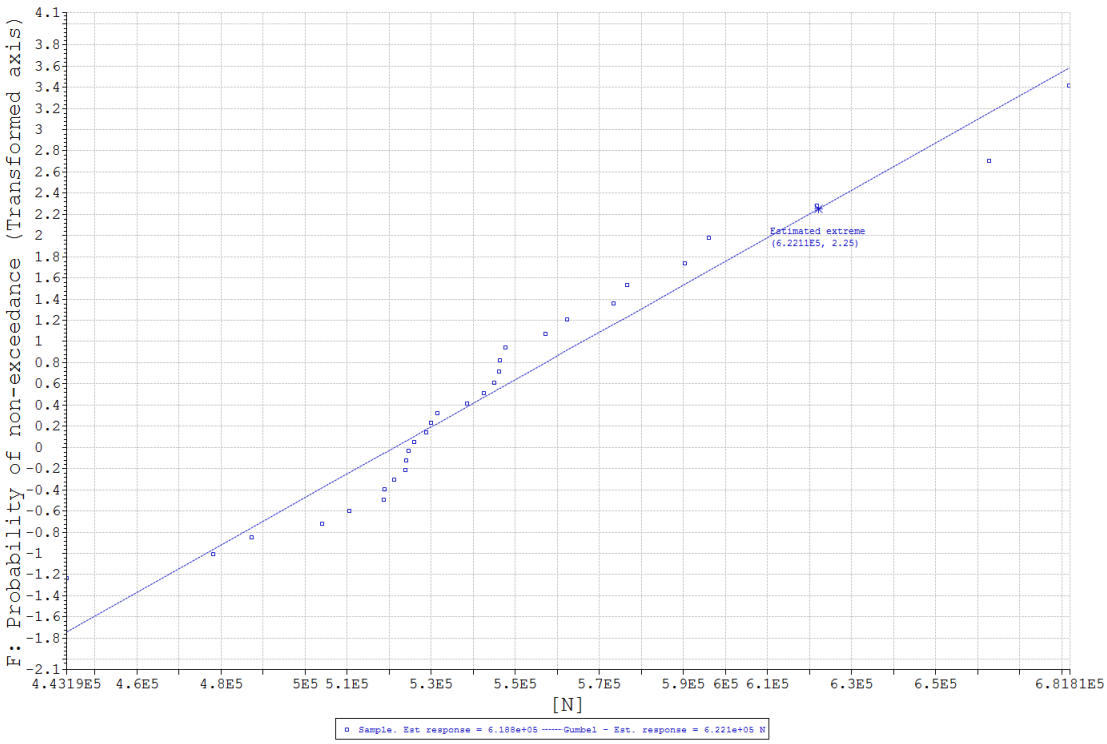

Figure C.4: Gumbel distribution for BN3L1

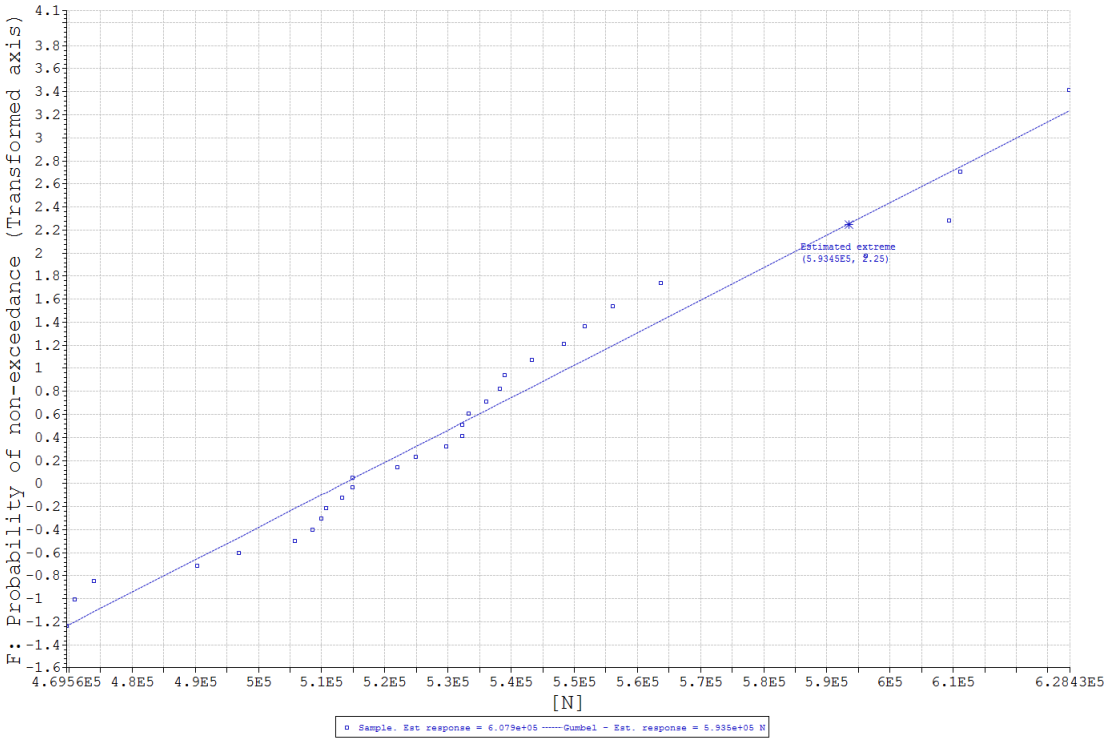

Figure C.5: Gumbel distribution for BN3L2

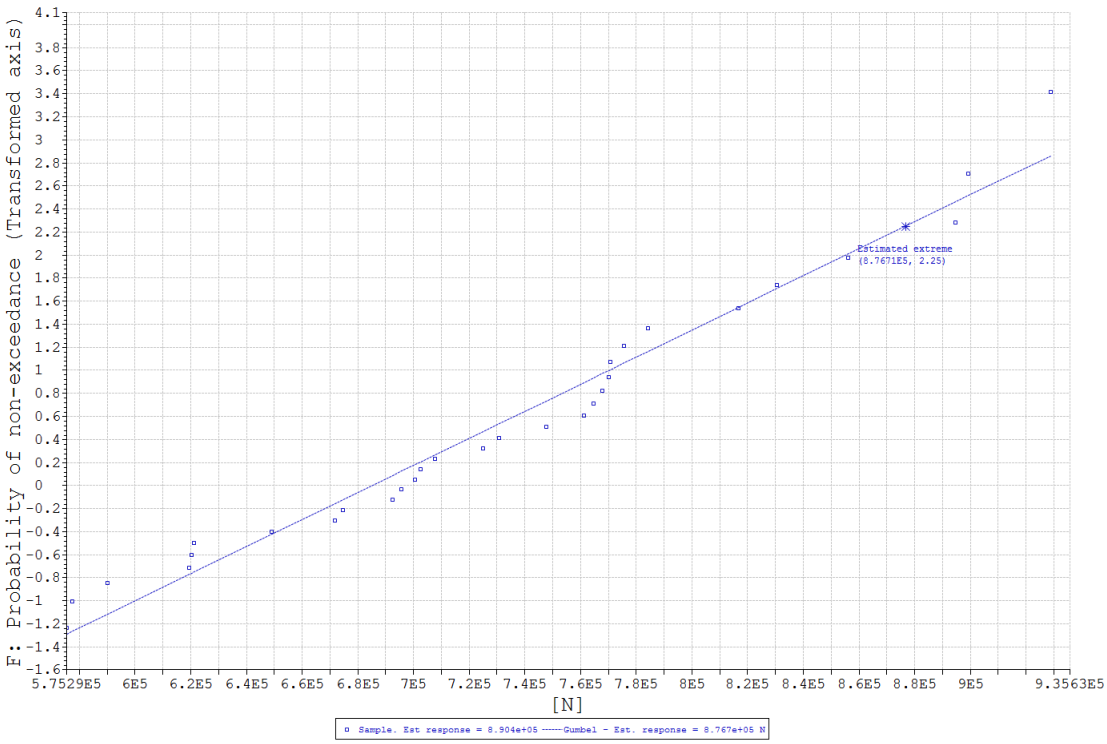

Figure C.6: Gumbel distribution for the BS4 surge force.

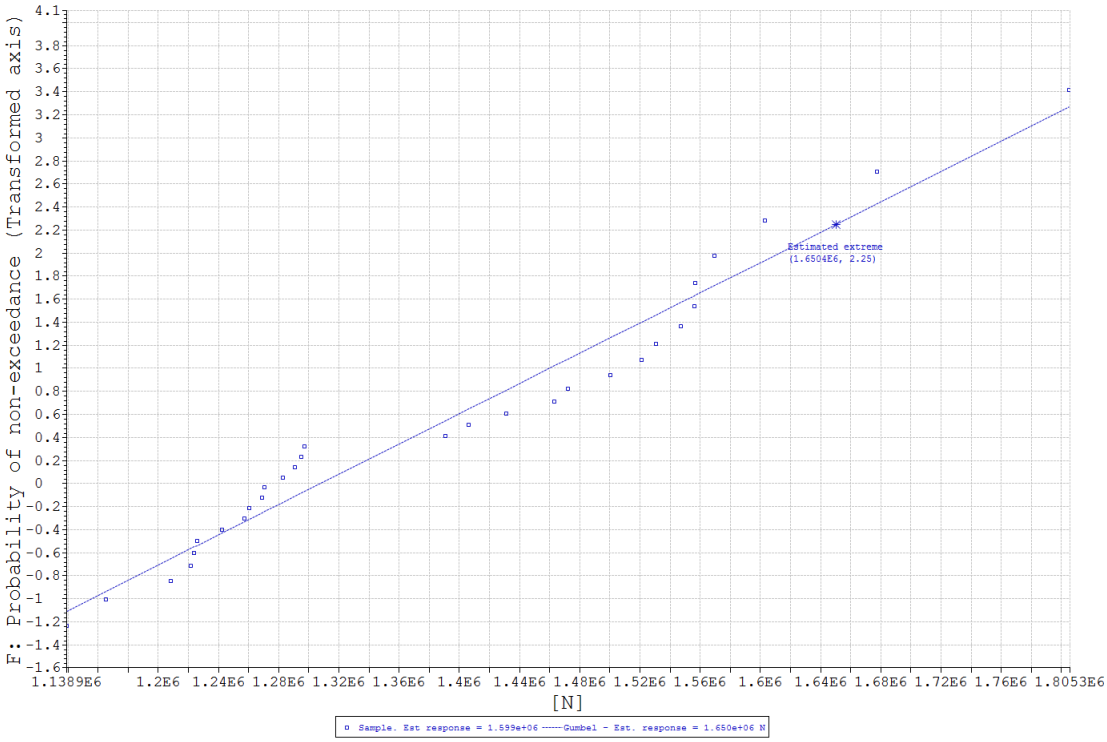

Figure C.7: Gumbel distribution for the BS4 sway force

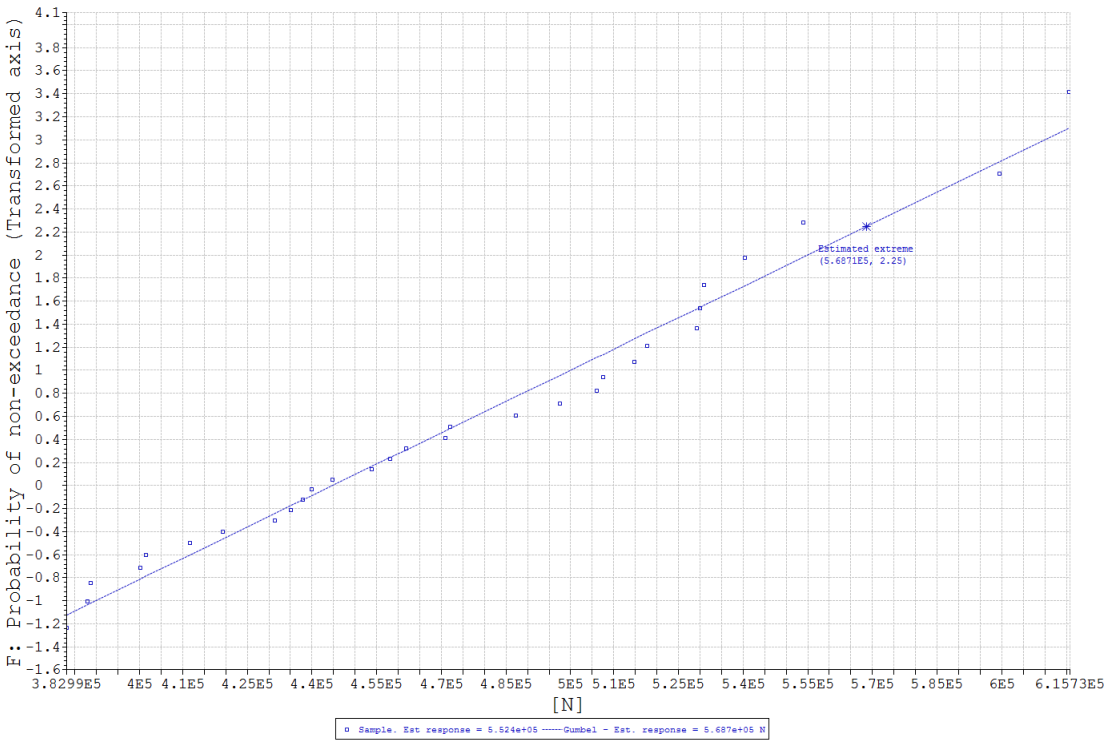

Figure C.8: Gumbel distribution for the BS4 heave force

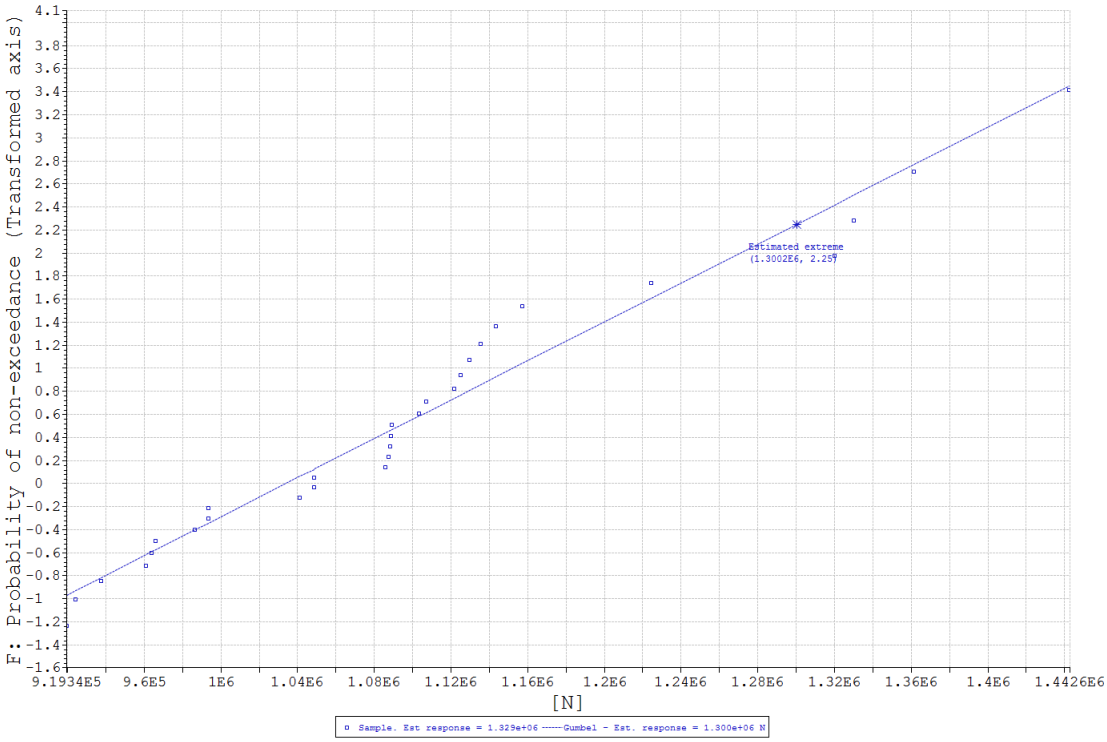

Figure C.9: Gumbel distribution for BS4L3

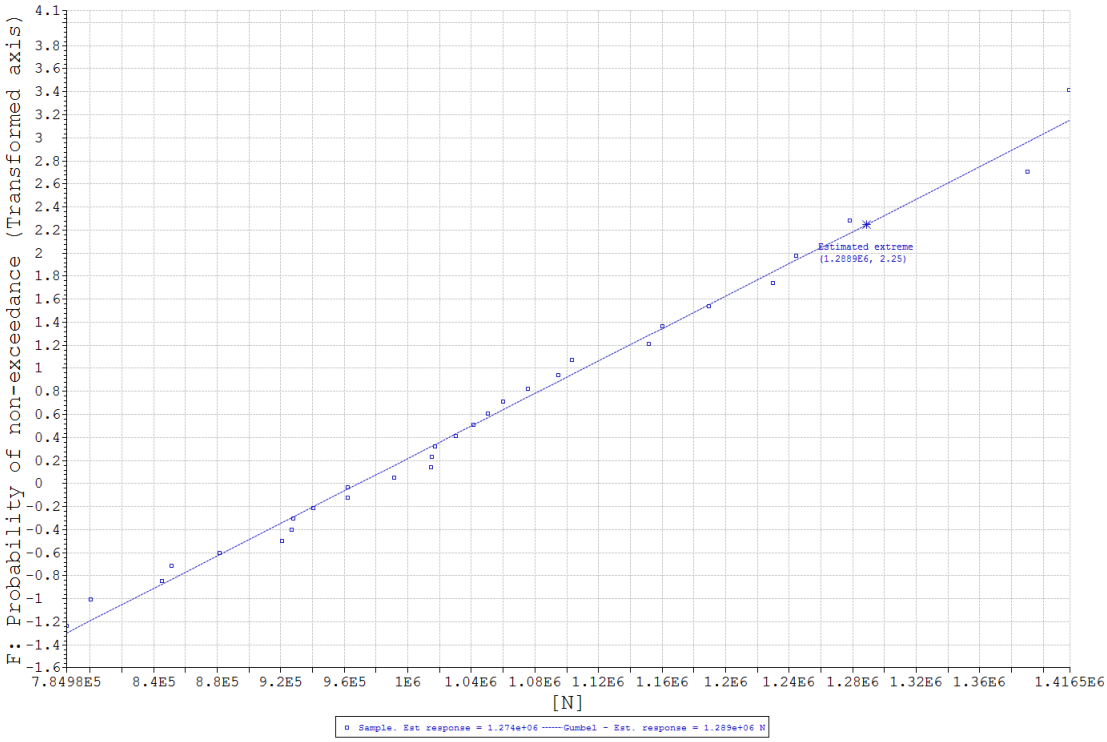

Figure C.10: Gumbel distribution for BS4L4

Sande 2013 winter storm

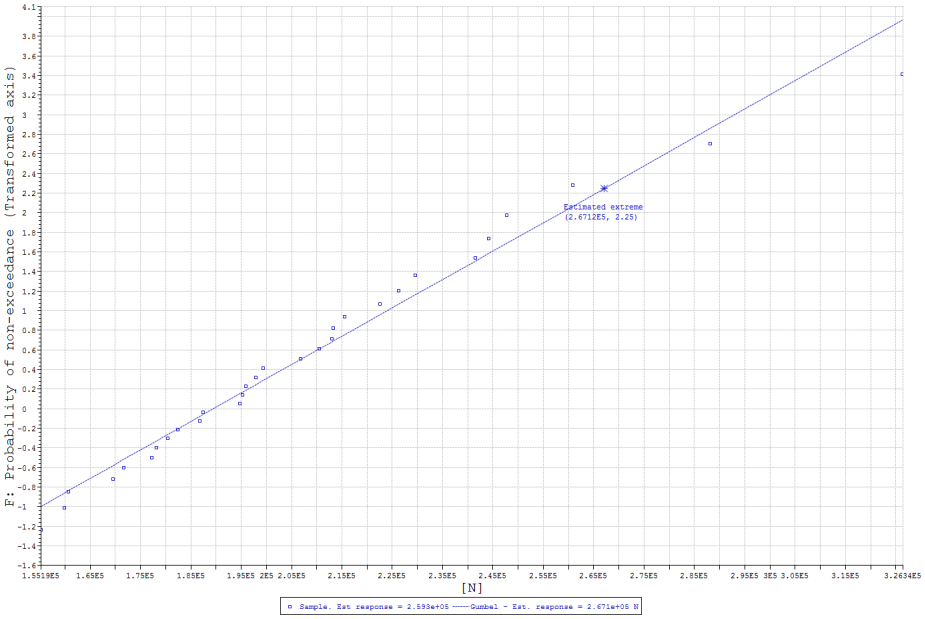

Figure C.11: Sande 2013 winter storm. Gumbel distribution for the BN3 surge force.

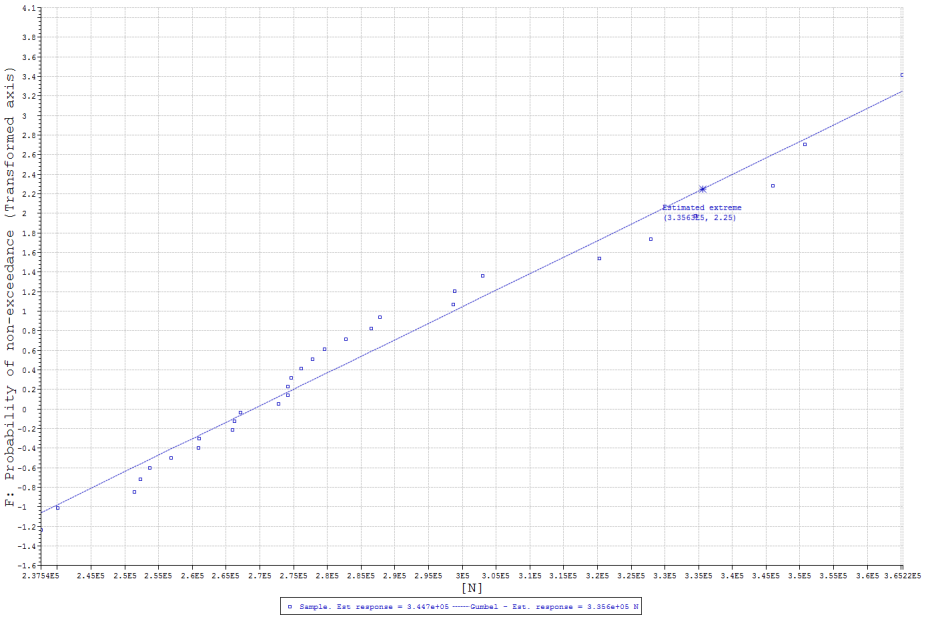

Figure C.12: Sande 2013 winter storm. Gumbel distribution for the BN3 sway force

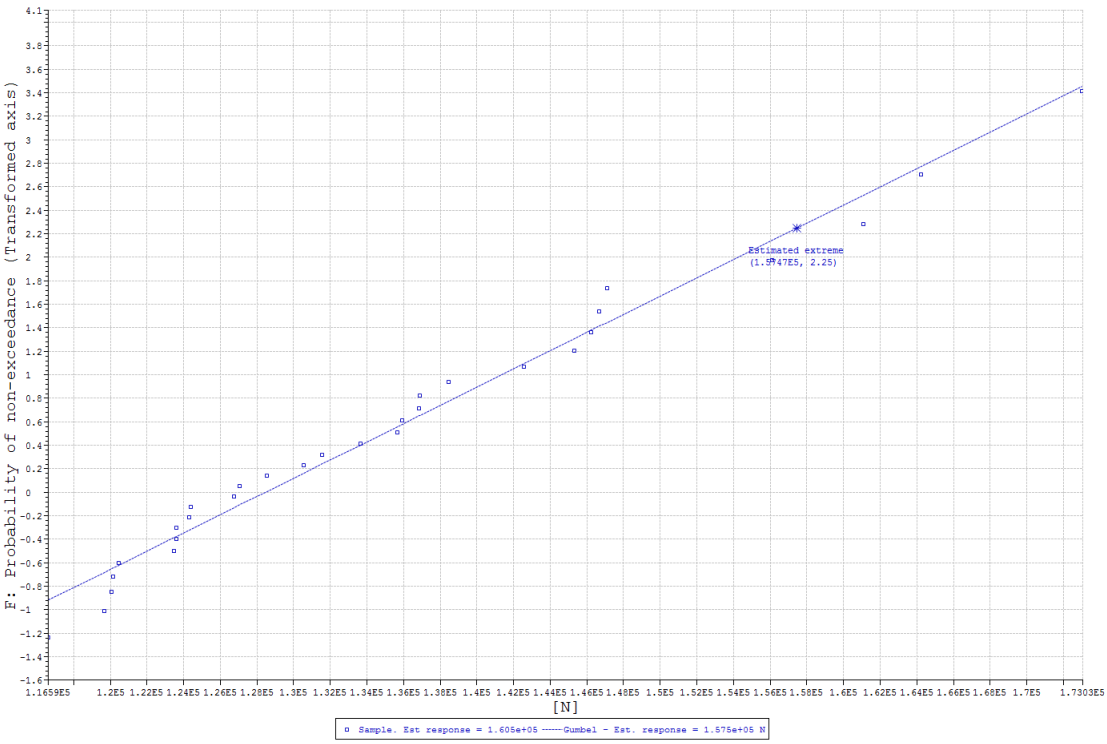

Figure C.13: Sande 2013 winter storm. Gumbel distribution for the BN3 heave force

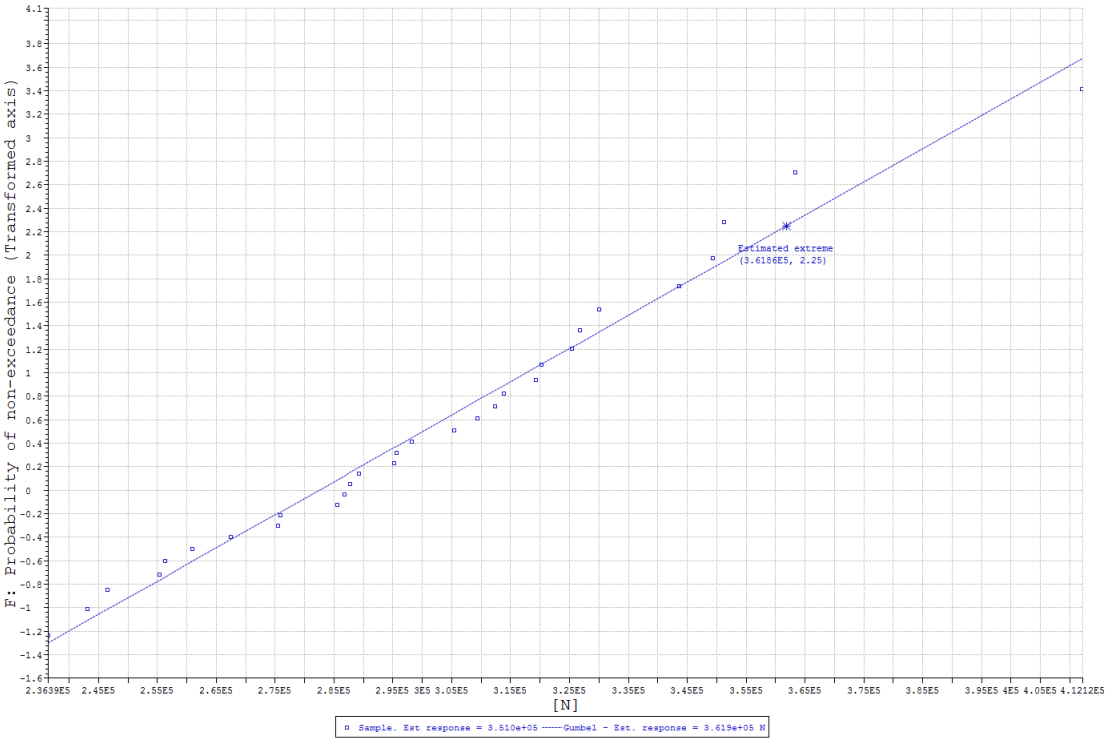

Figure C.14: Sande 2013 winter storm. Gumbel distribution for BN3L1

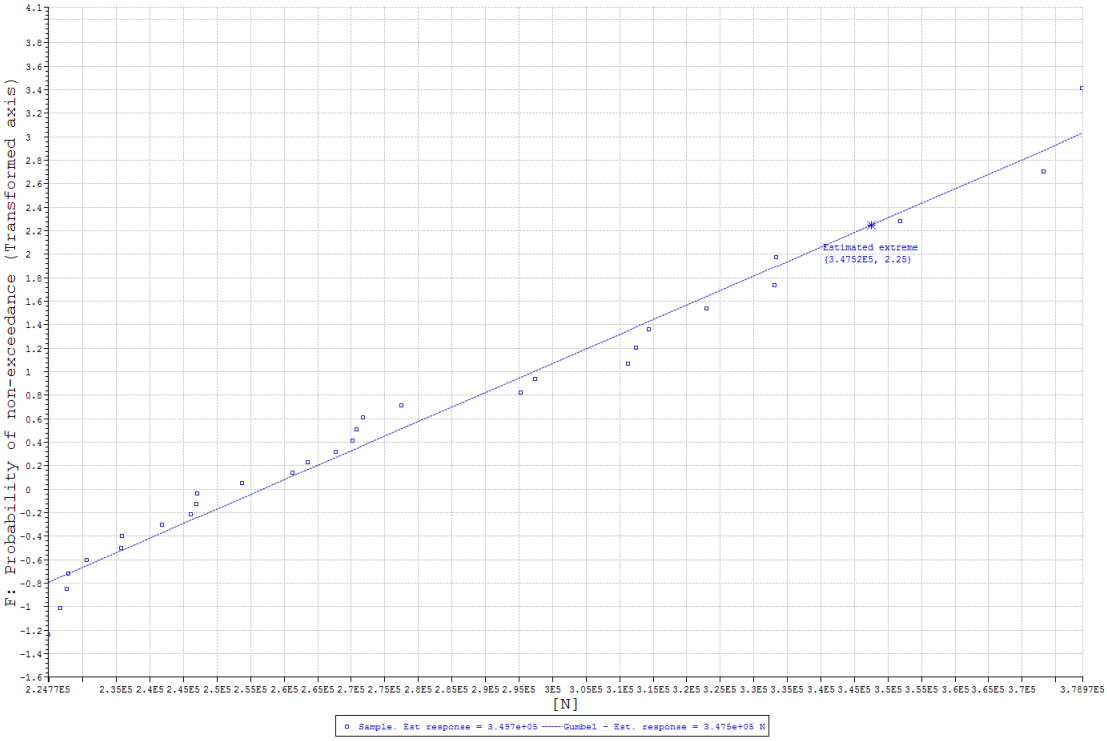

Figure C.15: Sande 2013 winter storm. Gumbel distribution for BN3L2

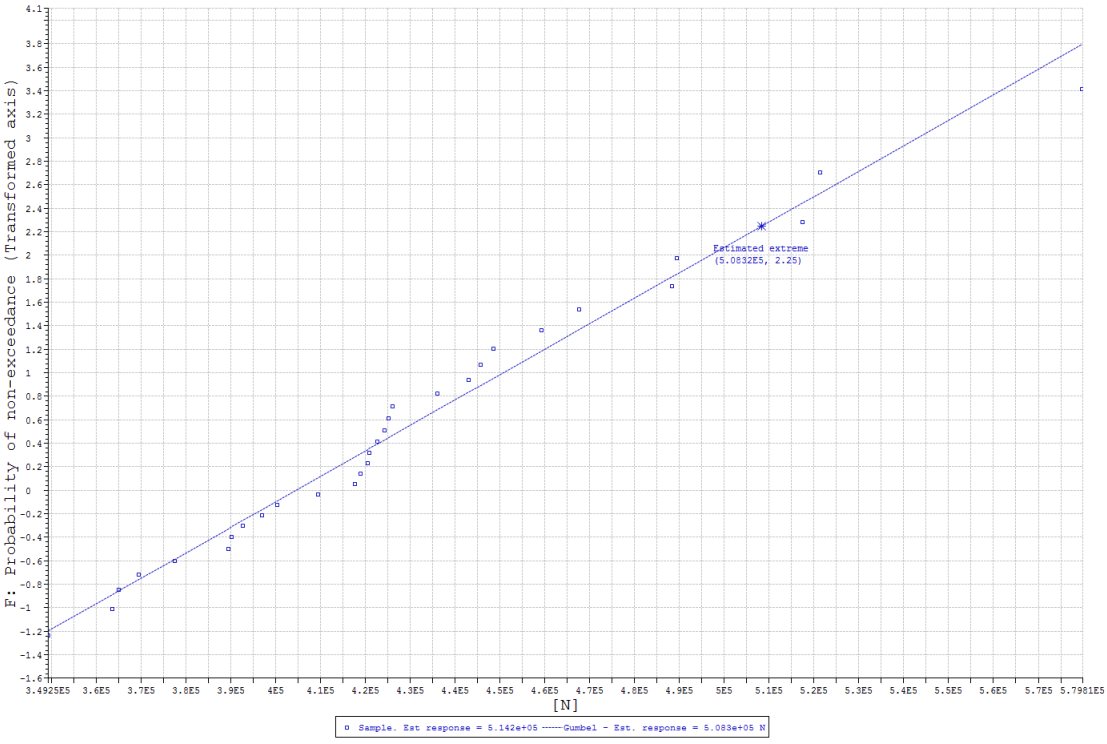

Figure C.16: Sande 2013 winter storm. Gumbel distribution for the BS4 surge force.

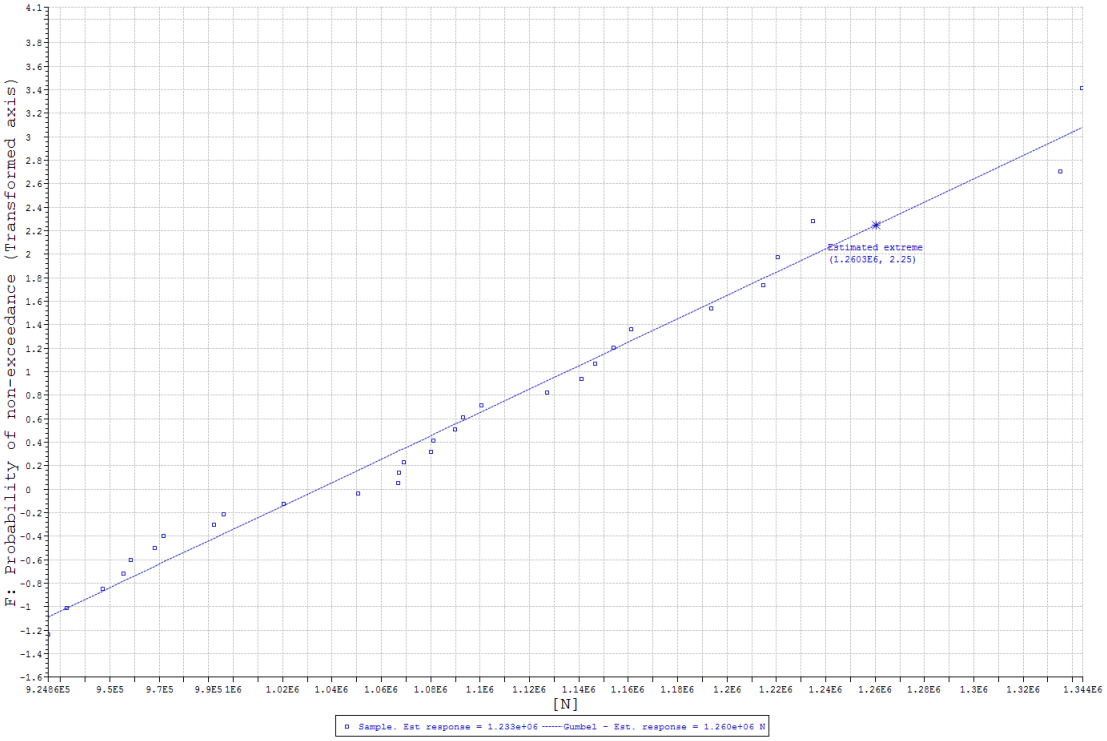

Figure C.17: Sande 2013 winter storm. Gumbel distribution for the BS4 sway force

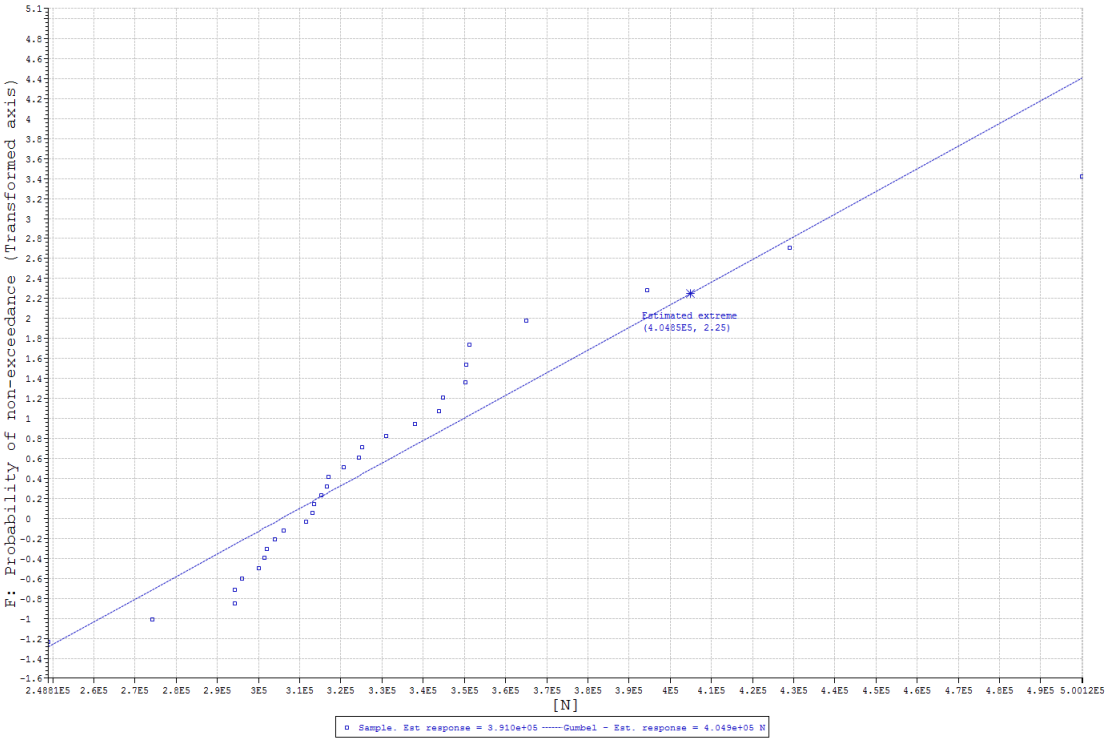

Figure C.18: Sande 2013 winter storm. Gumbel distribution for the BS4 heave force

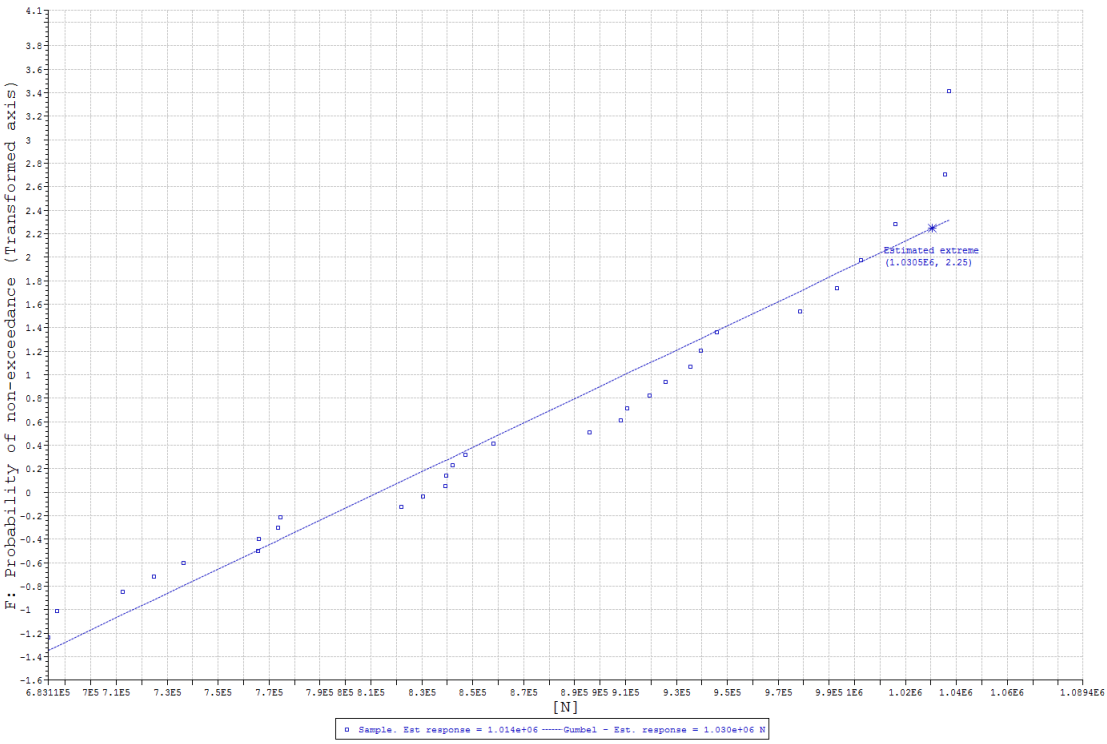

Figure C.19: Sande 2013 winter storm. Gumbel distribution for BS4L3

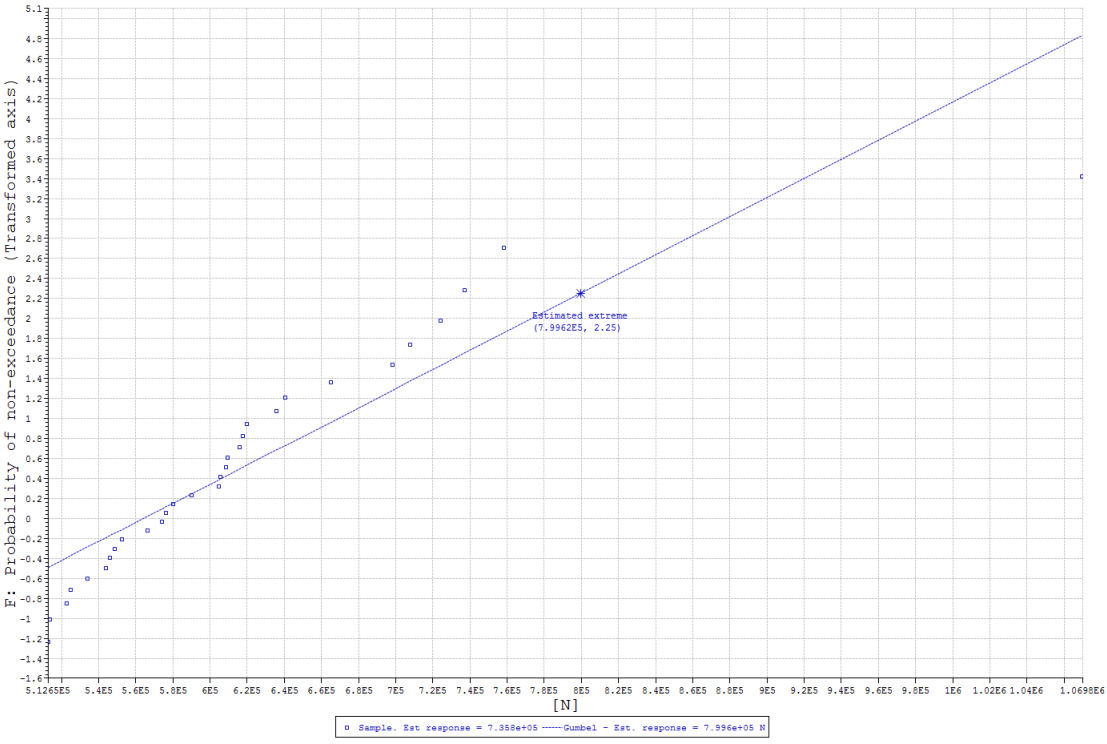

Figure C.20: Sande 2013 winter storm. Gumbel distribution for BS4L4

Gullholmen 2013 winter storm

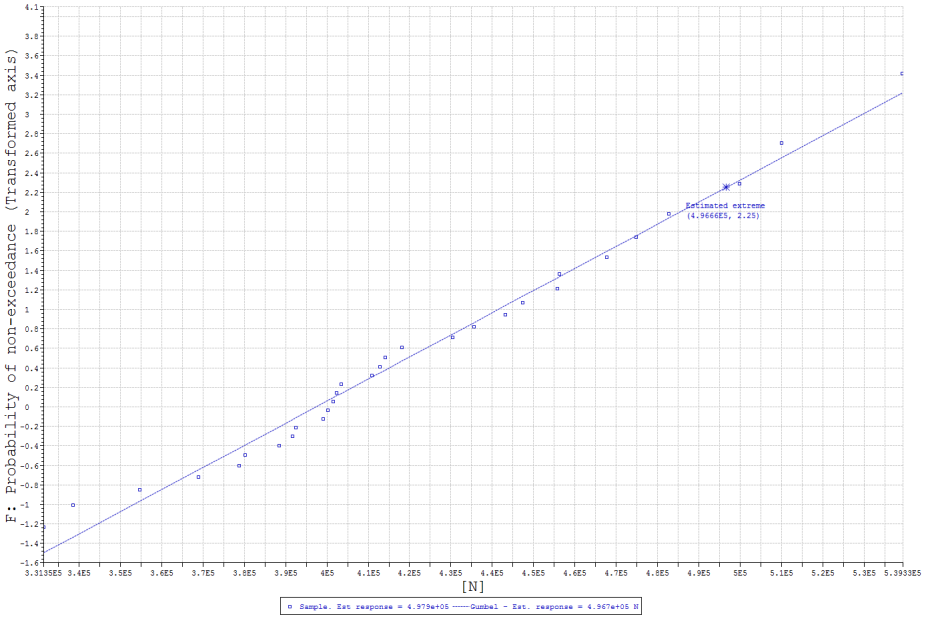

Figure C.21: Gullholmen 2013 winter storm. Gumbel distribution for the BN3 surge force.

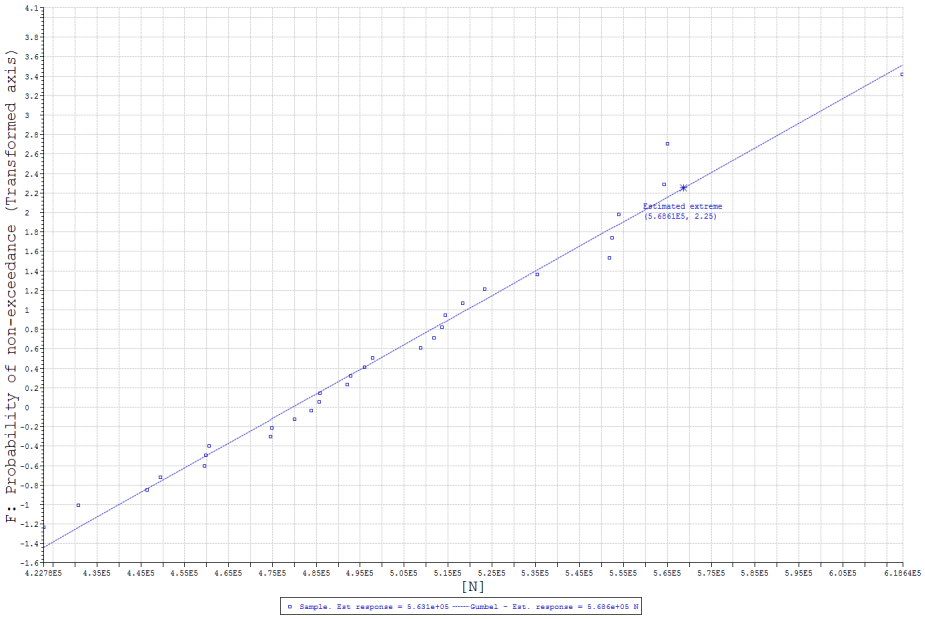

Figure C.22: Gullholmen 2013 winter storm. Gumbel distribution for the BN3 sway force

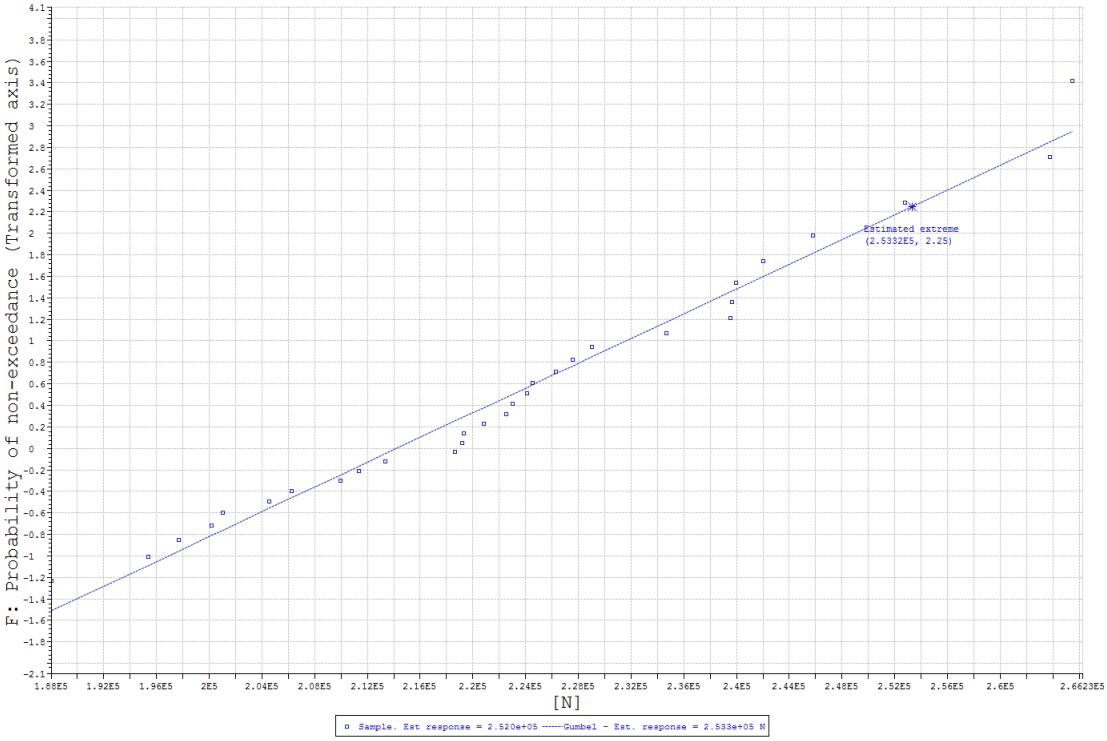

Figure C.23: Gullholmen 2013 winter storm. Gumbel distribution for the BN3 heave force

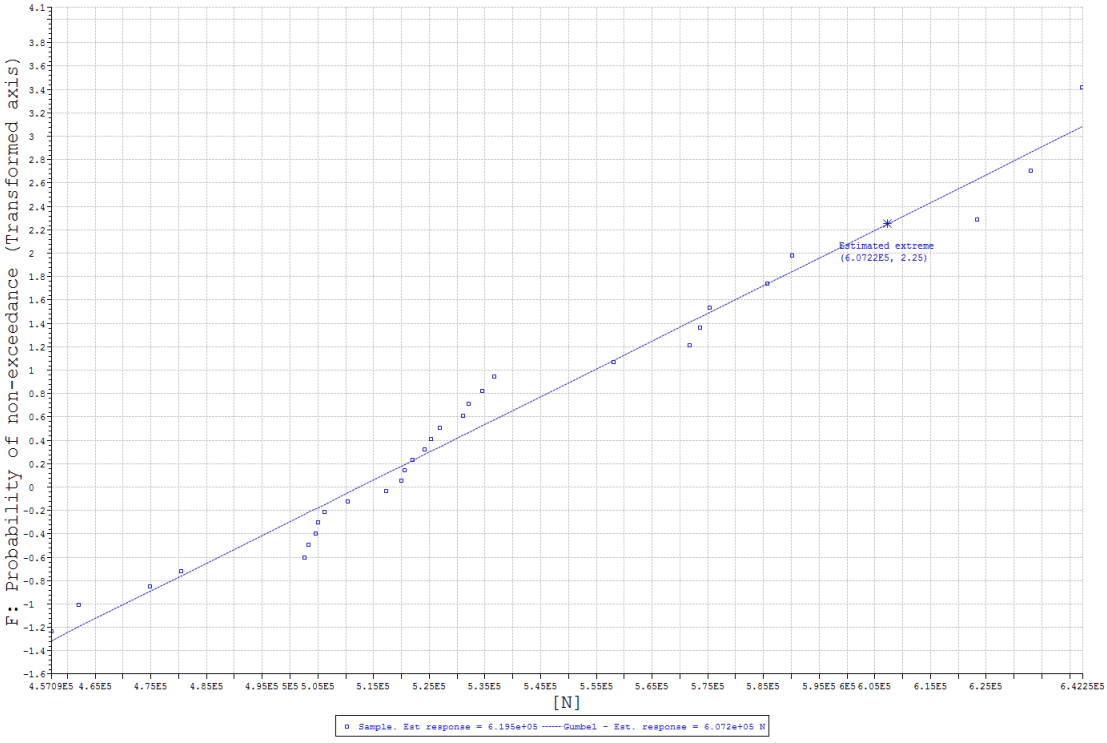

Figure C.24: Gullholmen 2013 winter storm. Gumbel distribution for BN3L1

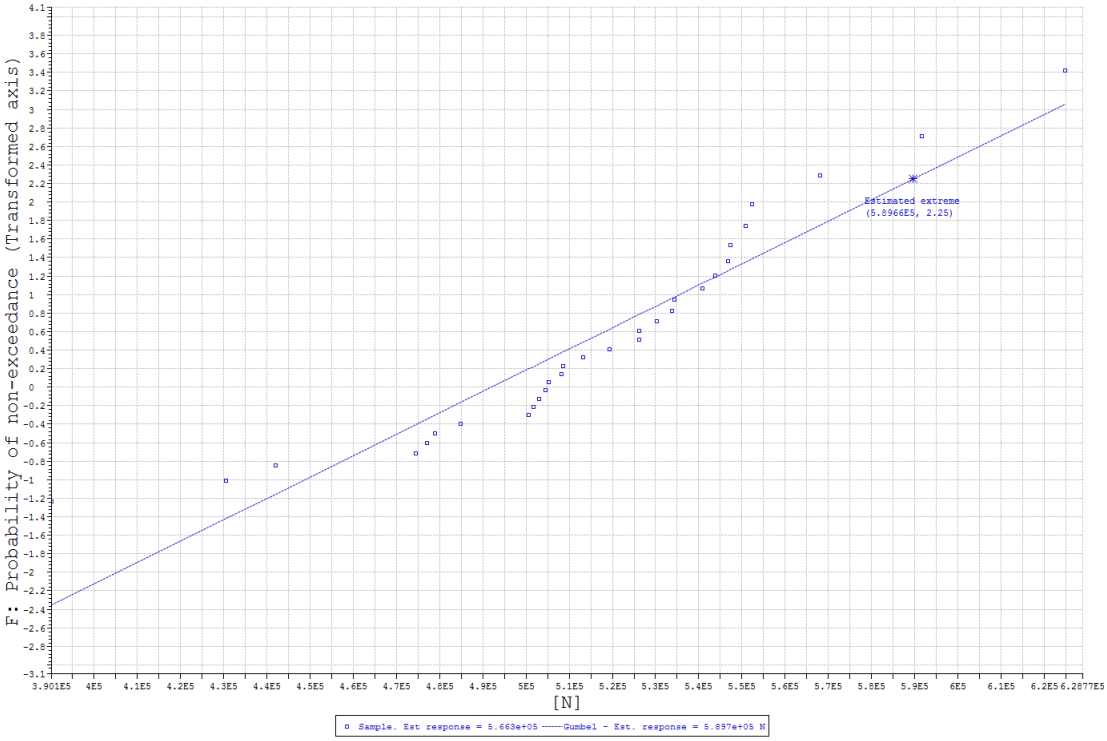

Figure C.25: Gullholmen 2013 winter storm. Gumbel distribution for BN3L2

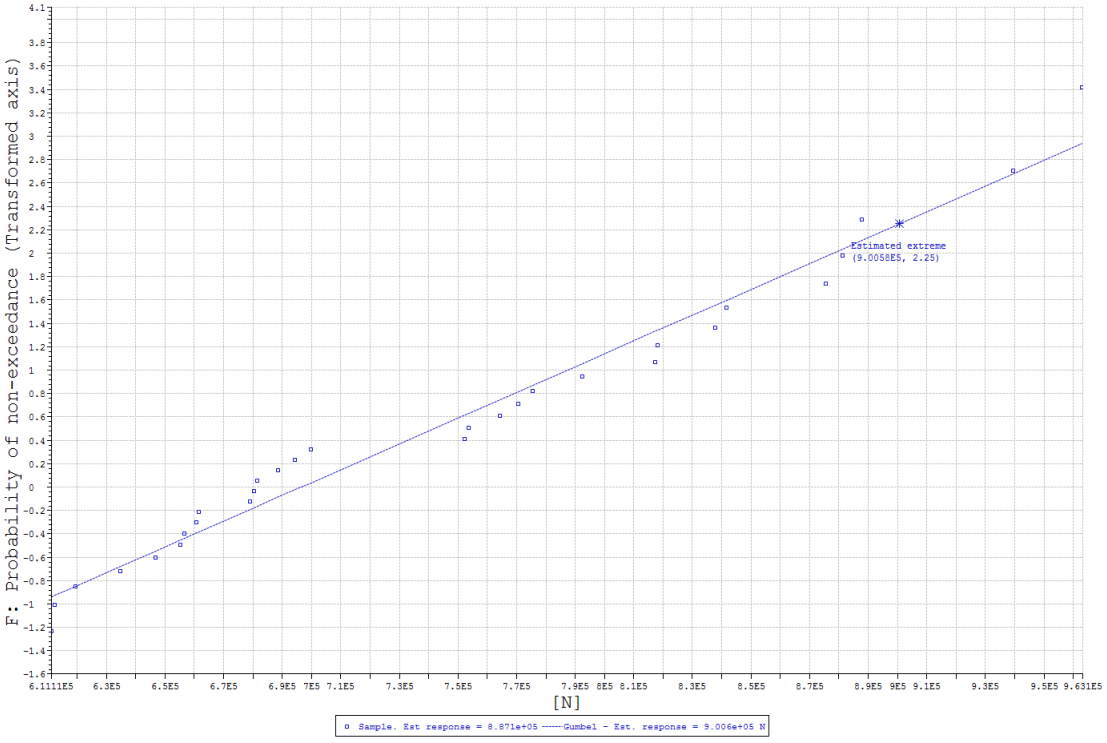

Figure C.26: Gullholmen 2013 winter storm. Gumbel distribution for the BS4 surge force.

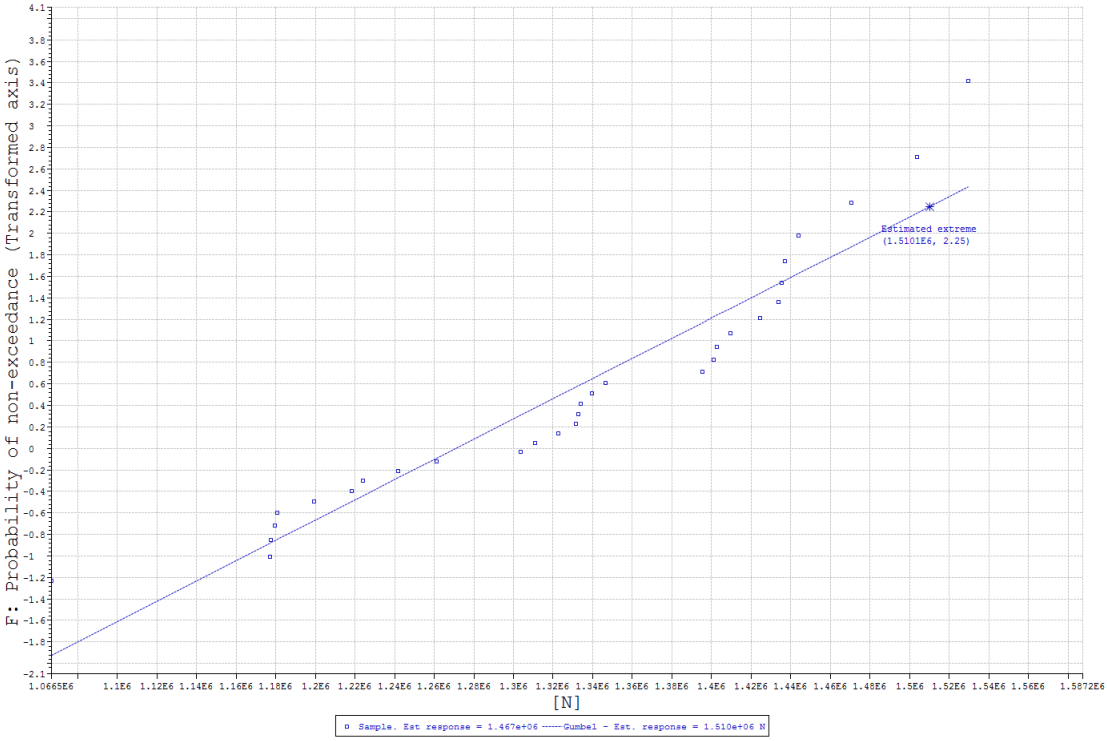

Figure C.27: Gullholmen 2013 winter storm. Gumbel distribution for the BS4 sway force

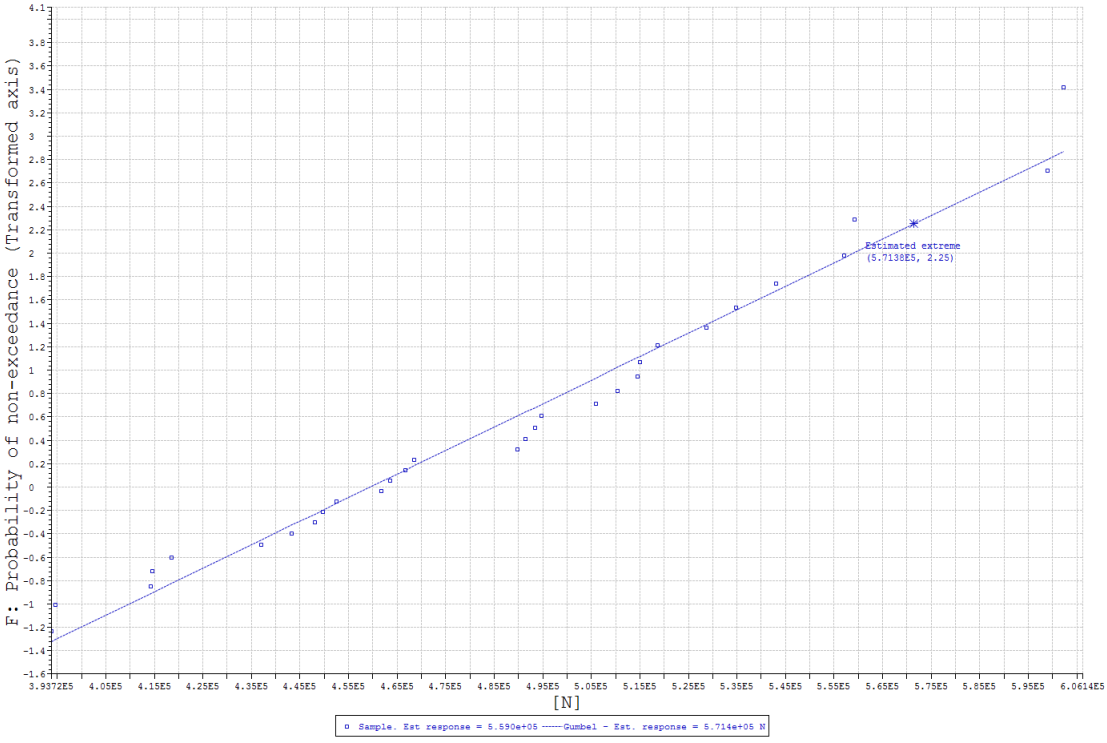

Figure C.28: Gullholmen 2013 winter storm. Gumbel distribution for the BS4 heave force

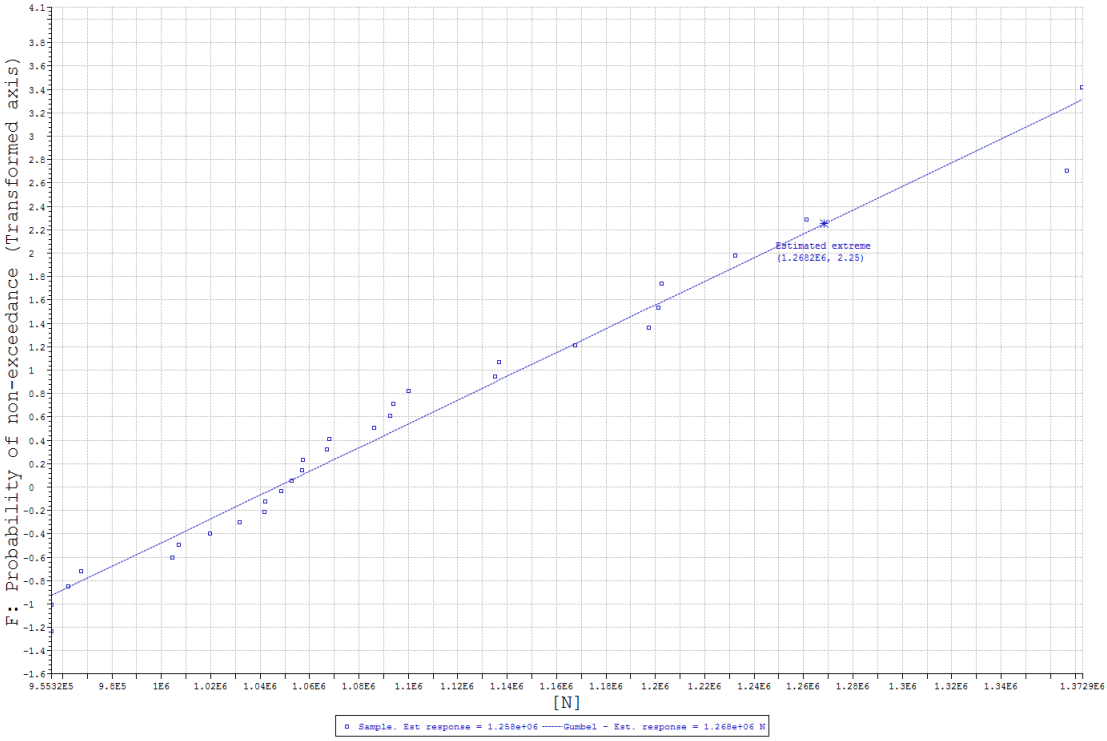

Figure C.29: Gullholmen 2013 winter storm. Gumbel distribution for BS4L3

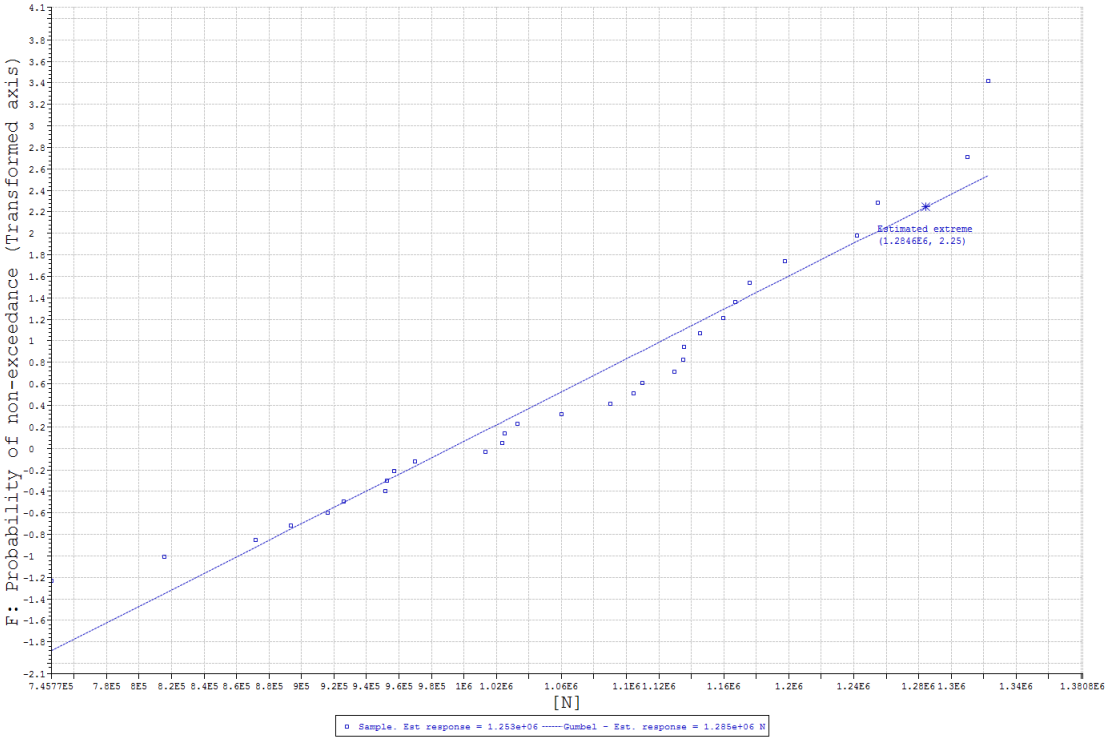

Figure C.30: Gullholmen 2013 winter storm. Gumbel distribution for BS4L4

C.2 Complete dynamic analysis results:

In this section the results from the 30 wave seed dynamic analyses may be found. The results are given for all elements.

Table C.1: Dynamic analysis results for BN1

Condition:	**Sande 50 year storm:**	**Sande 2013 storm:**	**Gullholmen 2013 storm:**
Surge x [N]:	5.59E+05	2.66E+05	5.77E+05
Sway y [N]:	6.99E+05	3.27E+05	6.50E+05
Heave z [N]:	2.12E+05	1.30E+05	2.02E+05
BN1LL1 [N]:	6.05E+05	2.76E+05	5.86E+05
BN1LL2 [N]:	6.53E+05	3.04E+05	6.13E+05
BN1L1 [N]:	4.97E+05	2.89E+05	5.02E+05
BN1L2 [N]:	4.60E+05	2.31E+05	4.41E+05

Table C.2: Dynamic analysis results for BN2

Condition:	**Sande 50 year storm:**	**Sande 2013 storm:**	**Gullholmen 2013 storm:**
Surge x [N]:	4.20E+05	1.70E+05	3.85E+05
Sway y [N]:	5.43E+05	2.70E+05	5.28E+05
Heave z [N]:	1.97E+05	1.29E+05	1.81E+05
BN2L1 [N]:	4.61E+05	2.74E+05	4.27E+05
BN2L2 [N]:	4.27E+05	2.45E+05	4.39E+05

Table C.3: Dynamic analysis results for BN3

Condition:	**Sande 50 year storm:**	**Sande 2013 storm:**	**Gullholmen 2013 storm:**
Surge x [N]:	5.19E+05	2.67E+05	4.97E+05
Sway y [N]:	6.05E+05	3.36E+05	5.69E+05
Heave z [N]:	2.59E+05	1.57E+05	2.53E+05
BN3L1 [N]:	6.22E+05	3.62E+05	6.07E+05
BN3L2 [N]:	5.93E+05	3.48E+05	5.90E+05

Table C.4: Dynamic analysis results for BS1

Condition:	**Sande 50 year storm:**	**Sande 2013 storm:**	**Gullholmen 2013 storm:**
Surge x [N]:	7.54E+05	4.73E+05	7.97E+05
Sway y [N]:	1.23E+06	7.09E+05	1.21E+06
Heave z [N]:	4.10E+05	2.32E+05	4.20E+05
BS1LL1 [N]:	2.30E+03	2.18E+03	2.36E+03
BS1LL2 [N]:	2.18E+03	2.18E+03	2.88E+03
BS1L1 [N]:	8.57E+05	5.19E+05	8.28E+05
BS1L2 [N]:	8.35E+05	5.29E+05	8.33E+05

Table C.5: Dynamic analysis results for BS2

Condition:	**Sande 50 year storm:**	**Sande 2013 storm:**	**Gullholmen 2013 storm:**
Surge x [N]:	6.66E+05	3.23E+05	6.07E+05
Sway y [N]:	1.29E+06	6.48E+05	1.11E+06
Heave z [N]:	3.51E+05	1.86E+05	3.34E+05
BS2L1 [N]:	7.96E+05	4.47E+05	7.15E+05
BS2L2 [N]:	6.84E+05	3.98E+05	7.19E+05

Table C.6: Dynamic analysis results for BS3

Condition:	**Sande 50 year storm:**	**Sande 2013 storm:**	**Gullholmen 2013 storm:**
Surge x [N]:	6.15E+05	3.73E+05	7.14E+05
Sway y [N]:	1.31E+06	7.85E+05	1.47E+06
Heave z [N]:	3.82E+05	2.56E+05	3.84E+05
BS3L1 [N]:	7.76E+05	4.79E+05	7.64E+05
BS3L2 [N]:	7.72E+05	4.49E+05	7.59E+05

Table C.7: Dynamic analysis results for BS4

Condition:	**Sande 50 year storm:**	**Sande 2013 storm:**	**Gullholmen 2013 storm:**
Surge x [N]:	8.77E+05	5.08E+05	9.01E+05
Sway y [N]:	1.65E+06	1.26E+06	1.51E+06
Heave z [N]:	5.69E+05	4.05E+05	5.71E+05
BS4L1 [N]:	9.67E+05	6.91E+05	9.41E+05
BS4L2 [N]:	8.73E+05	6.52E+05	8.93E+05
BS4L3 [N]:	1.30E+06	1.03E+06	1.27E+06
BS4L4 [N]:	1.29E+06	8.00E+05	1.28E+06

Bibliography

[1] Odd Faltinsen. *Sea loads on ships and offshore structures*, volume 1. Cambridge university press, 1993.

[2] DNV. Dnv-rp-c205 environmental conditions and environmental loads. 2010.

[3] Wind statistics from meteorologisk institutt. www.eklima.met.no. Last accessed: 2015-03-11.

[4] Tidal statistics from kartverket. http://www.sehavniva.no/sted/Vestfold/Sande/Selvik~59168/vannstand.html. Last accessed: 2015-03-12.

[5] Pronorm AS. Norsk standard ns 9415 flytende oppdrettsanlegg krav til utforming, dimensjonering, utførelse, installasjon og drift. 2003.

[6] Carl A Thoresen. *Port designer's handbook*. Thomas Telford, 2010.

[7] Bjørnar Pettersen. *Hydrodynamikk*. 2007.

[8] Willard J Pierson and Lionel Moskowitz. A proposed spectral form for fully developed wind seas based on the similarity theory of sa kitaigorodskii. *Journal of geophysical research*, 69(24):5181–5190, 1964.

[9] Klaus Hasselmann, TP Barnett, E Bouws, H Carlson, DE Cartwright, K Enke, JA Ewing, H Gienapp, DE Hasselmann, P Kruseman, et al. Measurements of wind-wave growth and swell decay during the joint north sea wave project (jonswap). 1973.

[10] Evert Bouws, H Günther, W Rosenthal, and CL Vincent. Similarity of the wind wave spectrum in finite depth water: 1. spectral form. *Journal of Geophysical Research: Oceans (1978–2012)*, 90(C1):975–986, 1985.

[11] D. Myrhaug. *Marine Dynamics Lecture notes 2009*. Department of marine technology, 2009.

[12] SIMO project team. Simo - theory manual version 4.0 rev.1. 2012.

[13] H Shin et al. Analysis of extreme tensions in a snapping cable. In *Proceedings of the 1st International Offshore and Polar Engineering Conference*, volume 2, pages 216–221. ISOPE, Golden, CO, 1991.

[14] DNV. Dnv-rp-h103 modelling and analysis of marine operations. 2010.

[15] Sigbjørnson R. Langen, I. *Dynamisk analyse av konstruksjoner*. 1979.

[16] Turgut Sarpkaya. Otc 2898 in-line and transverse forces on cylinders near a wall in oscillatory flow at high reynolds numbers. In *Proceedings-Offshore Technology Conference*, volume 3, page 161. Offshore Technology Conference, 1977.

[17] C. M. Larsen. *Marine Dynamics*. 2012.

[18] DNV. Dnv-os-e301 position mooring. 2010.

[19] Erwin Kreyszig. *Advanced Engineering Mathematics*. John Wiley and sons, Inc., 9 edition, 2006.

[20] Bernt J. Leira. *Stochastic Theory of Sealoads*. Department of marine technology, 2010.

[21] A Colin Cameron and Frank AG Windmeijer. An r-squared measure of goodness of fit for some common nonlinear regression models. *Journal of Econometrics*, 77(2):329–342, 1997.

[22] Standard Norge. Ns-en 1991-1-4:2005+na:2009 eurokode 1: Laster på konstruksjoner del 1-4: Allmene laster vindlaster. 2005.